Editor

Your TCD manuscript "Quantifying spatiotemporal variability of ice algal blooms and the impact on surface albedo in southwest Greenland" received two constructive reviews where both reviewers identified methodological issues and questions, which you already partly clarified in your author comments.

Now I would like to ask you to upload a revised version of the manuscript together with an author's response where you clearly address the comments of the reviewers. In this revised version I think it is specially important to address the topic of sensitivity of the 2BDA methods to changes in dust, ice properties, etc. and this may even include this sensitivity in your results (and not only discussion).

Response: We sincerely thank the editor and two anonymous reviewers for their insightful and constructive comments and suggestions. We have endeavored to address all the comments and improve the manuscript to our best. In particular, to address the comments regarding the sensitivity of the 2BDA index to glacier algae as compared to other factors, we included new sections (**3.3 Sensitivity analysis based on radiative transfer modelling, 4.2 Sensitivity analysis of 2BDA index to non-algal factors, and 5.1 Sensitivity to subpixel variability**) to analyze and discuss the impacts of dust presence, ice properties, and scale issues on 2BDA index. We used the radiative transfer model SNICAR and the spectral linear mixing method to analyze and discuss those factors. To support our statements, we added substantial details in the appendix and improved our figure presentations overall.

In this document, we provide point-by-point responses to the reviewer comments, a summary list of all relevant changes made in the manuscript, and a copy of the manuscript with changes highlighted. We believe that the manuscript has been greatly improved in this revision and we hope that the revised manuscript will be suitable for publication.

Anonymous Referee #1

Overall:

The authors have presented a paper that attempts to quantify biomass over the western Greenland Ice Sheet using the well known "rededge" technique that they refer to as "2BDA", which is often used for detecting chlorophyll containing biota such as photosynthetic algal blooms in oceanic and lacustrine environments, vegetation and crop mapping. Biomass quantification over the Greenland Ice Sheet is a worthy research goal because Greenland Ice Sheet glacier algae very likely play an important role in controlling the ablation zone albedo that is not yet accounted for in energy balance models. This is well within the scope of The Cryosphere and the scientific question is worthy of consideration in this journal. There are some very useful aspects to the paper, including demonstration that there are ablation zone albedo processes that SMB models currently do not account for, the albedo time series over the western ablation zone, and the comparison between different band ratios. However, there are some major issues that need to be addressed before I can recommend publication. More detail is provided below.

Response: We greatly appreciate the reviewer's careful review of our manuscript. Many thanks for suggesting to use SNICAR model to assess the sensitivity of 2BDA index to various dust concentrations. In this revision, we believe the manuscript has been greatly improved by incorporating the reviewer comments. Please see our responses below.

Major Comments:

1)There is past literature that emphasises the importance of discounting abiotically generated rededge signals before assuming them to be diagnostic of photosynthetic life (see Sparks et al. 2009; Seager et al. 2005). The vulnerability of the rededge to false positives is demonstrable using a simple radiative transfer model (easily replicated inbrowser via http://snow.engin.umich.edu/). Fig 1A shows the results from SNICAR runs where all variables were held constant except the mass concentrations of completely inorganic impurities (Flanner et al.'s (2009) "global average dusts, type 4"). The lowest 2 spectral albedo curves returned a false positive 2BDA result (1.002 and 1.005). In Figure 1B, the model is run again identically but with a hematiterich mineral dust taken from Polashenski et al. (2015), giving eight 2BDA false positives (1.004, 1.015, 1.026, 1.031, 1.039, 1.043 1.046). Tedesco et al. (2013) suggested that hematiterich red dusts are present in the GrIS ablation zone (we note that Cook et al. (in review) disagreed about that but their paper remains unpublished). Taking Tedesco et al. (2013) to be correct about the prevalence of red dusts on the Greenland ablation zone therefore invalidates the rededge as a biomarker due to the demonstrable potential for false positives. Convincing empirical data is required to demonstrate that the 2BDA signal is exclusively biological and robust to these types of false positive results.

A) B)

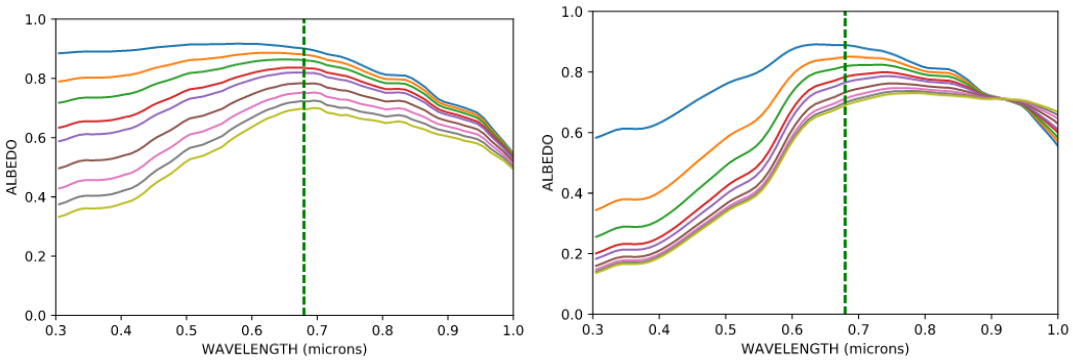

Fig 1: A) SNICAR runs with diffuse irradiance, homogenous snow with grain diameter 500 micron, density 400 kg m^3 and Flanner et al. (2009)'s "dust 4" in the upper 1 mm, in mass concentrations of 0.1, 0.3, 0.5, 0.8, 1.0, 1.5, 2.0, 2.5, 3.0 ugdust/gice. B) Identical SNICAR runs but with Polashenski et al. (2015)'s high hematite dust.

Response: We thank the reviewer for pointing out the issue of potential impacts by dusts. In this revision, we addressed this concern by conducting SNICAR simulations with various parameter settings as the reviewer suggested. We would like to clarify that our objective is not to define a universal biomarker for detecting photosynthetic life. To our understanding, the two papers the reviewer mentioned that address the potential false signal resulting from dusts (Sparks et al. 2009 and Seager et al. 2005; not in the reference list), are in the extraterrestrial context.

However, our research is conducted based on the understanding that widespread glacier algal blooms occur on the bare ice zone in southwest Greenland, which have been confirmed by numerous studies (Cook et al., 2020; Lutz et al., 2014; Remias et al., 2012; Ryan et al., 2018; Stibal et al., 2015; Stibal et al., 2017; Williamson et al., 2019; Yallop et al., 2012). Nevertheless, to evaluate the sensitivity of the 2BDA index to various dust sizes and concentrations, we performed radiative transfer modelling experiments using SNICAR, by setting the grain size of snow to 500 microns and 1500 microns. However, we cannot generate the same results using the dust concentrations specified by the reviewer (0.1, 0.3, 0.5, 0.8, 1.0, 1.5, 2.0, 2.5, 3.0 $\mu g_{dust}/g_{ice}$). Using these parameters, the 2BDA index is less than 0.97 for all dust sizes (dust 1, dust 2, dust 3, and dust 4) when the grain size is 1500 microns, and less than 0.98 when grain size is 500 microns. The 2BDA index would be over 1.0 only when the dust concentrations are greater than ~800 ppm.

In this revision, we added the section 3.3 (Sensitivity analysis based on radiative transfer modelling) and section 4.2 (Sensitivity analysis of 2BDA index to non-algal factors) to specifically analyze this issue. Using a grain size of 1500 microns produces a spectral curve that is closest to the MERIS bare ice spectra. The SNICAR experiments were performed with the following parameters: direct incident radiation, a solar zenith angle of 60 degrees, clear-sky conditions (for Summit Greenland), a snow grain effective radius of 1500 micron (to approximate the ice surface), a snowpack thickness of 100 m (to avoid any influence of the sub-snowpack albedo), a snowpack density of 400 kg/m^3, and dust concentrations of (0.1, 0.3, 0.5, 0.8, 1, 1.5, 2, 2.5, 3, 5, 8, 10, 30, 50, 80, 100, 300, 500, 800, 1000, 1500, 2000, 2500, and 3000 ppm) for four dust sizes (dust 1: 0.1–1.0μm; dust 2: 1.0–2.5μm; dust 3: 2.5–5.0μm; dust 4: 5.0–10.0 μm). We also tested different density values but

these did not affect the simulation results. In addition to the 2BDA index, we also calculated the impurity index for the SNICAR simulations, and found that the impurity index is more sensitive to dusts than the 2BDA index (Figure 4 in the revised manuscript, shown below). The figure (below) shows scatterplots of impurity index vs. 2BDA index calculated for the SNICAR simulations (with the diameter of circles representing the magnitude of dust concentrations for four different dust sizes), and density scatterplots from the MERIS data (impurity vs. 2BDA indices over bare ice). The results indicate that relatively high concentrations of dust would increase the 2BDA index, but would also result in a large increase in the impurity index. By contrast, the upper bound of the impurity index we calculated from the MERIS data is around 1.0, below the impurity index values for the highest dust concentrations. These results suggest that relatively high 2BDA values (especially above 0.99, corresponding to an impurity index of 1.0) are unlikely to be caused by dusts, because the presence of dusts would also result in an impurity index of above 1.0. This indicates that for our study area, the glacier algae identified with a 2BDA index greater than 0.99 are not likely to be false positives caused by dusts. Finally, even below this threshold, the slope of the 2BDA vs. impurity index is shallower than the SNICAR-generated curves, suggesting that the 2BDA index is generally more sensitive to chlorophyll-a than to dust.

With regard to the possible presence of hematite-rich dust, the samples of Tedesco et al. (2013) were from cryoconite holes, and are not necessarily representative of the ice surface; and the hematite concentration in those samples was actually very low. Cook et al. (2020) also found that the local bare-ice mineral dust is poor in hematite and rich in weakly absorbing quartz and feldspar minerals. Therefore, the hematite has a negligible influence on the detected chlorophyll-a signal at the red-NIR region.

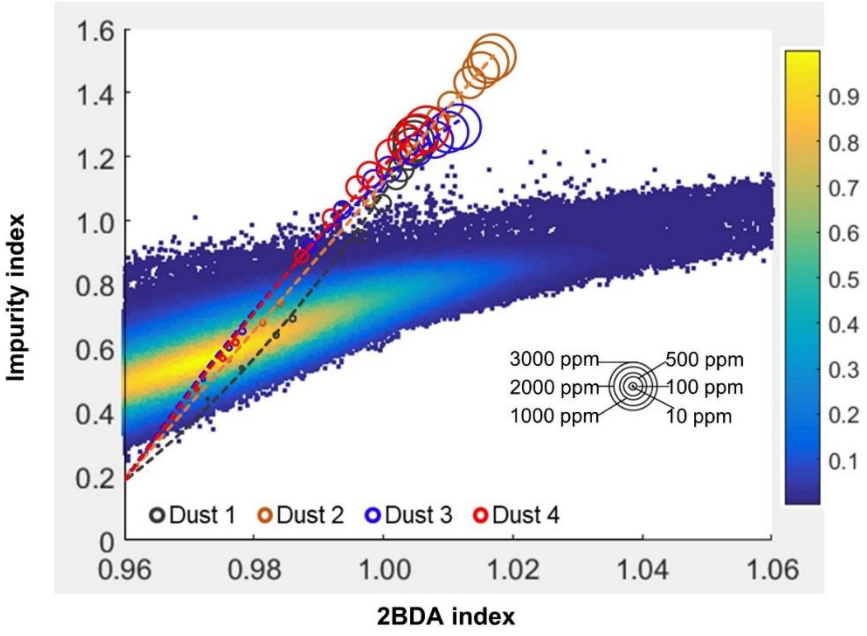

Figure 4 (in the revised manuscript). Impurity index vs. 2BDA index for MERIS bare ice pixels (density scatter plot with colours indicating relative frequency), excluding missing data in our study area, between 2004 and 2011. Circles show impurity vs. 2BDA index from SNICAR simulations with varying concentrations of dust (with four different dust sizes). The circle size corresponds to the dust concentration, and dashed lines show the polynomial regression for each of the

different dust sizes. The circle size corresponds to the dust concentration, and dashed lines show the polynomial regression for each of the different dust sizes.

2) The authors do not account for the spectral albedo of the ice itself. Ice albedo can vary dramatically independently of light absorbing particles and cause the 2BDA value to change, undermining the biomass quantification. Figure 2 shows identical simulations to Fig 1, except the grain size is increased to 1500 microns. False positive results are returned as before, but the value of the 2BDA indexes and therefore the retrieved biomass – change (Flanner et al. (2009) dust =1.0009 and 1.004; Polashenski et al. (2015) dust = 1.0018, 1.014, 1.026, 1.032, 1.040, 1.043, 1.045, 1.046). The retrieved biomass therefore changed without any change in impurity loading. On real glacier ice where the ice albedo can vary by tens of percent independently of impurity concentration due to weathering crust development, meltwater accumulation and drainage, topography, impurity mixing and glaciological structure, the potential for highly error prone retrievals is likely very high. The authors need to demonstrate that their band ratio is not vulnerable to this uncertainty, or that they can quantify and correct for it.

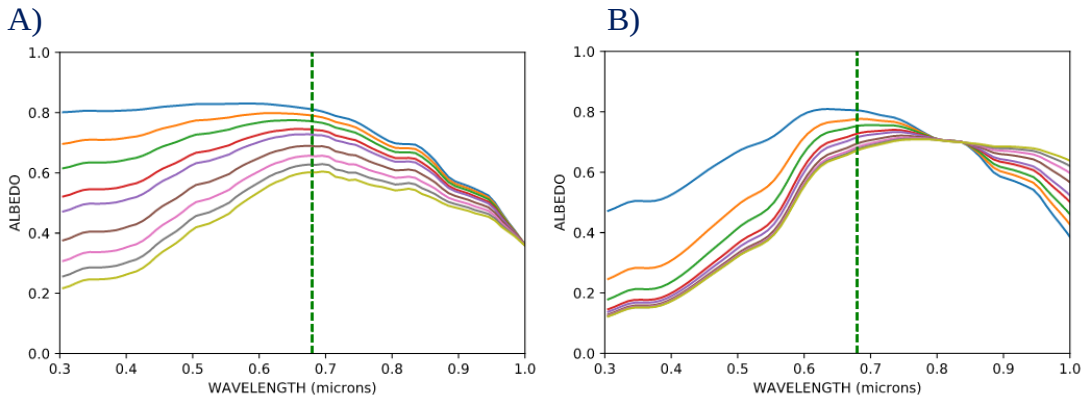

Fig 2: A) SNICAR runs with diffuse irradiance, homogenous 1500 micron, 400 kgm^3 snow with Flanner et al. (2009)'s "dust 4" in the upper 1 mm, in mass concentrations of 0.1, 0.3, 0.5, 0.8, 1.0, 1.5, 2.0, 2.5, 3.0 ugdust/gice. B) Identical SNICAR runs but with Polashenski et al. (2015)'s high hematite dust.

Response: The sensitivity of the 2BDA index to dust presence (over snow with a 1500 microns grain size to approximate ice) has been discussed above.

We agree on the point that ice albedo changes with impurity concentration, meltwater presence, topography and crevasses, as discussed by Ryan et al. (2018). But also, as suggested by Ryan et al. (2018), the distributed impurities explain most of the spatial variability of surface albedo. In addition, it should be noted that variations in albedo due to other factors including water, other impurities, and ice albedo does not necessarily affect the 2BDA index. Ice with different concentrations of air bubbles has a consistent spectral shape between 665 nm and 709 nm (Condom et al., 2018), and meltwater exhibits a similar pattern at this wavelength range, both of which are characterized by a decreasing reflectance from 665 nm to 709 nm. The sensitivity of the 2BDA index to glacier algae can be further demonstrated using the field dataset of Cook et al. (2020), as illustrated by Table C1 and Figure C2 (in the revised manuscript, shown below). The MERIS band ratio between 709 nm and 665 nm (both bands have bandwidths of 10 nm) is specifically designed

for chlorophyll-a, and less affected by dusts as we discussed above. To our knowledge, the meltwater, weathering crust, and crevasses do not cause the pattern of increasing reflectance from 665 nm to 709 nm. In our revised Figure 2d (shown below), it is clearly shown that the MERIS exhibits the red-NIR spectral signature caused by chlorophyll-a, which matches multiple field hyperspectral data measurements over algae-abundant dark ice (which are likely subject to varying ice conditions). We have added discussions in section 4.2 accordingly.

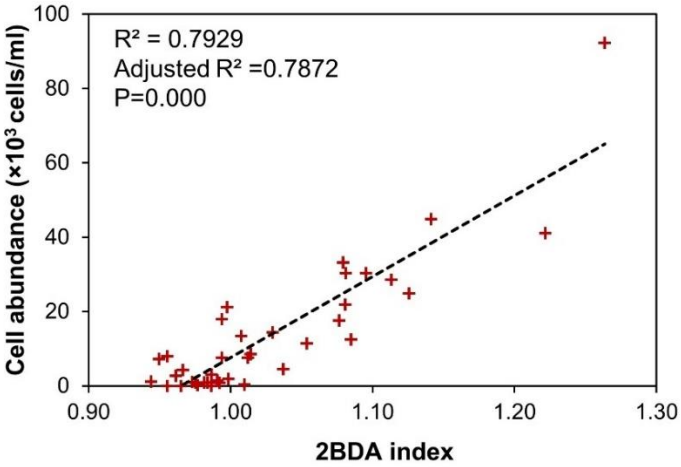

Figure C2 (in the revised manuscript). Scatterplot of measured cell abundance versus 2BDA index listed in Table C1 based on the published field dataset of Cook et al. (2020).

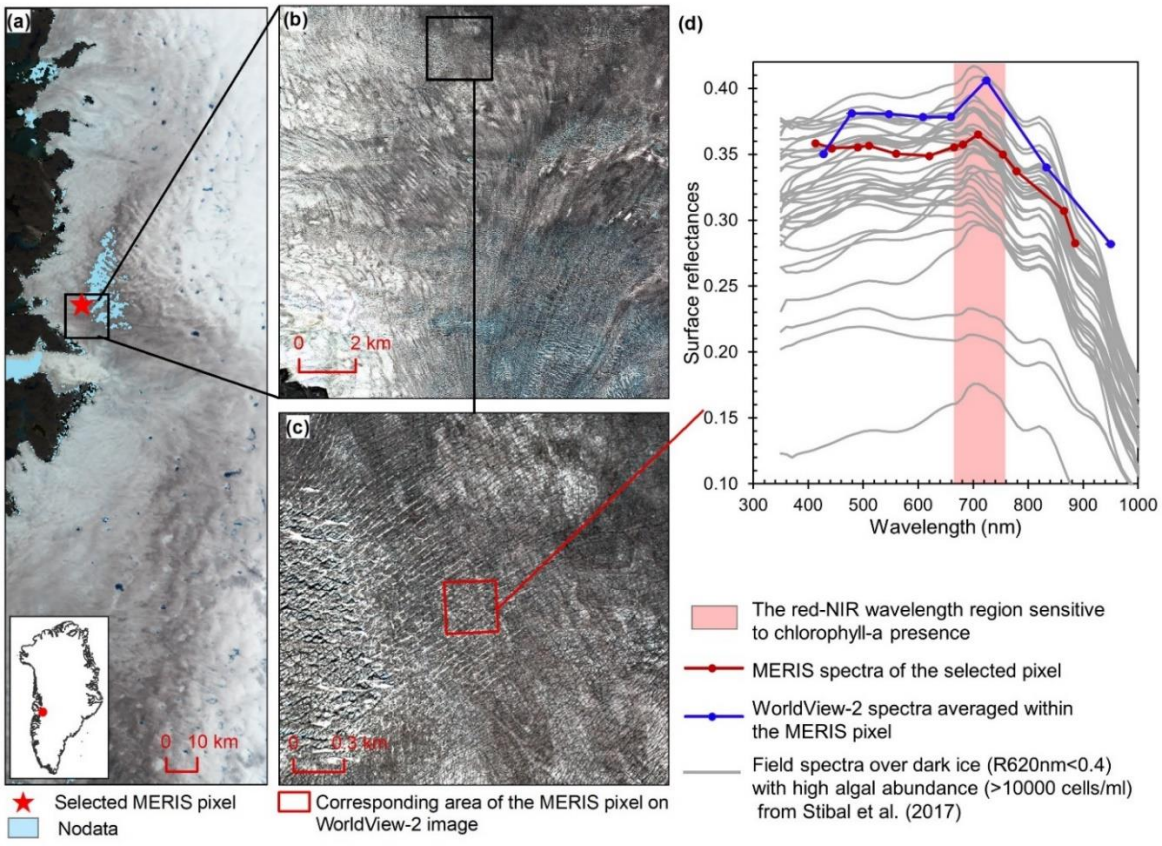

Figure 2 (in the revised manuscript). Comparison between MERIS, WorldView-2, and field spectra over algae-abundant dark ice. (a) MERIS Level-2 image (true colour composite) acquired on 5 July 2010. Pixels with missing data are shown in light blue. (b) WorldView-2 surface reflectance image acquired on 9 July 2010 over the square area in (a). (c) Zoomed-in WorldView-2 image, with the area (red square) corresponding to the selected MERIS pixel in (a). (d) Reflectance spectra for MERIS and WorldView-2 (2010), and field hyperspectral measurements collected over the algae-abundant dark ice at S6 by Stibal et al. (2017) in 2014.

3) The authors do not adequately address the problem of scale mismatches between the normal length scales of typical algal blooms (biomass varies dramatically over 110 m length scales) and the satellite used to gather their data (300 x 300m). Surface heterogeneity must surely introduce major uncertainties as the spectral reflectance of each pixel is the combined product of many highly variable surfaces. How would, for example, cryoconite, surface water, dust, crevasses and surface topography at the subpixel scale affect their biomass quantification? These unquantified factors must influence the predicted cell concentration independently of realworld changes to the mass concentration of algae, but they are not discussed in the paper.

Response: In this revision, we added section 5.1 (Sensitivity to subpixel variability) to discuss the scale issues. Based on our SNICAR experiments, and analysis of the 2BDA and impurity indices, the 2BDA index is less sensitive to the presence of dust, which means that the high 2BDA index is uniquely biological. Given the sensitivity of MERIS to the presence of chlorophyll-a, the 2BDA index can capture well the chlorophyll-a signal generated by glacier algae. To examine the potential impact of spatial heterogeneity on the MERIS 2BDA index, we performed spectral linear mixing experiments using the field hyperspectral measurements of Cook et al. (2020) for glacier algae and bare ice and the SNICAR-simulated spectra for dust. We obtained the mixed spectra (Figure C3 in the manuscript, shown below) by specifying the different areal percentage of algae/dust vs. bare ice, and calculated the corresponding 2BDA index for the mixed spectra. It is shown that the 2BDA index dramatically increases with the areal percentage of glacier algae, being consistent with the assumption that the 2BDA index is positively correlated with the algal abundance. In contrast, the 2BDA index has much less sensitivity to dust. The high-resolution UAV mapping by Ryan et al. (2018) suggests that the areal percentage of the distributed impurities is up to 65%~95% within individual MODIS pixels (500-meter resolution) over the dark zone in southwest Greenland. Our linear mixing experiments (Figure C3b) suggest that the MERIS 2BDA index can capture the glacier algae variability within the dark zone. In addition, our comparison between the MERIS spectra, WorldView-2 spectra, and field hyperspectral data (Figure 2 in the manuscript, shown above) shows that the chlorophyll-a signature at the red-NIR region is quite consistent between different source measurements with different spatial scales.

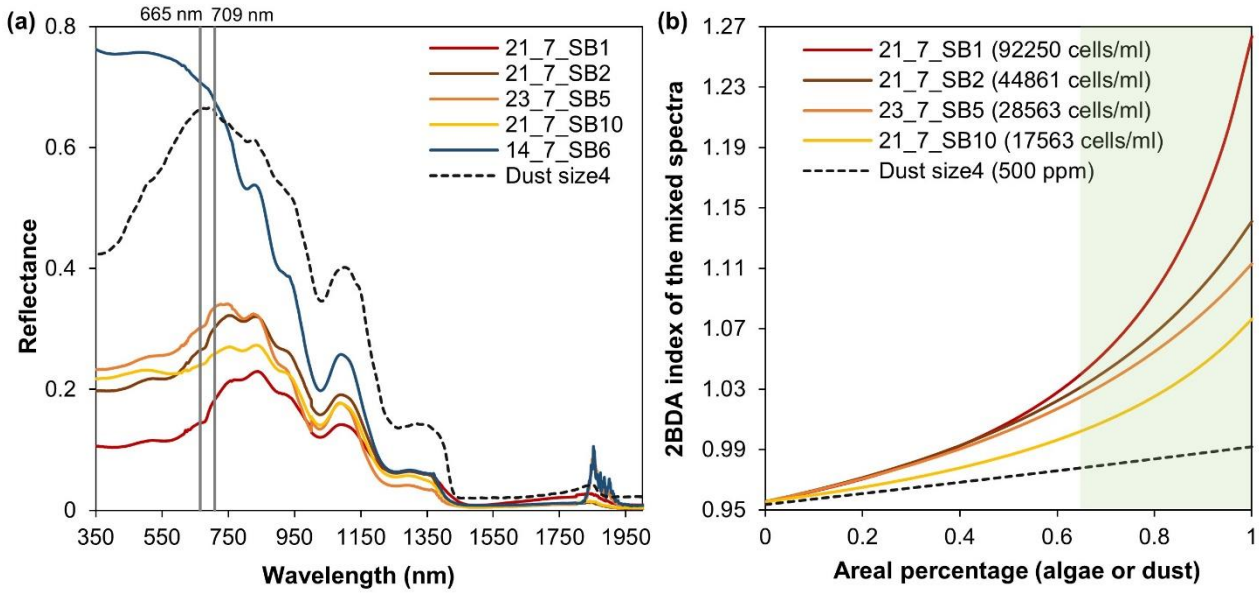

Figure C3 (in the revised manuscript). Spectral linear mixing experiments. (a) Field hyperspectral measurements of four algae-abundant samples (21_7_SB1, 21_7_SB2, 23_7_SB5, and 21_7_SB10) and one bare ice sample (zero algal abundance, 14_7_SB6) from Cook et al. (2020), and the SNICAR-simulated spectra for the dust scenario (size 4 at concentration of 500 ppm). (b) 2BDA index calculated from the linearly mixed spectra with varying areal percentage at subpixel scale for algae (different algal abundances) and dust scenarios.

4) There is insufficient detail regarding the use of field spectroscopic measurements as "ground truth". Only one single field spectrum is presented in the paper and the measurement conditions are not reported. Has it been picked because it matches well with the MERIS spectrum, is it a mean (in which case of how many samples, and what do the error bars look like) or is it the only available spectrum? How do other spectra in the field dataset compare? Can the authors provide evidence to suggest that centimeter scale field spectroscopy measurements are truly representative of the biomass over entire MERIS pixels?

Response: We have revised the text to include more details on how we used the field data by Stibal et al. (2015) and Stibal et al. (2017). In our study, we used those field data in a qualitative way to validate the spatial variations of algal concentration magnitude derived from the satellite data, and to compare the field hyperspectral measurements over algae-abundant ice with the MERIS spectra and WorldView-2 spectra. The field measurements are collected after the period of MERIS measurements, precluding direct comparison with field data. In this revision, we revised Figure 2d (shown above) to include additional field spectra collected over dark ice (R620nm<0.4) with high algal abundance (cell concentrations greater than 10000 cells/ml). As illustrated by Figure 2d, the spectral characteristics at the red-NIR region match well between MERIS spectra, WorldView-2 spectra and field spectra. The match between MERIS spectra (300 meter) and WorldView-2 spectra (2 meter) also indicate that the chlorophyll-a signal cannot be masked out because of large spatial scales, given the high areal percentage of the distributed impurities within the MERIS pixel, as illustrated by Figure 2 (in the revised manuscript) and given the estimation of Ryan et al. (2018) that the areal percentage of the distributed impurities is about 65~95% within individual MODIS pixels (500-meter resolution) in dark ice areas.

5) The authors are selective with their citing of literature under review. If they wish to include papers still under discussion they should explain why the issues of spatial scale encountered in 20 m Sentinel2 pixels discussed by Cook et al (in review) and Tedstone et al. (in review) do not also apply to their 300 m MERIS pixels. If they decide to stick to published literature they should explain how the presence of hematiterich dusts on the ablating Greenland Ice Sheet as reported by Tedesco et al. (2013) does not invalidate their assumption that the rededge is uniquely biological.

Response: We removed the references to all discussion papers since they are not referenceable. The paper by Cook et al. (2020) is now published, and we have included this citation in our introduction section and discussion section. We also mentioned the potential impact of hematite dust (Tedesco et al. 2013) on the 2BDA index in section 4.2. As we mentioned above, the hematite has a negligible impact on the 2BDA index in our context.

Specific Comments:

Title: As suggested by Daniel Remias in the open discussion forum, please adopt the generally accepted terminology "glacier algae" that distinguishes these algae from those found in sea ice.

Response: As suggested, we have changed 'ice algae' to 'glacier algae' throughout the text.

General point about chlorophyll: Referring to "chlorophyll" is somewhat ambiguous as it could imply total chlorophyll or one of several chlorophyll variants. Please be specific that you mean chlorophylla.

Response: We have revised the text as suggested.

L39: Any citation for yellow/orange snow algae? They are normally thought of as green or red.

Response: We have added the citation (Anesio et al., 2017) for the yellow/orange pigmentation of snow algae.

L71: The authors rightly criticise carotenoid based remote sensing methods because of possible false positives due to "dirt" but ignore the potential for equivalent rededge false positives due to dust.

Response: In this revision, we ran a number of SNICAR simulations with variant dust sizes and concentrations. Based on the SNICAR simulations, we calculated both the 2BDA and impurity indices for different dust configurations, and evaluated the potential impact of dust presence on 2BDA index. Please see details in the revised section 4.2 (Sensitivity analysis of 2BDA index to non-algal factors).

L75: The authors claim chlorophyll is the appropriate pigment to use to identify ice algae despite also stating that the coloration of the algae is primarily due to purpurogallin pigments. Why, then, is that not the appropriate pigment to use to identify glacier algae?

Response: Compared with the purpurogallin pigment, Chlorophyll-a is more appropriate for mapping glacier algae for the following reasons:

1) Chlorophyll-a is the primary photosynthetic pigment of glacier algae (Williamson et al., 2018). The ocean color satellite sensors like Envisat MERIS and Sentinel-3 OLCI are designed to capture the Chlorophyll-a signal from highly-absorptive and optically complex water bodies, which means that the ocean color sensors are highly sensitive to the chlorophyll-a presence, making them very useful tools for glacier algae detection based on the biological signatures.

2) According to the studies by Remias et al. (2012) and Williamson et al. (2018), the spectral signatures (absorption peaks) of the purpurogallin pigment are concentrated in the UV region (278 nm, 304 nm, and 389 nm, Remias et al.,2012). To our knowledge, no satellite sensor can detect these spectral signatures. Although the purpurogallin pigment is very likely to account for the brownish-grey colour of glacier algae, its absorption over the entire visible spectrum is quite uniform, making it difficult to differentiate from other dark impurities. In contrast, chlorophyll-a can generate very strong spectral signatures at the red and NIR region, which are supported by field hyperspectral measurements for both snow algae and glacier algae. (e.g. Ganey et al., 2017; Painter et al., 2001; Stibal et al., 2017; Cook et al., 2020).

   We have revised the text (introduction section) to discuss and compare the suitability of purpurogallin vs. chlorophyll-a for glacier algae mapping.

L75: "owing to its unique spectral signatures between 665 710nm (Gitelson, 1992; Painter et al., 2001; Wang et al., 2018)": Chlorophylla absorbs in narrow bands around 680 nm and 440 nm. Any effects extending up to 710 nm are due to interactions with the surrounding medium. This is why Painter et al. (2001) was able to use the narrow 680 nm absorption feature as a diagnostic tool for Chlorophylla detection.

Response: By 'unique spectral signatures between 665-710nm', we are referring to the absorption between 665-681 nm and the reflectance peak around 710nm. Painter et al. (2001) used the 680nm absorption feature by calculating the integral of the absorption scaled by its continuum spectra. Painter et al. (2001) retrieved the continuum spectrum by linearly interpolating the reflectance peaks at 630 nm and 700 nm, which similarly to our study, essentially used the relative difference between the absorption and reflectance features at the red-NIR region. Their method is specifically applicable for hyperspectral data like AVIRIS, but is limited for satellite multispectral data. We have revised the text to improve the clarity.

L79: "Quantification of ice algae biomass from satellite data based on the chlorophylla feature has received less attention since the chlorophyll related satellite bands designed for land generally have coarse spectral resolutions." This is just one of many reasons why remotely detecting algae over glacier ice is not simple. Other complexities include the complex pigmentation of the algae, the spatial resolution of the remote sensing instruments relative to the typical length scales of individual surface features (including algal blooms) and critically the optics of the underlying ice that vary dramatically over space and time and which are not yet well described. These issues are as important as the spectral resolution and must be acknowledged.

Response: We have revised the text (introduction section) to acknowledge these issues.

L100 – 120: Much more detail is required here. For example, how many actual field samples were used to validate your remote sensing retrievals? What were the biomasses measured at those sites? What were the measurement conditions? On which dates were spectra available at which sites? Were the measurement times conistent and how do they compare to the satellite overpass times? What was the sensor footprint size for the field measurements and how were these upscaled to the satellite pixel scale?

Response: We have revised this section and made clarifications on how we used the field measurements. It should be noted that we utilized those field data in a qualitative way for comparison with the satellite signals, rather than in a quantitative way for direct algal biomass inversion. The Envisat MERIS was operational from March 2002 to April 2012. To our knowledge, there were no algal field data coincident with the satellite data. In our study, we estimated the growth rate (population doubling time) and albedo reduction rate (for each population doubling) using a simple mathematical conversion and empirical relationship established from the Sentinel-3 OLCI data and field data (Wang et al. 2018). We did not directly estimate the algal biomass or abundance from MERIS data since no coincident field data are available. We attempted to apply the Sentinel-3 retrieved empirical relationship to estimate the population doubling time and albedo reduction rate due to algae, and the results match well with the spatial variability from previous field observations.

Figure 1: Please provide details of the field spectrum presented as the dashed line. Where/when was it collected and how does it compare to other field spectra presented in this paper?

Response: We have added more details in the figure caption (below) to describe the field spectrum.

Figure 1. Spectral response functions of (a) MERIS (red), OLCI (blue), and (b) MODIS (black), and WorldView-2 (orange) over the wavelength range of 350-1050 nm. All the MERIS and OLCI bands are within the 350-1050 nm range, where photosynthetic and photoprotective pigments have spectral responses. Four MODIS bands (over land) and eight WorldView-2 bands are within this spectral range, but with much coarser spectral resolutions. In both sub-plots, the dashed line shows hyperspectral ASD field spectrometer data (right vertical axis) collected over algae-abundant ice by Stibal et al. (2017), containing chlorophyll-a signal at the red-NIR wavelengths (red highlighted region). The plotted field spectrum (sample code: Ab.25.06.14.D1) was measured on 25 June 2014 at 67°04.779'N, 49°24.077'W (near the automatic weather station S6 along the K-transect), with an algal abundance measurement of 121664 cells/ml (Stibal et al., 2017).

L209: Chlorophylla is the primary photosynthetic pigment, but not the primary light absorbing pigment. In both the studies you have cited the chlorophylla absorption feature is actually extremely subtle – in fact in Cook et al. (in review) it was only really discernable in the derivative spectra and indistinguishable in the raw reflectance. In Stibal et al. (2017) the spectrum are presented with a very truncated yaxis to make the pigment feature discernable.

Response: We agree with the reviewer on the point that Chlorophyll-a is the primary photosynthetic pigment but not the primary light absorbing pigment. However, this does not mean that Chlorophyll-a cannot be used as the biomarker to detect glacier algae. According to the literature, the purpurogallin pigments are the primary light absorbing pigments for glacier algae. As we mentioned above, the characteristic spectral signatures generated by purpurogallin pigments (that might be used as biomarker for glacier algae detection) are concentrated in the ultraviolet region (278 nm, 304 nm, and 389 nm). To our knowledge, current satellite sensors cannot capture

the spectral signals at these wavelengths, which means that the spectral properties of purpurogallin pigments in the UV region cannot be utilized for glacier algae detection from space. The absorption features of the purpurogallin pigments are quite uniform over the entire visible spectrum, with no characteristic spectral signatures that can be used by satellite sensors to differentiate glacier algae from other dark materials. Although the Chlorophyll-a spectral signature (between 665 nm and 709 nm) generated by glacier algae is not as strong as the algal blooms in aquatic systems, the spectral characteristics of Chlorophyll-a are indeed present on the spectral curve, which are particularly obvious in the derivative spectra (shown in Cook et al. 2020) and the normalized spectra (revised Figure 3c, shown below).

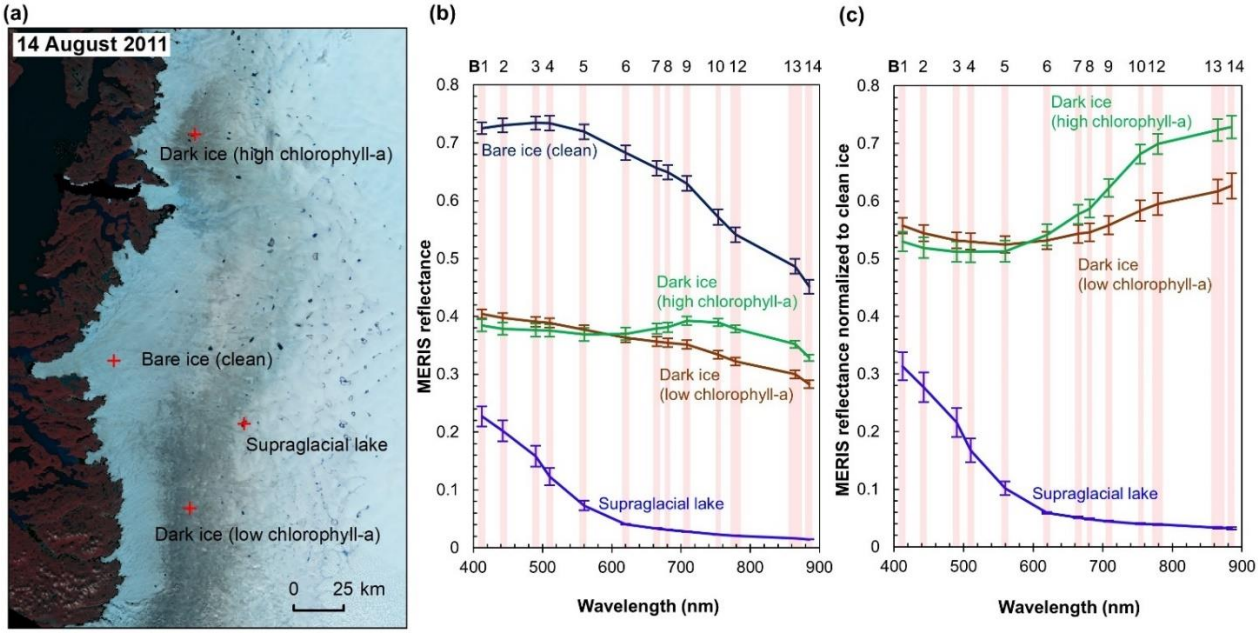

Figure 3 (in the revised manuscript). MERIS spectra of different surface types. (a) MERIS Level-2 image (false colour composite) acquired on 14 August 2011 and locations of the four sample sites. Each site has an area of 1.2 km by 1.2 km, composed of 16 MERIS pixels. (b) MERIS reflectance in 13 spectral bands over the four sites, illustrated by mean and standard deviation values for each band over each site. (c) Normalized reflectance relative to the clean ice spectra.

L211: "pure ice" has lower reflectance at red wavelengths compared to shorter wavelengths.

Response: We have revised the text as 'Pure ice has lower reflectance at 709 nm compared to shorter wavelengths (Hall and Martinec, 1985).'

L216220: This line of reasoning borrows heavily from studies of chlorophylla dominated species in other environments and still requires the rededge to be validated over glacier ice where LAP and meltwater mixing, complex pigmentation and ice optics are potential confounding variables.

Response: We agree that the mixture of dusts, algal pigments, meltwater, and ice optics could complicate the surface spectra. In this revision, we discussed the potential impacts of these variables on the 2BDA index by incorporating the SNICAR simulations. Although the 2BDA index is developed and well-validated for ocean color applications, the rationale for glacier algae detection based on the chlorophyll-a spectral signature at the red-NIR region is very similar to that of algal detection in aquatic environments, particularly for turbid case 2 waters (Blondeau-Patissier

et al., 2014; Matthews, 2011). Similar to the dark ice surface, the case 2 waters are also optically complex, largely affected by the colored dissolved organic matter (CDOM) and suspended sediments. The 2BDA index based on the 665nm and 709nm bands utilizes the reflectance peak near 709 nm, which has been widely tested and validated for the case 2 waters. Using Figure 2 (in the revised manuscript, shown above), we intend to show that the algae-laden ice has the chlorophyll-a spectral signature, which is consistent between the 300-meter MERIS spectra, 2-m WorldView-2 spectra, and the in-situ hyperspectral data. Multiple in situ spectra have been added to Figure 2 illustrating that the chlorophyll-a spectral signature is present across multiple measurement samples and dates.

Figure 2: How did the authors select the field spectrum to plot on this figure? Is this the average of all available? If so please provide error bars and number of observations. Also, 184 cells/mL reported in the legend is a tiny amount of algae, unlikely to explain the albedo reduction observed –is this a typo? What was the mineral dust type and concentration in the same area – could it also explain the rededge? How much of the albedo reduction can be attributed to the algae and how much to melt water/dust? If the absorption is mostly due to chlorophylla as the authors suggest, why is the absorption maximum outside of the chlorophyll absorption range shown in Fig 2c and why does it extend across the visible wavelengths? Why do the field spectra and remotely sensed spectra diverge below ~640 nm?

Response: The field spectrum we selected from Stibal et al. (2017) is used here as an example to show that the chlorophyll-a spectral characteristics (665-709 nm) over algae-abundant ice, and the satellite data (2-meter resolution WorldView-2 and 300-meter MERIS imagery) have similar spectral features at this red-NIR region. The selection criteria include high measured algal abundance (184184 cells/ml) and dark appearance (R620nm<0.45, consistent with the dark ice delineation criteria by Shimada et al., 2016 and Tedstone et al. 2017). To further illustrate the red-NIR spectral signature of glacier algae, we added multiple field spectra from locations where algal cell concentrations were measured at greater than 10,000 cells/ml to Figure 2, showing consistent spectral shapes in this wavelength region. For detailed information about the field data, including dust composition and albedo reduction caused by different variables, please refer to Stibal et al. (2017). As mentioned above, we have added a section analyzing the impact of dusts on 2BDA index in the revised discussion. 'The absorption maximum outside of the chlorophyll absorption range' can be explained by the purpurogallin pigments. The low absorption and uniform absorption in this range actually emphasizes the importance of using the 'red-edge' feature to detect glacier algae. We are not suggesting that 'the absorption is mostly due to chlorophyll-a', instead, we are suggesting to use the chlorophyll-a feature (absorption at 665 nm and reflectance peak at 709 nm) to detect glacier algae. We have revised the text to clarify this point. The divergence between the field spectra and satellite spectra below ~640 nm may be caused by two factors: 1) the uncorrected Rayleigh scattering effect that affects shorter visible wavelengths (particularly the blue band). and 2) spectral mixing with ice. Both can make the reflectance at shorter wavelengths higher, however, the reflectance ratio between 709 nm and 665 nm is less affected by these factors.

Figure 3: A) "Agust"->August;

Response: The typo has been corrected.

B) The authors present spectra for "dark → ice (more chlorophyll)" and "dark ice (less chlorophyll)". However, there does not seem to be any positive 2BDA signal in the latter spectrum at all. Is it actually "dark ice (no chlorophyll)"? If so, there are additional darkening processes occurring on the ice. What processes are darkening the ice in those areas and to what extent do those ice darkening processes also influence the biomass retrievals in areas where there is a positive 2BDA result? What effect does this have on retrieved biomass? What is the detection limit for the 2BDA method?

Response: We have corrected the figure to refer to "high chlorophyll-a" and "low chlorophyll-a". To illustrate the chlorophyll-a signal better, we also plotted the relative surface reflectances (MERIS) for different surface types normalized to the clean ice spectra (Figure 3c in the revised manuscript) since the primary background spectral signal is from ice. For both water and ice, the spectrum shows a decrease in reflectance from 665 nm to 709 nm, which is opposite to the chlorophyll-a spectrum. A 2BDA signal of less than one therefore does not imply that there is no chlorophyll-a present. A smaller rate of decrease could still be produced by low amounts of chlorophyll-a. Using the 2BDA index, we do not intend to classify the ice surface into 'algae' vs. 'no algae'. We use the 2BDA index to show the magnitude of glacier algal blooms varying over space and time. We think it is more appropriate to use 'high chlorophyll-a' and 'low chlorophyll-a' to describe those two sites. We agree with the reviewer that more discussions and investigations are needed to quantify the impacts of other darkening processes on 2BDA index. In this revision, we added the analysis of dust impacts on 2BDA index based on SNICAR simulations in section 4.2 (Sensitivity analysis of 2BDA index to non-algal factors). We found that by combining the 2BDA index with the Impurity Index, we can exclude the possibility of false positives when the 2BDA index is greater than 0.99.

L413: Cook et al. (in review) mention that a rededge signal was present in most of their algal hyperspectral data but they do not mention false positive rates and they opted not to use that method for their spatial upscaling. It would therefore be useful to know the false positive rate in the present study and how it scales to 300m MERIS pixels.

Response: Cook et al. (2020, published online) showed that the 'red-edge' spectral signal due to chlorophyll-a is present in their hyperspectral measurements for algae-covered ice, which further supports the chlorophyll-a signal we observed in the 300-meter MERIS image and the 2-meter WorldView-2 image. In this revision, we revisited the field dataset of Cook et al. (2020). They provided coincident data of cell abundance and hyperspectral measurements for a number of field sites (Table C1 in the revised manuscript). Based on their field datasets, we calculated the 2BDA index for each sample, and Figure C2 (in the revised manuscript, shown above) shows the strong correlation between cell abundance and 2BDA index based on the Cook et al. (2020) field data. To investigate potential scale issues, we added a discussion section (5.1 Sensitivity to subpixel variability) to analyze the sensitivity of 2BDA index to subpixel variability of glacier algae vs. dust by performing spectral linear mixing experiments based on the Cook et al. (2020) field spectral data and the SNICAR-simulated dust spectral data. As we discussed above, the MERIS 2BDA index is capable of capturing the glacier algae at the 300-meter resolution scale. This is further supported by the comparison between the WorldView-2 image (2-meter resolution) and

the MERIS image (Figure 2 in the revised manuscript, shown above). Although we can observe spatial heterogeneity within one MERIS pixel, the dark materials are widespread over the entire area. This is also consistent with the UAV mapping results by Ryan et al. (2018), showing that the areal percentage of the distributed impurities is up to 90% within individual MODIS pixels (500-meter resolution) over the dark zone in southwest Greenland. Nevertheless, it is important to investigate the pixel mixture problems more rigorously in the future and the limit of algae distribution within each pixel that can cause detectable chlorophyll-a signal. Based on our discussion on dust impacts and the spatial scale of MERIS imagery, we think that using MERIS data is more likely to cause false negatives instead of false positives given the sensor detection limit to weaker chlorophyll-a signals.

L416: It is not clear to me from the manuscript precisely how you have inferred algal cell abundance. Please provide further methodological details.

Response: The methods for computing algal population doubling were described in Section 4.3 (Lines 363-376 in the original manuscript). However, this section may have been somewhat unclear. In this revision, we have clarified how the population doubling time was estimated based on the fitted coefficients between 2BDA and time (section 4.5 in the revised manuscript). We did not directly infer the algal cell abundance using the 2BDA index, instead, we used the empirical relationship established based on the Sentinel-3 OLCI band ratio and previous field measurements (Wang et al., 2018) and mathematical conversions.

L450460: Another explanation for this is that the overall ice albedo is lower, there may be smoother ice and more water at the surface, and rather than there being less algae, the rededge signal is simply erased by an overall dampening of the spectrum across all wavelengths (i.e. putting dark impurities on dark ice has a less detectable effect that putting the same impurities on otherwise bright ice). Can the authors demonstrate that this is not the case?

Response: As we have discussed above, the 2BDA index is sensitive to the absorption and reflectance peaks of chlorophyll-a, which is not a feature of other surface types. As the 2BDA index is a ratio of two different wavelength bands, a uniform reduction in "background" albedo should have a small effect. A change in the shape of the "background" spectrum (the relative reflectance at 709 nm relative to 665 nm would be required to have a large impact on 2BDA. Observed spectra shown in Figure 2 (in the revised manuscript, shown above) suggest that differences in the average magnitude of the reflectance spectrum do not appear have a strong impact on the shape of the reflectance spectra, and therefore likely do not strongly impact the 2BDA index either.

References:

Cook et al. (in review) Glacier algae accelerate melt rates on the south western Greenland Ice Sheet, The Cryopshere, https://www.thecryospherediscuss.net/tc201958/#discussion

Painter, T. H., Duval, B., and Thomas, W. H.: Detection and quantification of snow algae with an airborne imaging spectrometer, Appl. Environ. Microbiol., 67, 5267–5272, https://doi.org/10.1128/AEM.67.11.52675272.2001, 2001.

Tedesco, M., Foreman, C., Anton, J., Steiner, N., Schwartzman, T.: Comparative analysis of morphological, mineralogical and spectral properties of cryoconite in Jakobshavn Isbr?, Greenland, and Canada Glacier, Antarctica. Annals of Glaciology, 54(63), 147157. doi:10.3189/2013AoG63A417, 2013.

Tedstone, A. J., Cook, J. M., Williamson, C. J., Hofer, S., McCutcheon, J., IrvineFynn, T., Gribbin, T., and Tranter, M.: Algal growth and weathering crust structure drive variability in Greenland Ice Sheet ice albedo, The Cryosphere Discuss., https://doi.org/10.5194/tc2019131, in review, 2019.

Anonymous Referee #2

Overview

This manuscript uses data from the MERIS satellite sensor to seek to quantify glacier algae bloom dynamics over the south west Greenland ablation zone. They justify their use of this sensor for detecting algal blooms by reference to their previous work using the very similar Sentinel-3 OLCI on the same topic (Wang et al, 2018), by selected references to some field observations, and by wider reference to remote sensing of ocean-borne algal blooms.

Response: We greatly appreciate the reviewer's careful reading and useful suggestions, which have improved our manuscript. In this revision, we believe that we have sufficiently addressed the concerns raised by the reviewer. Please see our responses below.

Major comments

The manuscript tests several remote sensing ratio indices and shows that, to some extent, the 2BDA approach retrieves a different signal to that obtained by the 'bulk' Impurity Index or simple red band threshold approaches. This is a useful exercise in seeking to understand what signals can be retrieved from the MERIS/OLCI sensors.

As the manuscript is presented currently, I have some major concerns which prevent me from recommending publication in The Cryosphere.

There are known problems with seeking to apply band ratios/indices designed for chlorophyll-a retrieval from water bodies but which this manuscript does not engage with. I appreciate that the main studies which highlight these problems, by Cook et al. (TCD) and Tedstone et al. (TCD), are currently undergoing review and so were unlikely to have been available at the time when this study was started. But nevertheless, there is a lack of discussion of the wider literature on this issue; instead, Wang et al (2018) is cited as proof that chlorophyll-a-focused band ratios are appropriate for detecting glacier algae blooms, but I find that discussion of these problems is lacking there too, and so their 2018 paper is not an especially strong foundation on which to base the present study.

Response: In this revision, we added the section 3.3 (Sensitivity analysis based on radiative transfer modelling) and section 4.2 (Sensitivity analysis of 2BDA index to non-algal factors) to analyze and discuss the sensitivity of the 2BDA index to dust presence using SNICAR simulations with varying dust sizes and concentrations (more details are in the response to reviewer#1). Our results indicate that the 2BDA index is much less sensitive to dust presence than the impurity index,

and in our context (with impurity index mostly less than 1.0), the high 2BDA index (greater than 0.99) is unlikely caused by dust. Given that the 2BDA index is specifically designed for chlorophyll-a retrieval and the narrow bandwidths of MERIS, the 2BDA index (especially at values greater than 0.99) is uniquely biological due to glacier algae.

Since discussion papers are not referenceable, we did not cite any discussion paper in this revision. The papers by Cook et al. (2020) and Tedstone et al. (2020) were published very recently, and have been added to our references. Cook et al. (2020) discussed the 'red-edge' feature of glacier algae caused by chlorophyll-a, and we have revisited their field data in this revision. In addition, we cited the paper by Williamson et al. (2020) who also noted the chlorophyll-a absorption feature at ~675 nm besides the purpurogallin absorption.

As I understand it, the core of this problem is two-fold: (1) the optics of bare ice are insufficiently well understood to be able to guarantee that the reduction in reflectance around 667 nm compared to 710 nm is uniquely biological; and (2) other light absorbing impurities may interfere or present the same signal. Thus, based on published field evidence, there is little evidence that the band ratio approach is uniquely biological. Cook et al. (TCD) and Tedstone et al. (TCD) have more information on this and note that phenolic compounds for in the dominant glacier algae species can obscure potentially diagnostic spectral features. This being the case, NDCI etc may simply be measuring some combination of slightly different surface characteristics to the Impurity Index approach, rather than yielding information specifically on glacier algae growth. Thus, regarding inter-annual mapping of 'dark ice' vs glacier algae, there may be little advance on Shimada et al. (2016) or Tedstone et al. (2017), both of whom considered inter-annual variability in 'dark ice' dynamics over the timescales addressed here.

Response: We agree that the optics of bare ice and light absorbing impurities can complicate the spectral signal, but we respectfully disagree that "based on published field evidence, there is little evidence that the band ratio approach is uniquely biological". Current field studies (Stibal et al., 2017; Cook et al., 2020) presented the field hyperspectral data of dark ice with abundant glacier algae, and their data show the chlorophyll-a signature at the red-NIR region. However, they did not apply the band ratio approach, which doesn't necessarily mean that 'there is little evidence that the band ratio approach is uniquely biological'. As we discuss below, the ice/snow optics have little impact on the 2BDA index, and based on radiative transfer modelling experiments (response to reviewer #1, and revised section 4.2), the upper limit of the dust impact on the 2BDA index is around 0.99. In contrast, the impurity index is more sensitive to dust presence. In the revised text, we have added more discussion and figures to show the difference between impurity index and 2BDA index. We also respectfully disagree with the statement 'Thus, regarding inter-annual mapping of 'dark ice' vs glacier algae, there may be little advance on Shimada et al. (2016) or Tedstone et al. (2017), both of whom considered inter-annual variability in 'dark ice' dynamics over the timescales addressed here', since according to our results (Figure 5 in the manuscript), there are differences between 2BDA index, impurity index, and the R620nm reflectance that Shimada et al. (2016) and Tedstone et al. (2017) used for dark ice delineation. We would like to argue that their method doesn't account for any biological signal specific to glacier algae, and is more likely to be influenced by meltwater presence, ice optics and other impurities.

On justification of the 2BDA, Wang et al. (2018) point to Painter et al. (2001) as evidence that glacier algae can detected using chlorophyll-a indices. However, Painter et al refers to the specific case of snow algae growing on snow surfaces, which is not relevant here as this study engages only with bare ice surfaces. Thus, retrievals in this study can in fact be based only on paired cell counts and field spectra acquired by Stibal et al. (2017), a study which also indicates that chlorophyll-a-based approaches could be useful for remote sensing. However, the spectra that Stibal et al (2017, Figure 3) present refers only to high algal abundance ice, over centimetres patch scales, which is not representative of OLCI or MERIS 300 m data. Some consideration of the scale mismatch is therefore required.

Response: We respectfully disagree with the reviewer on the point that the specific case of snow algae growing on snow surfaces is not relevant to the discussion of glacier algae growing on bare ice surfaces. There are differences between snow and ice spectra, but both of them are characterized by decreased reflectance at 709 nm as compared with 665 nm. The spectral signature of ice and snow themselves exhibit a slope opposite to that of the chlorophyll-a spectra at this region. Although snow algae and glacier algae are distinct species, they both generate chlorophyll-a for photosynthetic activity and chlorophyll-a is their major photosynthetic pigment. The colours of snow algae and glacier algae are different mainly because snow algae generate secondary carotenoids which have a reflectance peak in red band. However, according to Painter et al. (2001), this carotenoid feature does not block the chlorophyll-a absorption signal around 680 nm. Therefore, Painter et al. (2001) were able to detect snow algae using the chlorophyll-a signature between 630 nm and 700 nm using the absorption at 680 nm and the reflectance features at 630 nm and 700 nm. Glacier algae have brownish-grey colour because they generate purpurogallin pigments, and at the same time, they also generate chlorophyll-a for photosynthesis (similar to snow algae). However, as we noted in response to the first reviewer, compared with the purpurogallin pigment, Chlorophyll-a is more appropriate for mapping glacier algae for the following reasons:

1) Chlorophyll-a is the primary photosynthetic pigment of glacier algae (Williamson et al., 2018). The ocean color satellite sensors like Envisat MERIS and Sentinel-3 OLCI are designed to capture the Chlorophyll-a signal from highly-absorptive and optically complex water bodies, which means that the ocean color sensors are highly sensitive to chlorophyll-a presence, making them very useful tools for glacier algae detection based on the biological signatures.

2) According to the studies by Remias et al. (2012) and Williamson et al. (2018), the spectral signatures (absorption peaks) of the purpurogallin pigment are concentrated in the UV region (278 nm, 304 nm, and 389 nm, Remias et al.,2012). To our knowledge, no satellite sensor can detect these spectral signatures. Although the purpurogallin pigment is very likely to account for the brownish-grey colour of glacier algae, its absorption over the entire visible spectrum is quite uniform, making it difficult to differentiate from other dark impurities. In contrast, chlorophyll-a can generate very strong spectral signatures in the red and NIR region, which is supported by field hyperspectral measurements for both snow algae and glacier algae. (e.g. Ganey et al., 2017; Painter et al., 2001; Stibal et al., 2017; Cook et al., 2020).

As we clarified in the text, we used the field measurements by Stibal et al. (2017) for qualitative evidence to show that the MERIS spectra, WorldView-2 spectra, and field hyperspectral data are consistent in terms of the spectral shape over algae-abundant ice. In this revision, we improved Figure 2d (in the revised manuscript) to include more field spectra data from Stibal et al. (2017) to illustrate that the chlorophyll-a spectral signature at the red-NIR region is present across multiple measurement samples and dates. Additionally, the recently published paper by Cook et al. (2020) also discussed the 'red-edge' feature present in their field data, which is attributed to the chlorophyll-a generated by glacier algae. Examining the field measurements and hyperspectral data of Cook et al. (2020), we find a strong sensitivity of the 2BDA index derived from field hyperspectral data with coincident measured cell abundance. We have added Table C1 and Figure C2 showing the relationship between cell abundance and the 2BDA index.

In regard to the scale issues, we added section 5.1 (Sensitivity to subpixel variability) to discuss the effects of spatial scale on the 2BDA index. Based on our SNICAR experiments, and analysis of the 2BDA and impurity indices, the 2BDA index is less sensitive to the presence of dust, which means that the high 2BDA index is uniquely biological. Given the sensitivity of MERIS to the presence of chlorophyll-a, the 2BDA index can effectively capture the chlorophyll-a signal generated by glacier algae. To examine the potential impact of spatial heterogeneity on the MERIS 2BDA index, we performed spectral linear mixing experiments using the field hyperspectral measurements of Cook et al. (2020) for glacier algae and bare ice and the SNICAR-simulated spectra for dust. We obtained the mixed spectra (Figure C3 in revised the manuscript, shown below) by specifying the different areal percentage of algae/dust vs. bare ice, and calculated the corresponding 2BDA index for the mixed spectra. It is shown that the 2BDA index dramatically increases with the areal percentage of glacier algae, being consistent with the assumption that the 2BDA index is positively correlated with algal abundance. In contrast, the 2BDA index has much less sensitivity to dust. The high-resolution UAV mapping by Ryan et al. (2018) suggests that the areal percentage of the distributed impurities is up to 65%~95% within individual MODIS pixels (500-meter resolution) over the dark zone in southwest Greenland. Our linear mixing experiments (Figure C3b, shown below) suggest that the MERIS 2BDA index can capture the glacier algae variability within the dark zone. In addition, our comparison between the MERIS (300-meter resolution) spectra, WorldView-2 (2-meter resolution) spectra, and field hyperspectral data (Figure 2 in the manuscript, shown below) shows that the chlorophyll-a signature at the red-NIR region is quite consistent between different source measurements at different spatial scales. Therefore, MERIS data can effectively capture the glacier algae signal over southwest Greenland; nevertheless, we agree with the reviewer that more investigations on the scale and spectral mixing issues are needed in future studies. Besides, as we noted in our response to reviewer #1, we excluded the possibility of false positives caused by dusts when the 2BDA index is greater than 0.99.

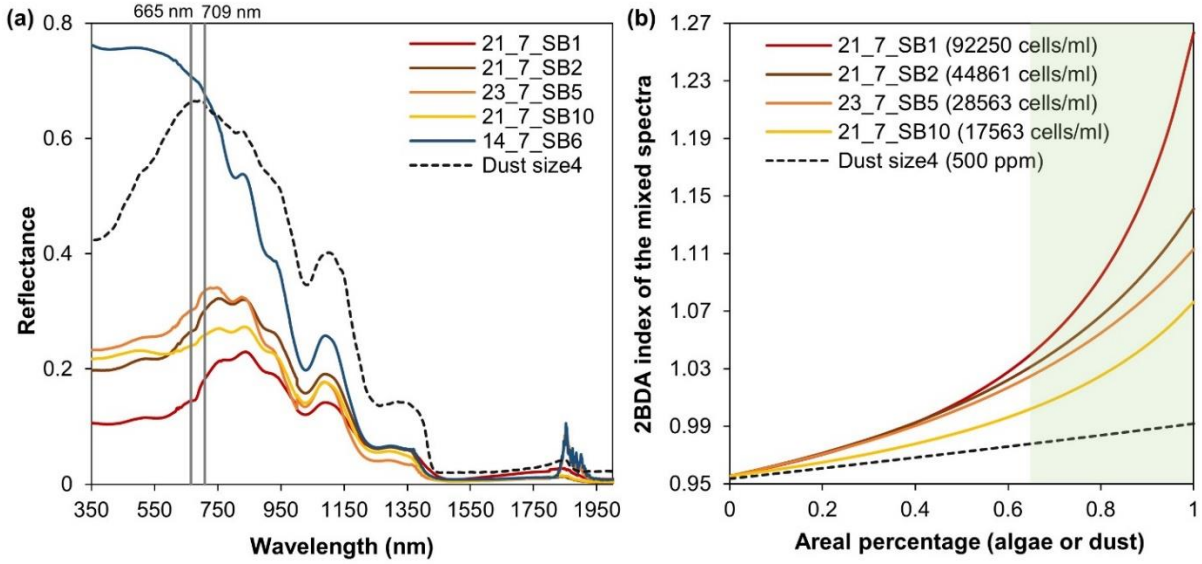

Figure C3 (in the revised manuscript). Spectral linear mixing experiments. (a) Field hyperspectral measurements of four algae-abundant samples (21_7_SB1, 21_7_SB2, 23_7_SB5, and 21_7_SB10) and one bare ice sample (zero algal abundance, 14_7_SB6) from Cook et al. (2020), and the SNICAR-simulated spectra for the dust scenario (size 4 at concentration of 500 ppm). (b) 2BDA index calculated from the linearly mixed spectra with varying areal percentage at subpixel scale for algae (different algal abundances) and dust scenarios.

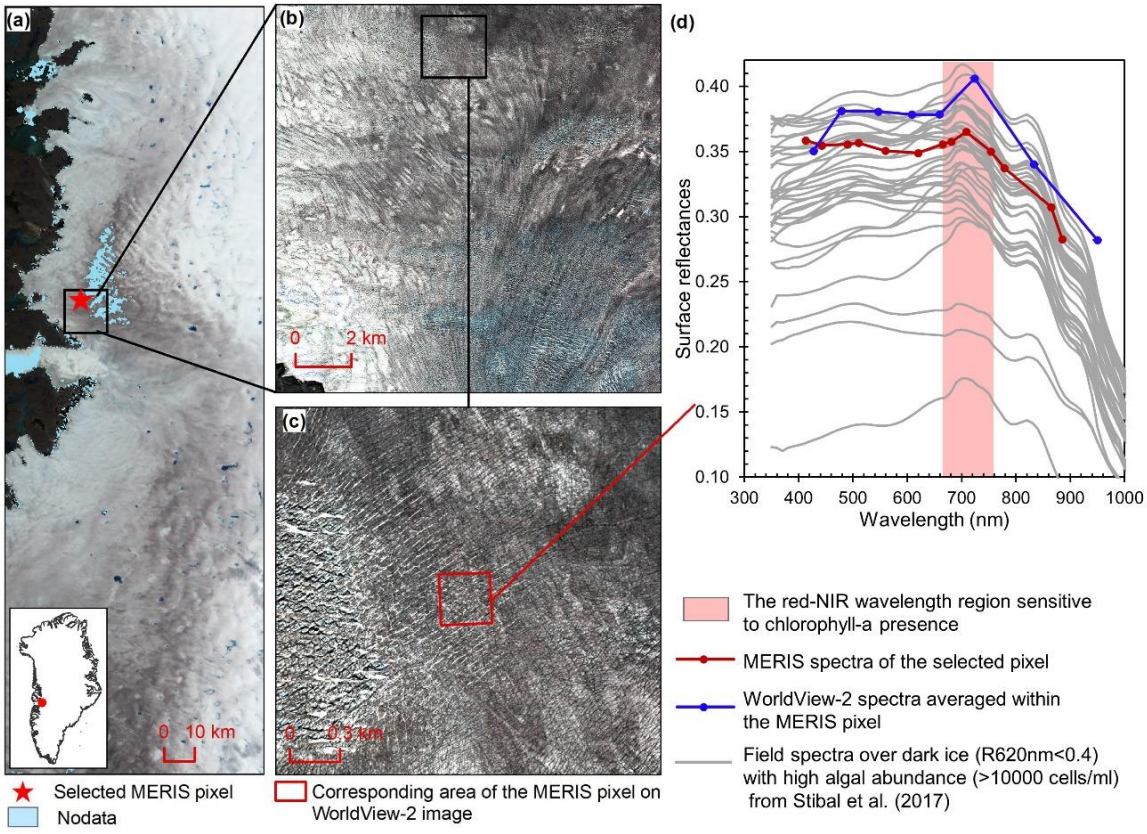

Figure 2 (in the revised manuscript). Comparison between MERIS, WorldView-2, and field spectra over algae-abundant dark ice. (a) MERIS Level-2 image (true colour composite) acquired on 5 July 2010. Pixels with missing data are shown in light blue. (b) WorldView-2 surface reflectance image acquired on 9 July 2010 over the square area in (a). (c) Zoomed-in

WorldView-2 image, with the area (red square) corresponding to the selected MERIS pixel in (a). (d) Reflectance spectra for MERIS and WorldView-2 (2010), and field hyperspectral measurements collected over the algae-abundant dark ice at S6 by Stibal et al. (2017) in 2014.

Possibly a more minor concern: the cell counts used as field validation in this manuscript are very high, at 105 cells ml (Figure 2d), but I'm not sure that we would expect to see such high counts over these larger spatial scales (e.g. Williamson et al.,2018, FEMS). Furthermore, the field spectra seem to have quite high reflectance for the quoted cell counts compared to other field spectra in the literature, e.g. Figure A1 in Tedstone et al. (2017, TC). The field spectra shown here seems to be that in Stibal et al. (2017, GRL, Figure 3), but a cell count is not quoted there and so I raise this question here in case there has been an error in transforming Stibal et al's data for this study.

Response: In this revision, we clarified in the text on how we used the field data by Stibal et al. (2017). The field hyperspectral measurements collected by Stibal et al. (2017) were used for qualitative purposes for comparison with the MERIS spectra over dark ice to validate the chlorophyll-a spectral signature at the red-NIR region, specifically the bands of 709 nm and 665 nm used for 2BDA index calculation. We have revised Figure 2d (shown above) by adding multiple in situ spectra collected over the algae-abundant dark ice (R620nm<0.4, and algal concentration >=10000 cells/ml) to illustrate that the chlorophyll-a spectral signature is present across multiple measurement samples and dates. We have double checked the original data published by Stibal et al. (2017) and ensured the correctness of our plotted spectra.

The study also presents data that undermines its application of a Chlorophyll-a based band ratio approach. Figure 3b shows some averaged MERIS surface reflectance curves. Dark Site (Less Chlorophyll) has higher reflectance at 665 than 709 nm and so with 2BDA this site would presumably diagnose as 'clean ice' by comparison to the Clean Ice spectrum plotted above it. I do not see any comment upon this issue elsewhere in the text.

Response: We respectfully disagree with the reviewer that our presented data in Figure 3 undermines its application of a Chlorophyll-a based band ratio approach. As we responded to reviewer#1, we have corrected the figure to refer to "high chlorophyll-a" and "low chlorophyll-a". For both water and ice, the spectrum shows a decrease in reflectance from 665 nm to 709 nm, which is opposite that of the chlorophyll-a spectrum. A 2BDA signal of less than one therefore does not imply that there is no chlorophyll-a present. A smaller rate of decrease could still be produced by low amounts of chlorophyll-a. Using the 2BDA index, we do not intend to classify the ice surface into 'algae' vs. 'no algae'. We use the 2BDA index to show the magnitude of glacier algal blooms varying over space and time. We think it is more appropriate to use 'high chlorophyll-a' and 'low chlorophyll-a' to describe those two sites. To illustrate the chlorophyll-a signal better, we have revised the text to discuss this issue and added a subplot (Figure 3c in the manuscript, shown below) to show the normalized MERIS surface reflectances relative to the clean ice spectrum.

We agree with the reviewer that more discussions and investigations are needed to quantify the impacts of other darkening processes on 2BDA index. In this revision, we added the analysis of dust impacts on 2BDA index based on SNICAR simulations in section 3.3 (Sensitivity analysis

based on radiative transfer modelling) and section 4.2 (Sensitivity analysis of 2BDA index to non-algal factors). We found that by combining the 2BDA index with the Impurity Index, we can exclude the possibility of false positives when the 2BDA index is greater than 0.99.

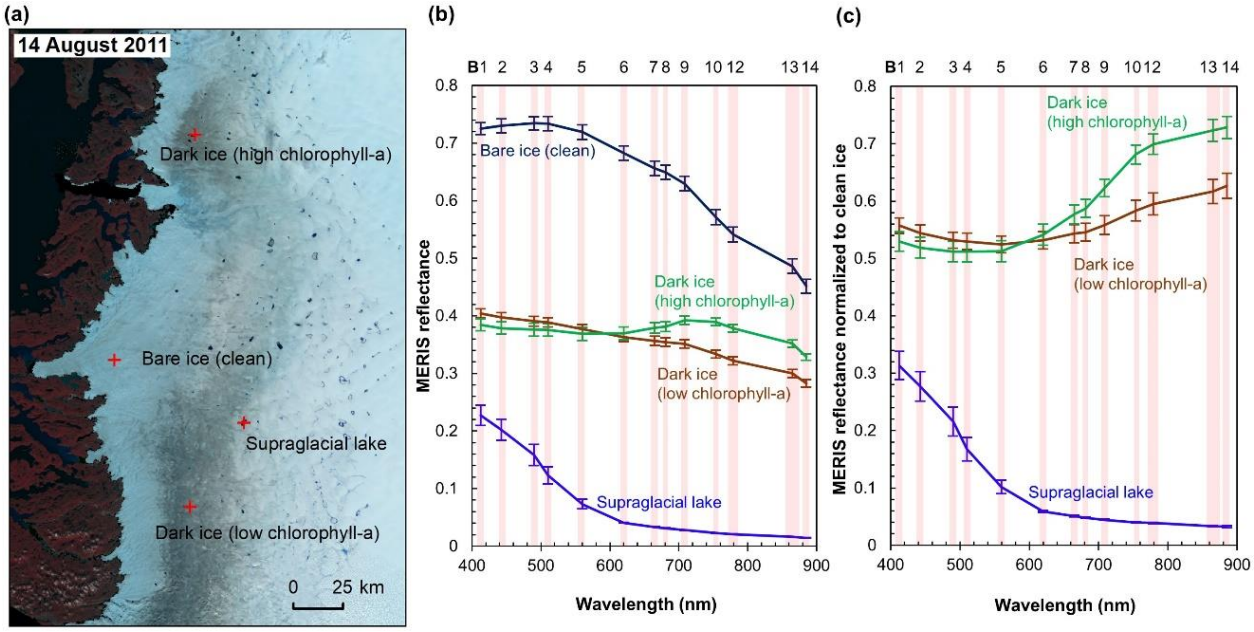

Figure 3 (in the revised manuscript). MERIS spectra of different surface types. (a) MERIS Level-2 image (false colour composite) acquired on 14 August 2011 and locations of the four sample sites. Each site has an area of 1.2 km by 1.2 km, composed of 16 MERIS pixels. (b) MERIS reflectance in 13 spectral bands over the four sites, illustrated by mean and standard deviation values for each band over each site. (c) Normalized reflectance relative to the clean ice spectra.

I'm very confused about how the algal population doubling times were calculated. This is a critical part of the manuscript as it underpins the assertion that there is a 0.02-0.04 reduction rate in albedo for each algal population doubling.

Response: The methods for computing algal population doubling time were described in Section 4.3 (Lines 363-376 in the original manuscript). However, this section may have been somewhat unclear. In this revision, we have clarified how the population doubling time was estimated based on the fitted coefficients between 2BDA and time (section 4.5 in the revised manuscript).

Overall, I would urge nuanced engagement with the question of how confident can we be that the differences between 2BDA, Impurity Index and Dark Ice metrics are due solely to algae and not to other processes that might affect this band ratio? I suggest that this needs much clearer explanation in the methods about how Stibal et al's field data were used in this manuscript, and some nuanced discussion of the uncertainties surrounding Chlorophyll-a indices on ice surfaces. If these issues are addressed then the revised manuscript may be suitable for publication.

Response: As we mentioned above, we have analyzed the sensitivity of 2BDA index and impurity index to dust presence by using the SNICAR simulations with variant dust sizes and concentrations (Section 4.2, Figure 4 in the manuscript). We have excluded the possibility of false positives for glacier algae detection caused by dusts using the 2BDA index (particularly greater than 0.99).

We have clarified in the text on how we used the field data from Stibal et al. (2017). The match between the MERIS spectra, WorldView-2 spectra, and field spectra (Figure 2 in the manuscript, shown above) indicates the chlorophyll-a signal can be effectively captured by MERIS.

Minor comments

I agree with the short comment by Daniel Remias that this manuscript should use the terminology 'glacier algae' in preference to 'ice algae'.

Response: As suggested, we have changed 'ice algae' to 'glacier algae' through the text.

The introduction includes wide-ranging references to both glacier algae and snow algae. Detailed discussion of the snow algae literature is not relevant here as this study focuses only on bare ice surfaces, so the introduction would benefit from being focused solely on glacier algae.

Response: We respectfully disagree with the reviewer on this point. We think it is important to discuss the differences between snow algae and glacier algae, as the differences may not be clear to a broader audience, as well as the similarities and techniques that can help inform our current study.

P3 L71: define what is meant by 'dirt'.

Response: We used 'dirt' according to the studies by Painter et al. (2001) and Takeuchi et al. (2006). However, since glacier algae do not generate secondary carotenoids like snow algae, the spectral characteristics of carotenoids are not relevant to our study. To avoid ambiguity, we have removed the statement 'the spectral characteristics of dirt may resemble those of carotenoids' from the manuscript.

P8 L209. Cook et al. (2019, Cryosphere Discussions) are cited for the first time here. If it is being cited then it should be introduced earlier during the lit. review section of the Introduction. Alternatively, if taking the view that Cook et al is under discussion and that it isn't 'referenceable', then all references to it should be removed.

Response: This paper is currently published online (Cook et al., 2020). We have included it in the introduction and updated the reference.

P9 L226: please quantify how the 'best' means of quantifying ice algae was obtained. This is not clear, either here or in the subsequent text.

Response: We have rewritten the paragraph to improve the clarity.

P9 L229: Dumont et al. (2014) focussed on impurity loading upon snow surfaces. Please comment further on the suitability of the Impurity Index for ice surfaces.

Response: The Impurity Index (Dumont et al., 2014) is the ratio between the natural logarithms of the spectral albedos at 545–565 nm (visible green band) and at 841–876 nm (NIR band). This index was built upon the hypothesis that the surface reflectances at visible wavelengths are more sensitive to impurity content than at the NIR wavelengths, and Dumont et al. (2014) found that the

Impurity Index is almost insensitive to grain size based on their field measurements and radiative transfer modelling results. Given the similar spectral shapes of snow and ice and the general assumption in radiative transfer modelling that ice has larger grain size than snow, we think it is suitable to apply the Impurity Index to the ice surface. Besides, Dumont et al. (2014) quantified the impurity content using this index over the Greenland Ice Sheet for the May–July period from 2003 to 2013, including the bare ice zone in southwest Greenland. We have added more details in the text to describe the impurity index.

Results, section 4.1: I find this section very difficult to read. It would benefit from re-writing and introduction of paragraph breaks.

Response: This section has been rewritten as suggested and additional paragraph breaks have been added for clarity.

Fig. 3a: typo, August spelt 'Agust' Fig. 3b: provide MERIS band numbers at top of plot to aid cross-comparison back to Table 1. The colours of the two dark ice spectra lines are too similar to be able to tell them apart in print.

Response: We have revised the figure as suggested. We also added a subplot to show the normalized MERIS reflectances to the clean ice spectrum, showing the spectral signature of chlorophyll-a better.

P11 L275: full stop missing after '1400 m'.

Response: We have revised the text accordingly.

P12 L278-290: I do not follow the arguments being made in this section. Further, I disagree with the statement made in reference to Fig. 4, that 'Similar to the Impurity Index, the dark ice area is not only limited to the algae-abundant areas'. My examination of Fig 4 suggests that this is cherry-picking as conversely I saw plenty of evidence of a very good match between the two indices. As the authors central premise is that the 2BDA is 'uniquely biological' and so therefore yielding details not provided by the Impurity index or Dark ice index I propose that quantification beyond eye-balling the associated plots is required – ideally some statistical approach.

Response: In this revision, we changed the color scheme for each variable (2BDA, Impurity Index, R620nm, and MODIS bare ice albedo). The revised figure shows better the differences between those variables. Figure 5a (in the revised manuscript, shown below) clearly shows that along the central dark zone, 2BDA is highest at the elevation level of 1200-1400m, and comparatively the Impurity index is highest at the elevation level of 1000-1200m. The R620nm used for dark ice delineation in previous studies (Shimada et al. 2016; Tedstone et al. 2017) has the lowest value at the elevation level of 1000-1200m, more consistent with the Impurity Index. To show the spatial variation in more detail, we have also added a supplementary figure (Figure A1 in the revised manuscript, shown below) to illustrate the variations of different indices with elevation (at a 20-meter interval), which also shows the differences clearly. We have rewritten the text accordingly.

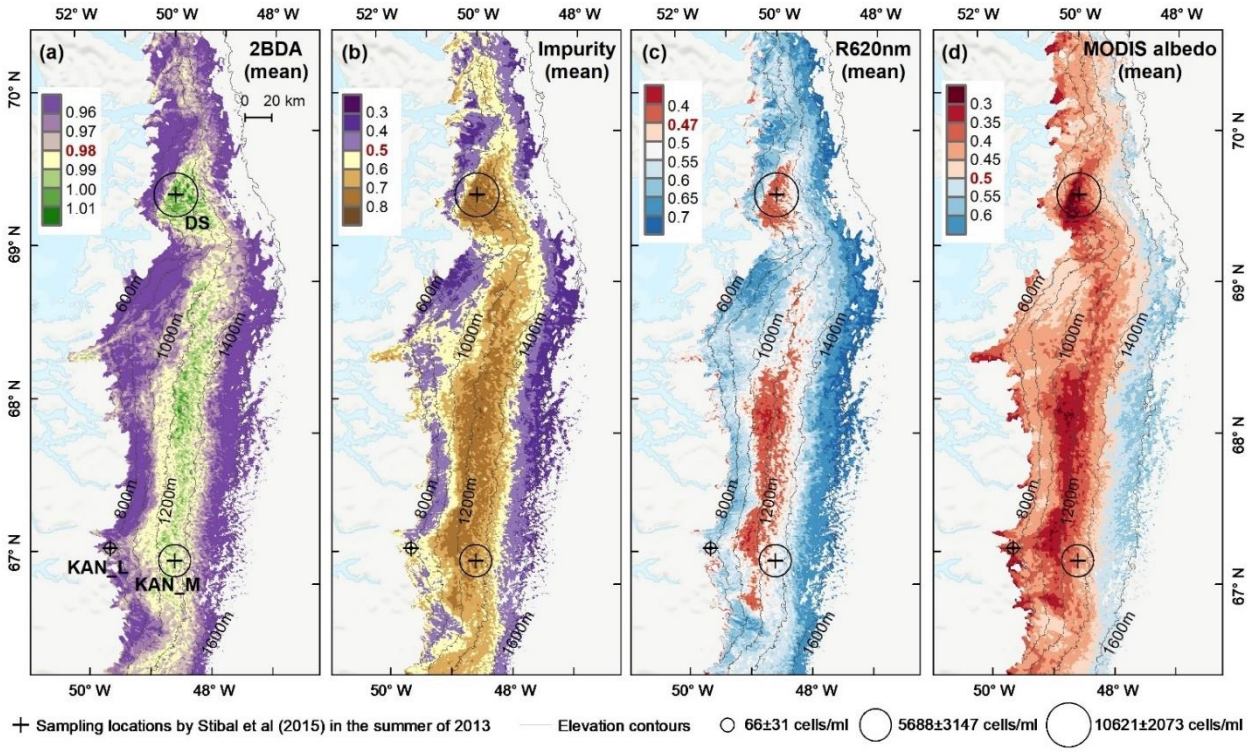

Figure 5 (in the revised manuscript). Spatial patterns of the mean 2BDA index (a), impurity index (b), reflectance at 620 nm (c), and MODIS broadband albedo (d) over the bare ice zone during July and August from 2004 to 2011. The elevation contours illustrate the spatial variations of each variable with altitude. The cross labels show the spatial locations of the field sites DS, KAN_L, and KAN_M and magnitude of glacier algal abundance (circle labels) measured by Stibal et al. (2015) in 2013.

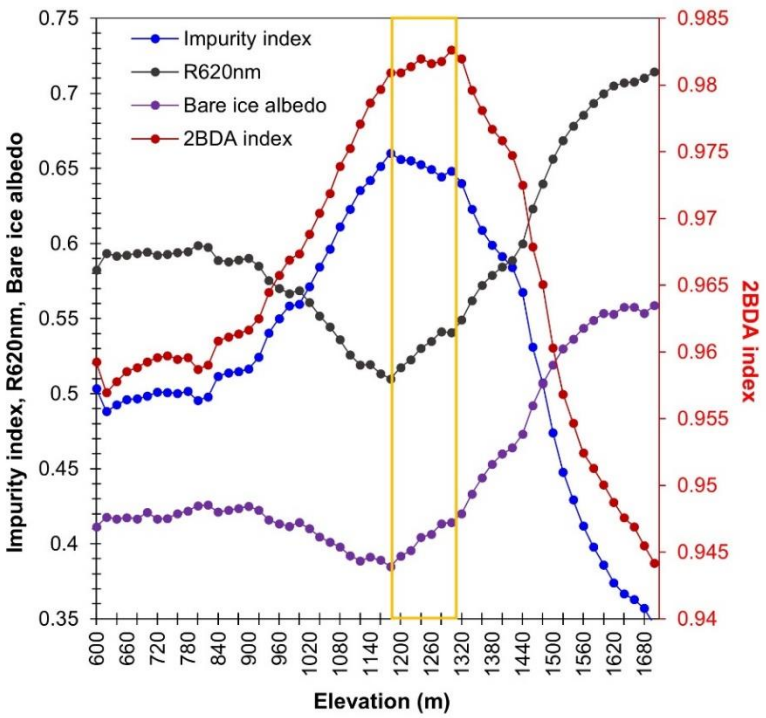

Figure A1 (in the revised manuscript). Spatial variations of the average 2BDA index, impurity index, 620 nm reflectance, and MODIS albedo over bare ice at different elevations within the study area (20-meter elevation interval). For surface elevation, we used the 30-meter resolution MEaSUREs Greenland Ice Mapping Project (GIMP) Digital Elevation Model (Howat et al., 2014; 2015).

P12 L288-290: this study has no field data for the wavy patterns caused by ancient ice outcropping and does not provide any zoomed satellite imagery which shows them, so the reference to Wientjes and Oerlemans (2010) strikes me as somewhat speculative.

Response: The study by Wientjes and Oerlemans (2010) indeed has no field data for the wavy patterns caused by ancient ice outcropping, but they do show the zoomed in ASTER satellite image (15-meter resolution) in their Figure 8 to illustrate the observed wavy patterns which are typical for outcropping tilted layers of ice. In our context, the 2BDA index indicates that along the central dark zone, there were more glacier algae distributed at the elevation level of 1200-1400m as compared with the 1000-1200m elevation level. However, the darkening index (R620nm, e.g. Shimada et al., 2016 and Tedstone et al., 2017) and the Impurity Index (Dumont et al., 2014) indicate that the 1000-1200m elevation zone also contains high impurity content, suggesting that other darkening processes potentially played an important role in this area. Therefore, we discussed the possibility of ancient ice outcropping in this area based on Wientjes and Oerlemans (2010). In this revision, we provided additional evidence (Figure A2 in the revised manuscript, shown below) to support this observation, using 2-meter resolution WorldView-2 images to show the differences between those two elevation zones. The WorldView-2 image (Figure A2b) clearly shows the wavy patterns mentioned by Wientjes and Oerlemans (2010) at 1000-1200m, and very different textures are visible at 1200-1400m (Figure A2c) where high algae content was identified using the 2BDA index.

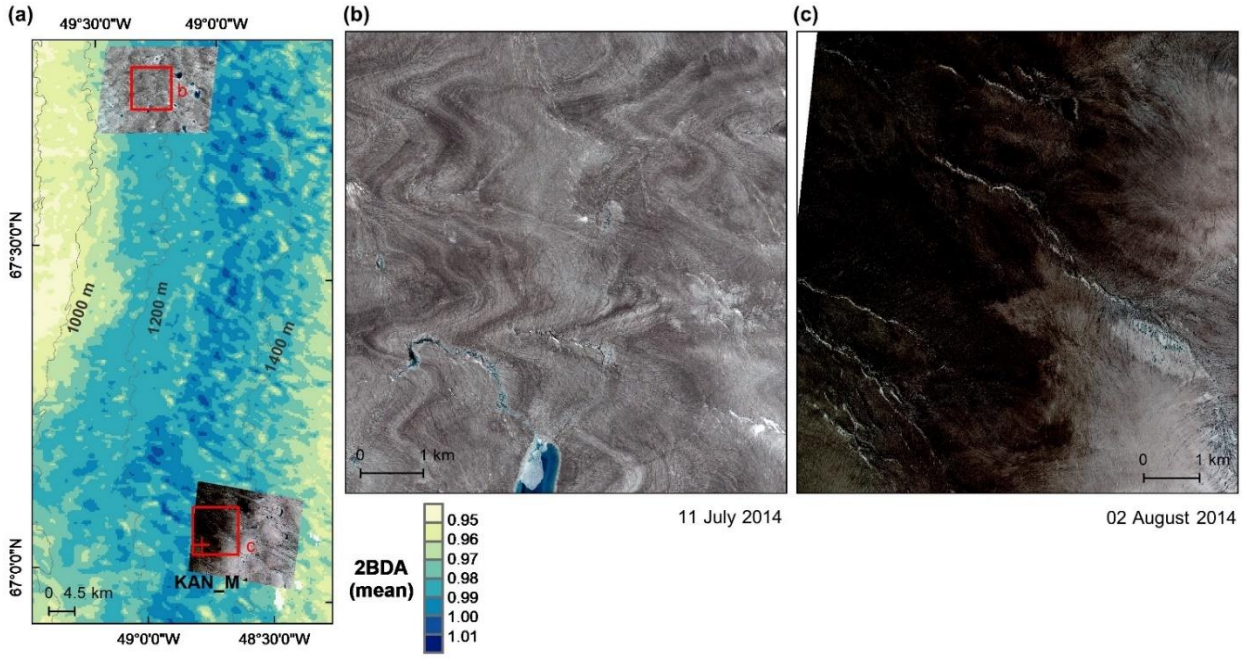

Figure A2 (in the revised manuscript). Average 2BDA index (2004-2011) for a subset of our study area (a) and comparison between WorldView-2 imagery over a dark ice site with low 2BDA index at 1000-1200m elevation (b) and a dark ice site with high 2BDA index at 1200-1400m elevation (c). The WorldView-2 image in (b)

illustrates the 'wavy' pattern that Wientjes and Oerlemans (2010) suggested was caused by ancient ice outcropping.

P13 L302: 'exhibits different spatiotemporal variations'. Are these differences statistically significant? They are almost impossible to identify by eye, apart from in one or two years of record 2BDI. Consider doing some elevational binning to support your case.

Response: In this revision, we grouped the annual 2BDA and Impurity Index time series into different elevation bins (600-800m, 800-1000m, 1000-1200m, and 1200-1400m), to better illustrate the differences, and calculated the average values for each elevation bin. We also added a supplementary figure (Figure A3, shown below) in the appendix to show the annual time series of 2BDA and Impurity indices for different elevation levels, and revised the text accordingly.

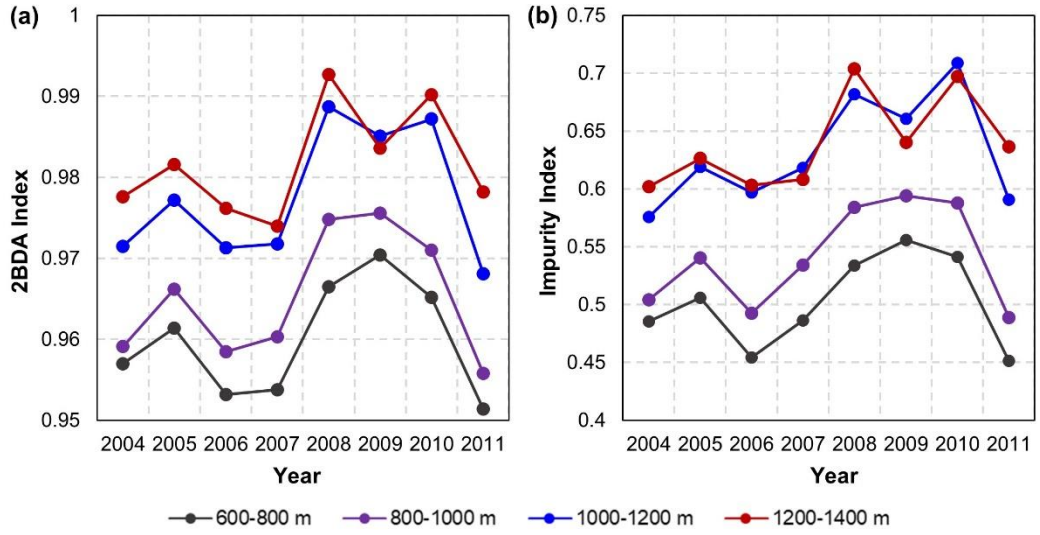

Figure A3 (in the revised manuscript). Interannual variability of the 2BDA index (a) and impurity index (b) at the elevation levels of 600-800m, 800-1000m, 1000-1200m, and 1200-1400m within the study area.

Fig. 5: add 2BDA and Impurity index labels to each row of subplots.

Response: We have revised the figure as suggested.

Fig. 6: What p-value where these trends culled at, if at all? I also note that the R2 values in the referenced appendix plot are very small.

Response: We added the p-value maps to Figure A4 (in the revised manuscript) to show the spatial extent where the annual 2BDA index, Impurity Index, and MODIS broadband albedo have statistically significant annual trends from 2004 to 2011 which are limited to a few areas. Although the trends in most areas are not statistically significant at the 95% confidence level, we still think it is useful to examine the patterns of interannual trends for the different indices. We have revised the text to make note of the locations where Figure A4 shows statistically significant trends.

Fig. 7: Please provide some indication of measurement spread at each point, e.g. +/- 1 s.d. I would also prefer to see just the 2014 MERIS data for comparison with the 2014 algal abundance time series, rather than the aggregate 2004-2011 time series which is shown currently. Previous work

e.g. Shimada et al. (2016) and Tedstone et al. (2017) has shown that there is considerable inter-annual variability and so I think more value here could come from detailed analysis of how algal growth proceeds in each season.

Response: Since the Envisat MERIS was operational from March 2002 to April 2012, we are unable to provide a 2014 MERIS time series coincident with the 2014 field data. In this revision, we removed the figure from our manuscript. To consider the algal growth in different seasons, we extracted the seasonal growth functions (2BDA vs. time) for different seasons and compared with the growth function extracted from the 'climatological' averages over the two example sites KAN_M and DS (Figure A5 in the revised manuscript, shown below).

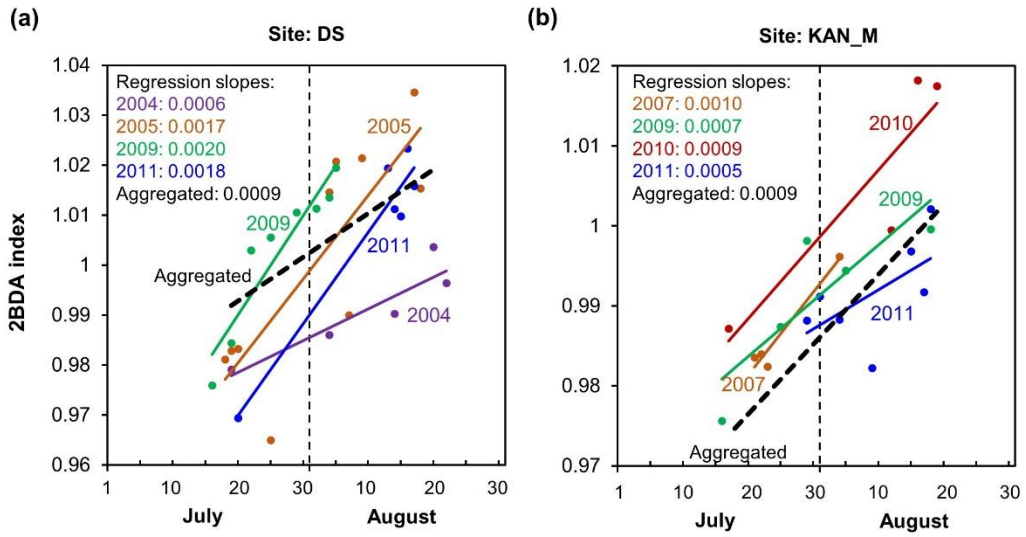

Figure A5 (in the revised manuscript). Temporal trends of 2BDA index from mid-July to Mid-August in different years at sites DS (a) and KAN_M (b).

P16 L342-359: very wordy. Requires paragraphing. Also consider in here which assertions can be retained once major review comments are addressed. It remains particularly difficult to follow the links with the field data despite close reading of the m/s.

Response: We have rewritten and restructured this section, and have added more text describing how and why we compared the remote sensing data to previous field data.

Fig. 8: (a) panels use inter-annual averages of each day and are therefore not especially useful at the process-level: like any other process, algal growth is not actually dependent on time but on a range of processes. Examination of individual years with varying melt season characteristics would therefore be more useful. At the very least, it would be good to see faint lines for each year plotted into the background of these panels. Associated question: how much 'noise' is there in individual years relative to the 'climatological' averages being shown?

Response: We aggregated the daily data in different years to estimate the overall seasonal trend since the data for some years are not sufficient to obtain a reliable seasonal trend. We agree that algal growth is a complicated process, being affected by multiple factors like nutrients, meltwater, sunlight, temperature, and so on, which needs further investigation in the future by combining in

situ and remote sensing observations with meteorological and regional climate modelling data. However, characterizing the seasonal trend of algal growth over time is still useful for understanding the average patterns of seasonal growth across multiple years. In this revision, we added a supplementary figure (Figure A5, shown above) to show the temporal variations of 2BDA index in different years over the sites KAN_M and DS (algae-abundant area), showing that the regression slope of 2BDA vs. time is quite consistent between different years despite some variability at the DS site.

Fig. 8c and section 4.4: is the chosen breakpoint of 20 August statistically significant?

Response: We choose 20 August as the breakpoint because for most of the years we studied, snowfall happened after 20 August and covered the bare ice surface where glacier algae grow. In this revision, we removed the points with p-value greater than 0.05 from Figure 8b and Figure 8c.

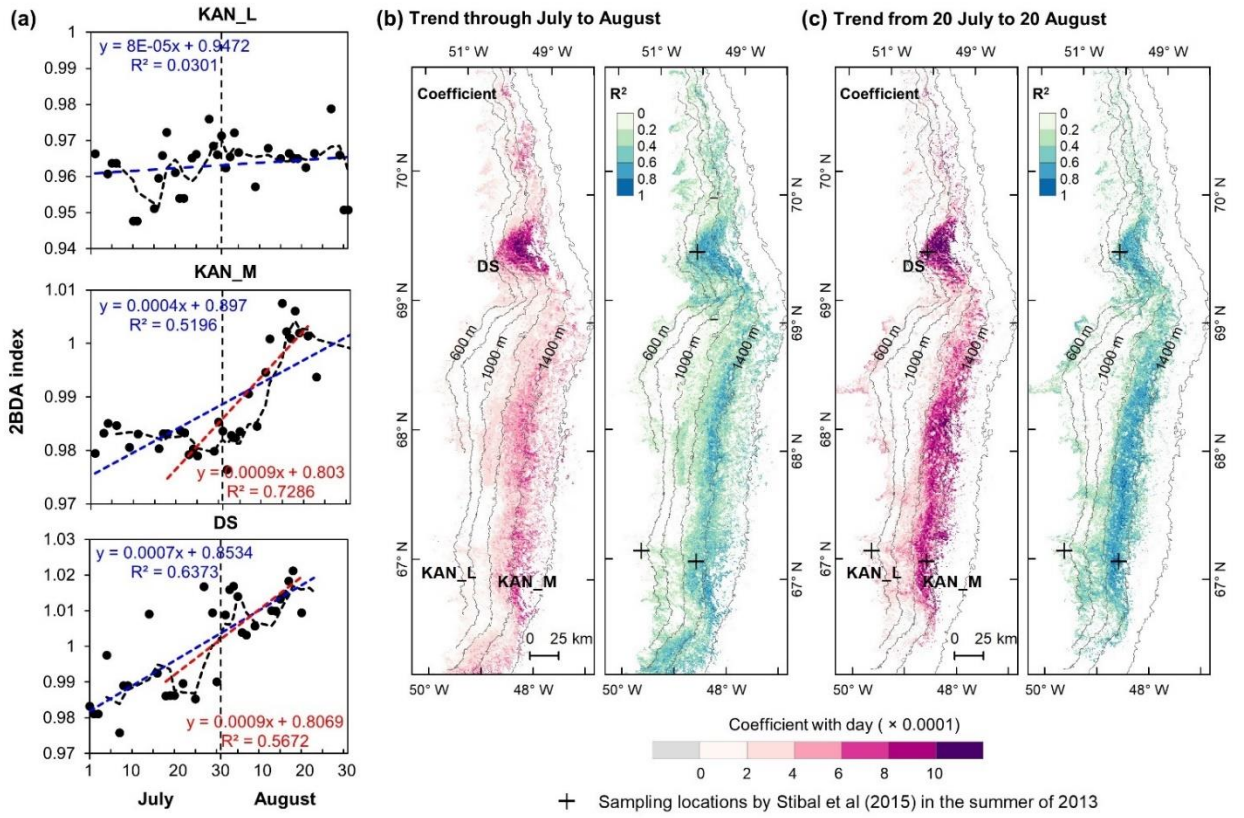

Figure 8 (in the revised manuscript). Temporal trends of the 2BDA index over July and August. (a) 2BDA time series and temporal trend analysis over the KAN_L, KAN_M, and DS sites. (b) Regression slope and R2 estimates of the temporal trend analysis for the period of July–August (for areas where the p value <=0.05). (c) Regression slope and R2 estimates of the temporal trend analysis for the period of 20 July–20 August (for areas where the p value <=0.05).

Discussion: excessively wordy in places, can be shortened without loss of meaning. Fig. 11: provide colorbar to interpret density colors. Consider providing R2 values instead of just R.

Response: We have revised the discussion section to improve clarity. We added the colorbar to Figure 11 as suggested. We use R instead of R^2 as our focus is to discuss the correlations between MAR albedo and MODIS albedo, and between the albedo bias and 2BDA index. The metric R

describes the strength of linear association between two variables, while R^2 is generally used in regression models to represent the amount of variability in y (dependent variable) that can be explained by the regression model, which is not the focus in our context.

Text of page 22: this paragraph is overly long. It requires a re-structure.

Response: We have restructured this part into three paragraphs and have revised the text.

P22 L456-459: might be worth noting here that this is opposite to the results of Tedstone et al. (2017).

Response: We have added discussion of the Tedstone et al. (2017) study as suggested.

L460: 'For each of the two variables'

Response: We have changed the text accordingly.

P23 L474-481: reads hugely speculatively, especially given the relative lack of process-level understanding about ice algae available in the literature.

Response: This statement is indeed somewhat speculative, but we have provided these suggestions based on our analysis as a point of discussion for future study. We restructured and rewrote this section to clarify that these statements are somewhat speculative and more work is necessary to better understand these relationships.

Fig. 13a,b: why was a white mid-point of _0.97 chosen? Aren't algae judged to be present at values < 1?

Response: We didn't intend to use 0.97 as a thresholding point. We changed the color scheme to avoid the confusion caused by color scheme. We also moved the subplots (a) and (b) to the appendix (Figure B1). As noted in the response to reviewer #1, there is no particular threshold for which algae are deemed to be present or not present. Algae may still be present at 2BDA values less than 1, as the background bare ice spectrum shows a decrease from 665 to 709 nm. However, as we note in response to reviewer #1, there is a higher likelihood of dust impacting the 2BDA index below values of 0.99.

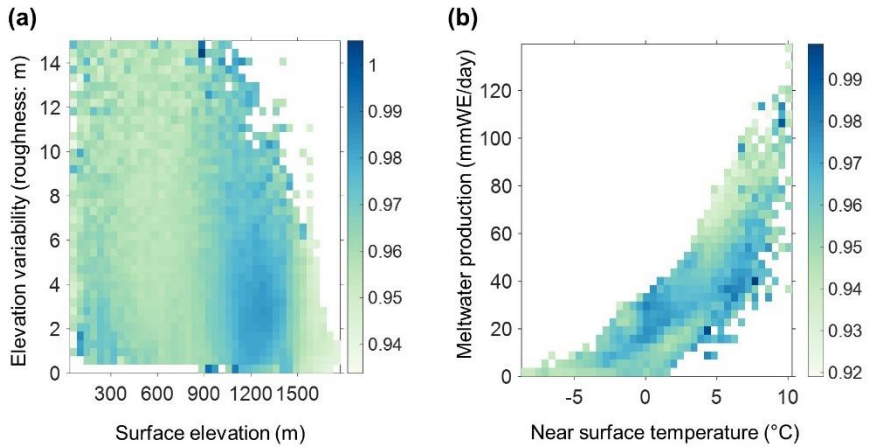

Figure B1 (in the revised manuscript). (a) 2BDA index versus surface elevation and roughness (elevation variability within each MERIS pixel). (b) 2BDA index versus near surface temperature and meltwater production simulated by MAR. The colour bars in (a) and (b) indicate the average 2BDA index for each two-dimensional bin defined by the two variables on the horizontal and vertical axes.

Fig. 13c,d,e: I am not sure what the relevance of providing these data are. At the very least it would be useful to add some kind of annual 2BDI and Impurity Index time series for comparison with the provided metrics.

Response: We added the annual 2BDA time series to the figure as suggested. This analysis is meant to be a preliminary investigation of possible relationships between algae and climate forcing, and is provided as a discussion point for future research.

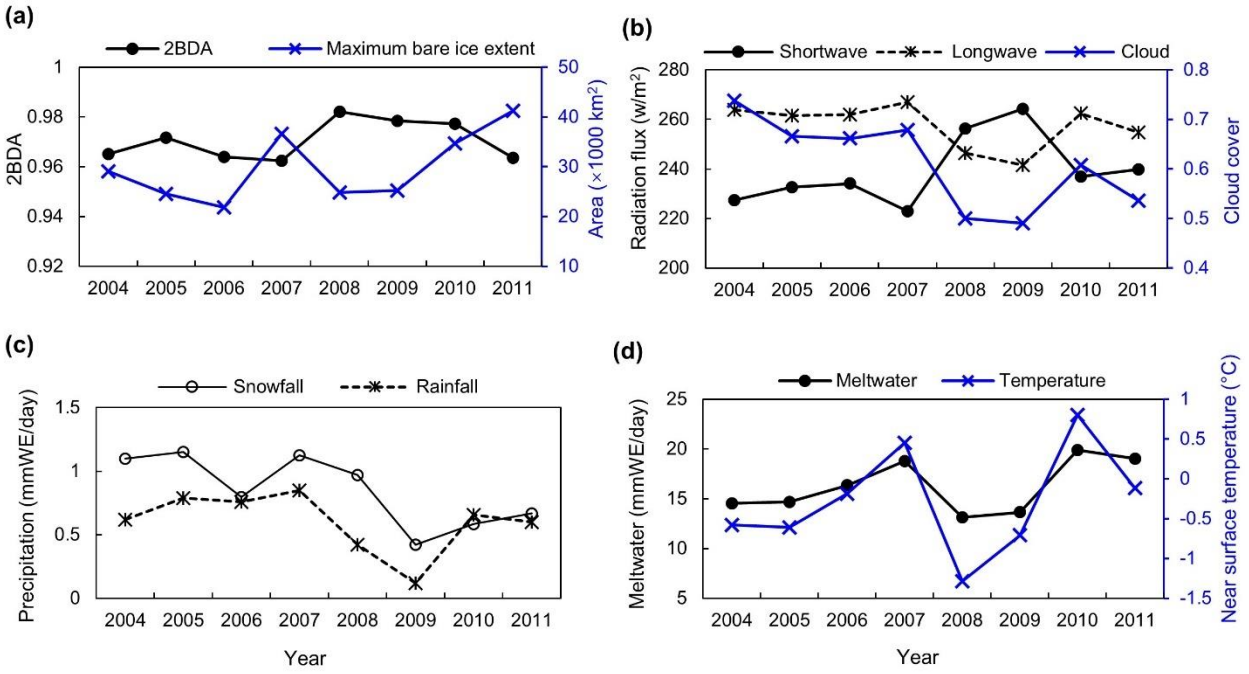

Figure 13 (in the revised manuscript). (a) Average 2BDA index over bare ice and maximum bare ice area from 2004 to 2011 (MERIS). (b) July-August mean of downward shortwave and longwave radiation fluxes and cloud cover over the study area from 2004 to 2011 (MAR). (c) July-August mean of rainfall and snowfall (MAR). (d) July-August mean of meltwater production and near surface temperature (MAR).

Reference for the response

Anesio, A. M., Lutz, S., Chrismas, N. A. M. and Benning, L. G.: The microbiome of glaciers and ice sheets, *NPJ Biofilms Microbiomes*, 3, 10, 2017.

Blondeau-Patissier, D., Gower, J. F. R., Dekker, A. G., Phinn, S. R. and Brando, V. E.: A review of ocean color remote sensing methods and statistical techniques for the detection, mapping and analysis of phytoplankton blooms in coastal and open oceans, Prog. Oceanogr., 123, 123–144, 2014.

Condom, T., Dumont, M., Mourre, L., Sicart, J. E., Rabatel, A., Viani, A. and Soruco, A.: Technical note: A low-cost albedometer for snow and ice measurements – theoretical results and application on a tropical mountain in Bolivia, Geoscientific Instrumentation, Methods and Data Systems, 7(2), 169–178, doi:10.5194/gi-7-169-2018, 2018.

Cook, J. M., Tedstone, A. J., Williamson, C., McCutcheon, J., Hodson, A. J., Dayal, A., Skiles, M., Hofer, S., Bryant, R., McAree, O., McGonigle, A., Ryan, J., Anesio, A. M., Irvine-Fynn, T. D. L., Hubbard, A., Hanna, E., Flanner, M., Mayanna, S., Benning, L. G., van As, D., Yallop, M., McQuaid, J. B., Gribbin, T. and Tranter, M.: Glacier algae accelerate melt rates on the south-western Greenland Ice Sheet, The Cryosphere, 14(1), 309–330, doi:10.5194/tc-14-309-2020, 2020.

Dumont, M., Brun, E., Picard, G., Michou, M., Libois, Q., Petit, J.-R., Geyer, M., Morin, S. and Josse, B.: Contribution of light-absorbing impurities in snow to Greenland's darkening since 2009, Nat. Geosci., 7, 509, 2014.

Ganey, G. Q., Loso, M. G., Burgess, A. B. and Dial, R. J.: The role of microbes in snowmelt and radiative forcing on an Alaskan icefield, Nat. Geosci., 10, 754, 2017.

Lutz, S., Anesio, A. M., Jorge Villar, S. E. and Benning, L. G.: Variations of algal communities cause darkening of a Greenland glacier, FEMS Microbiol. Ecol., 89(2), 402–414, 2014.

Matthews, M. W.: A current review of empirical procedures of remote sensing in inland and near-coastal transitional waters, Int. J. Remote Sens., 32(21), 6855–6899, 2011.

Painter, T. H., Duval, B., Thomas, W. H., Mendez, M., Heintzelman, S. and Dozier, J.: Detection and quantification of snow algae with an airborne imaging spectrometer, Appl. Environ. Microbiol., 67(11), 5267–5272, 2001.

Remias, D., Schwaiger, S., Aigner, S., Leya, T., Stuppner, H. and Lütz, C.: Characterization of an UV-and VIS-absorbing, purpurogallin-derived secondary pigment new to algae and highly abundant in Mesotaenium berggrenii (Zygnematophyceae, Chlorophyta), an extremophyte living on glaciers, FEMS Microbiol. Ecol., 79(3), 638–648, 2012.

Ryan, J. C., Hubbard, A., Stibal, M., Irvine-Fynn, T. D., Cook, J., Smith, L. C., Cameron, K. and Box, J.: Dark zone of the Greenland Ice Sheet controlled by distributed biologically-active impurities, Nat. Commun., 9(1), 1065, 2018.

Shimada, R., Takeuchi, N. and Aoki, T.: Inter-Annual and Geographical Variations in the Extent of Bare Ice and Dark Ice on the Greenland Ice Sheet Derived from MODIS Satellite Images, Front. Earth Sci., 4, 2293, 2016.

Stibal, M., Gözdereliler, E., Cameron, K. A., Box, J. E., Stevens, I. T., Gokul, J. K., Schostag, M., Zarsky, J. D., Edwards, A., Irvine-Fynn, T. D. L. and Jacobsen, C. S.: Microbial abundance in surface ice on the Greenland Ice Sheet, Front. Microbiol., 6, 225, 2015.

Stibal, M., Box, J. E., Cameron, K. A., Langen, P. L., Yallop, M. L., Mottram, R. H., Khan, A. L., Molotch, N. P., Chrismas, N. A. M., Calì Quaglia, F., Remias, D., Smeets, C. J. P. P., van den Broeke, M. R., Ryan, J. C., Hubbard, A., Tranter, M., van As, D. and Ahlstrøm, A. P.: Algae Drive Enhanced Darkening of Bare Ice on the Greenland Ice Sheet, Geophys. Res. Lett., 44(22), 2017GL075958, 2017.

Takeuchi, N., Dial, R., Kohshima, S., Segawa, T. and Uetake, J.: Spatial distribution and abundance of red snow algae on the Harding Icefield, Alaska derived from a satellite image, *Geophys. Res. Lett.*, 33(21), 570, 2006.

Tedesco, M., Foreman, C., Anton, J., Steiner, N., Schwartzman, T.: Comparative analysis of morphological, mineralogical and spectral properties of cryoconite in Jakobshavn Isbr?, Greenland, and Canada Glacier, Antarctica. Annals of Glaciology, 54(63), 147157. doi:10.3189/2013AoG63A417, 2013.

Tedstone, A. J., Bamber, J. L., Cook, J. M., Williamson, C. J., Fettweis, X., Hodson, A. J. and Tranter, M.: Dark ice dynamics of the south-west Greenland Ice Sheet, The Cryosphere, 11(6), 2491–2506, 2017.

Wang, S., Tedesco, M., Xu, M. and Alexander, P. M.: Mapping Ice Algal Blooms in Southwest Greenland From Space, Geophys. Res. Lett., 45(21), 11,779–11,788, 2018.

Williamson, C. J., Anesio, A. M., Cook, J., Tedstone, A., Poniecka, E., Holland, A., Fagan, D., Tranter, M. and Yallop, M. L.: Ice algal bloom development on the surface of the Greenland Ice Sheet, FEMS Microbiol. Ecol., 94(3), doi:10.1093/femsec/fiy025, 2018.

Wientjes, I. G. M. and Oerlemans, J.: An explanation for the dark region in the western melt zone of the Greenland ice sheet, The Cryosphere, 4(3), 261–268, 2010.

Yallop, M. L., Anesio, A. M., Perkins, R. G., Cook, J., Telling, J., Fagan, D., MacFarlane, J., Stibal, M., Barker, G., Bellas, C., Hodson, A., Tranter, M., Wadham, J. and Roberts, N. W.: Photophysiology and albedo-changing potential of the ice algal community on the surface of the Greenland ice sheet, ISME J., 6(12), 2302–2313, 2012.

Summary list of all relevant changes made in the manuscript

	Sections	**Changes**
	Author info	We changed the correspondence email address as **wangshujie23@gmail.com**
Text	1 Introduction	We rewrote paragraphs #5 and #6 to address the reviewers' comments, particularly about using the spectral feature of chlorophyll-a instead of the purpurogallin pigment.
	2.1 Study area and previous field observations	We added more details about the field datasets and how we used them in this study.
	3.2 Chlorophyll-a indices and impurity index	We added more details on the different indices, particularly the discussion about the impurity index as Reviewer#2 suggested.
	3.3 Sensitivity analysis based on radiative transfer modelling	We added this new section in this revision to describe how we used the SNICAR model to examine the sensitivity of 2BDA index to dust presence.
	4.1 Comparison between different ratio indices	We rewrote most of this section as Reviewer#2 suggested. In the course of making corrections to the manuscript we discovered a minor error in calculating the 3BDA index (which was not used to produce any results in the manuscript). The change does not affect any of our results or conclusions and we have corrected the manuscript with the correct 3BDA values.
	4.2 Sensitivity analysis of 2BDA index to non-algal factors	We added this new section to analyze and discuss the sensitivity of the 2BDA index to dust presence and ice properties.
	4.3 Spatial variability	We improved the readability of this section.
	4.4 Interannual variability	For clarity, we moved some of the text to this new section and improved the writing for better readability.
	4.5 Seasonal trends of algal growth over July and August	We improved the writing of this section and provided more methodological details about calculation of population doubling times.
	5 Discussion	We restructured the Discussion into three sections: 5.1 Sensitivity to subpixel variability, 5.2 Relationship between regional climate model albedo bias and glacier algae, and 5.3 Potential drivers for glacier algae variability.
	5.1 Sensitivity to subpixel variability	We added this new section to discuss the sensitivity of 2BDA index to the scale of MERIS data, by performing spectral linear mixing experiments using the field data and SNICAR-simulated data.

	5.3 Potential drivers for glacier algae variability	We restructured and rewrote this part by incorporating Reviewer#2's comments.
Figures	Figure 1	Added more descriptions about the field spectrum in the figure caption
	Figure 2	Added more field spectra of glacier algae-laden ice based on Stibal et al. (2017), to illustrate the consistency of the chlorophyll-a spectral signal between MERIS, WorldView-2, and field data.
	Figure 3	Revised as Reviewer#2 suggested, and added a subplot to show the reflectance spectra of different surface types normalized to the bare ice spectra.
	Figure 4	New figure added in this revision, to support the sensitivity analysis of the 2BDA index to dust presence based on SNICAR simulations and MERIS data.
	Figure 5	Figure 4 in the original manuscript. Changed color scheme for better illustrating the spatial variability of different indices.
	Figure 6	Figure 5 in the original manuscript. Changed as Reviewer#2 suggested. Changed color scheme for better illustration.
	Figure 8	Changed subplots (b) and (c) by removing the pixels with P value greater than 0.05.
	Figure 11	Changed as Reviewer#2 suggested by adding color bar.
	Figure 13	Added the time series of 2BDA index and maximum bare ice extent as a subplot, and moved the original subplots (a) and (b) to Appendix B as Figure B1.
	Other changes	Removed the original Figure 7 from the manuscript.
Appendix	Figure A1	New supplementary figure added in this revision, to show the different spatial variability of different indices varied with elevation levels.
	Figure A2	New supplementary figure added in this revision, to illustrate the wavy patterns potentially caused by dust outcropping at 1000-1200m elevation based on high-resolution WorldView-2 imagery.
	Figure A3	New supplementary figure added in this revision, to show the interannual variability of 2BDA index and impurity index at the elevation levels.
	Figure A4	Changed from the original Figure A1. Added the maps of P values.
	Figure A5	New supplementary figure added in this revision, to show the temporal trends of 2BDA index through mid-July to Mid-August in different years at sites DS (a) and KAN_M (b).
	Figure B1	Moved from the original Figure 13(a) and (b). Changed color scheme to avoid ambiguity as noted by Reviewer#2.
	Table C1	New supplementary table added in this revision, obtained from the field data of Cook et al. (2020), which provides additional evidence showing the positive correlations between 2BDA index and algal cell abundance.
	Figure C2	New supplementary figure added in this revision, plotted based on Table C1.
	Figure C3	New supplementary figure added in this revision, showing the spectral linear mixing results to support the discussion section 5.1 about the scale issues.

Quantifying spatiotemporal variability of ~~ice~~glacier algal blooms and the impact on surface albedo in southwest Greenland

Shujie Wang[1], Marco Tedesco[1,2], Patrick Alexander[1,2], Min Xu[3], Xavier Fettweis[4]

[1]Lamont-Doherty Earth Observatory, Columbia University, Palisades, NY 10964, USA.
[2]NASA Goddard Institute for Space Studies, New York, NY 10025, USA.
[3]Department of Geography, University of Alabama, Tuscaloosa, AL 35401, USA.
[4]Department of Geography, University of Liège, Liège 4000, BELGIUM

Correspondence to: Shujie Wang (~~swang@ldeo.columbia.edu~~wangshujie23@gmail.com)

Abstract. Albedo reduction due to light-absorbing impurities can substantially enhance ice sheet surface melt by increasing surface absorption of solar energy. ~~Ice~~Glacier algae have been suggested to play a critical role in darkening the ablation zone in southwest Greenland. It was very recently found that the Sentinel-3 Ocean and Land Colour Instrument (OLCI) band ratio R_{709nm}/R_{673nm} can characterize the spatial patterns of ~~ice~~glacier algal blooms. However, Sentinel-3 was launched in 2016 and current data are only available over three melting seasons~~.~~ (2016-2019). Here, we demonstrate the capability of the MEdium Resolution Imaging Spectrometer (MERIS) for mapping ~~ice~~glacier algae from space and extend the quantification of ~~ice~~glacier algal blooms over southwest Greenland back to the period 2004–2011. Several band ratio indices (MERIS chlorophyll-a indices and the impurity index) were computed and compared with each other ~~and against field measurements~~. The results indicate that the MERIS two-band ratio index (2BDA) R_{709nm}/R_{665nm} is very effective in capturing the spatial distribution and temporal dynamics of ~~ice~~glacier algal growth on bare ice in July and August. We analyzed the interannual (2004–2011) and summer (July–August) trends of algal ~~abundance~~distribution and found significant ~~increasing trends of ice~~seasonal and interannual increases in glacier algae close to the Jakobshavn Isbrae Glacier and along the middle dark zone between the altitudes of 1200 m and 1400 m. Using broadband albedo data from the Moderate Resolution Imaging Spectroradiometer (MODIS) we quantified the impact of ~~ice~~glacier algal growth on bare ice albedo, finding a 0.02~0.04 reduction rate in albedo for each algal population doubling. Our analysis indicates the strong potential for the satellite algal index to be used to reduce bare ice albedo biases in regional climate model simulations.

1 Introduction

Snow and ice play a critical role in regulating the global energy balance through high surface albedos (Skiles et al., 2018; Warren, 1982). The presence of light-absorbing impurities, including abiotic materials (such as mineral dust and black carbon; e.g. Flanner et al., 2007; Goelles and Bøggild, 2017; Wientjes et al., 2011) and biogenic materials primarily produced by microbial processes (Chandler et al., 2015; Ryan et al., 2018; Stibal et al., 2017; Williamson et al., 2019), can

substantially reduce the surface albedo of snow and ice and thus enhance surface melt. Increased meltwater further decreases surface albedo, triggering a positive feedback mechanism between meltwater production and albedo ~~decay~~decline (Box et al., 2012; Tedesco et al., 2011, 2016).

Snow algae and ~~ice~~glacier algae are among the main microbial communities in supraglacial environments, which are distributed in Greenland, Antarctica, Alaska, Svalbard, ~~Himalaya~~the Himalayas, Siberia, the Rocky Mountains, ~~and~~or the European Alps (Anesio et al., 2017). Algal growth on glaciers and ice sheets not only plays an important role in local and regional carbon and nutrient cycles but is also crucial for regulating surface melt processes through the reduction in snow and ice albedo resulting from dark algae pigmentation (Lutz et al., 2014; Remias et al., 2012; Stibal et al., 2017; Yallop et al., 2012). Snow algae (mainly Chlorophyceae) are psychrophiles residing in glacial snow or ~~snowfield~~snowfields and bloom on the snow surface after the onset of melting (Lutz et al., 2016, 2017). The visible colour of snow algae varies from green~~,~~ to yellow to orange and red, and is determined by the pigments (chlorophylls, xanthophylls, and secondary carotenoids, etc.) produced in different life stages~~. Ice~~ (Anesio et al., 2017). Glacier algae (Zygnematales) are different from snow algae, and grow on the bare ice glacier surface when liquid water, nutrients, and photosynthetically active radiation are sufficient (Lutz et al., 2018; Stibal et al., 2017; Yallop et al., 2012). The earliest documentation about ~~ice~~glacier algae dates to 1872.~~ ~~ During an expedition to Greenland in 1870, Adolf Erik Nordenskiöld and fellow explorers found 'a brown polycellular alga' on the ice surface and within cryoconite holes (Nordenskiöld, 1872). Several field studies (Lutz et al., 2018; Stibal et al., 2015, 2017; Uetake et al., 2010; Yallop et al., 2012) have investigated the species composition and cell structures of ~~ice~~glacier algal communities. The primary ~~ice~~glacier algal species are Ancylonema nordenskiöldii, Mesotaenium berggrenii, and Cylindrocystis brebissonii, which are green microalgae and produce pigments including chlorophyll-a, chlorophyll-b, beta-carotene, lutein, and violaxanthin. Ancylonema nordenskiöldii and Mesotaenium berggrenii also generate a phenolic purpurogallin pigment (purpurogallin carboxylic acid-6-O-b-D-glucopyranoside) which absorbs ultraviolet and visible radiation (Remias et al., 2012; Yallop et al., 2012). It has been suggested that this purpurogallin pigment accounts for the brownish-grey colour of the algae-laden ice (~~Tedstone~~Remias et al., ~~2017~~2012; Yallop et al., 2012).

Recent studies have revealed a significant impact of ~~ice~~glacier algal blooms on bare ice albedo in Greenland (Stibal et al., 2017; Tedstone et al., 2020; Williamson et al., 2018). Along the ablation zone over the southwest Greenland Ice Sheet, a dark ice band appears every summer season (Shimada et al., 2016; Tedstone et al., 2017). It was previously thought that this surface darkening was primarily caused by outcropping of ancient dust (Wientjes and Oerlemans, 2010). Recently, widespread ~~ice~~glacier algal blooms were observed in the field and the dark pigments generated by ~~ice~~glacier algae were argued to be a primary control on the presence of the dark band (Ryan et al., 2018; Stibal et al., 2017; Williamson et al., 2018~~).~~; Williamson et al., 2020). Field sampling and spectral measurements indicate that ~~ice~~glacier algae have a greater effect on albedo reduction than other nonalgal impurities (Stibal et al., 2017). However, current field measurements of ~~ice~~glacier algal abundance and surface albedo are limited to a very few sites and melting seasons, and it is logistically difficult to use ~~the~~ laboratory techniques to measure ~~ice~~glacier algae at a regional scale. The impact of ~~ice~~glacier algal development on surface albedo over large spatial and temporal scales has not yet been quantified.

Remote sensing provides a synoptic and efficient way to characterize geospatial phenomena across large spatial scales. To date, using remote sensing methods to quantify snow or ~~ice~~glacier algae extent or concentration is limited to a few studies (e.g. Cook et al., 2020; Ganey et al., 2017; Huovinen et al., 2018; Painter et al., 2001; Takeuchi et al., 2006; Wang et al., 2018). Painter et al. (2001) estimated the algal abundance of the snow alga Chlamydomonas nivalis over a snow-covered region in the Sierra Nevada of California from ~~the~~ Airborne Visible/Infrared Imaging Spectrometer (AVIRIS) hyperspectral imagery based on chlorophyll-a absorption features between 630 nm and 700 nm. Despite the high capability of airborne hyperspectral imaging data for detecting ~~chlorophyll~~chlorophylls, the availability of hyperspectral imaging data is constrained over space and time. Several studies (e.g. Takeuchi et al. 2006; Ganey et al. 2017; Huovinen et al. 2018) mapped red snow algae based on carotenoid absorption features using satellite red and green bands. ~~However,~~

Mapping glacier algae using remote sensing is complicated by a number of factors, including the complex pigmentation of glacier algae, insufficient spectral and spatial resolution of satellite data, and the impact of dusts and underlying ice optics that are not yet well understood. The use of carotenoid features ~~in mapping ice~~is not applicable to glacier algae ~~is questionable~~, as ~~ice algae~~they do not, to our knowledge, generate secondary carotenoids like snow algae~~, and additionally, the spectral characteristics of dirt may resemble those of carotenoids~~ (Painter et al., 2001; Takeuchi et al., 2006). ~~While the~~The brownish-grey colour of ~~ice~~glacier algae is attributed to the purpurogallin ~~pigment,~~ pigments, but the characteristic absorption peaks of purpurogallin pigments are concentrated in the ~~detailed~~ultraviolet spectrum at 278 nm, 304 nm, and 389 nm (Remias et al.,2012), which are not detectable by current satellite sensors. At visible wavelengths, the absorption by purpurogallin pigments is quite uniform, making it difficult to differentiate between glacier algae and other dark impurities from satellite data based on purpurogallin spectral ~~and optical~~ properties ~~of purpurogallin are not well understood, and the proper remote sensing bands/wavelength necessary to detect it are not yet known. Instead,~~.

The spectral signature of chlorophyll-a, the primary photosynthetic pigment~~, is generally used as a~~ generated by glacier algae, however, is well-suited for mapping glacier algae using satellite remote sensing techniques. Chlorophyll-a is widely used as a biomarker to detect ~~algae~~or quantify algal blooms from remote sensing data ~~owing to its unique spectral signatures between 665-710 nm ((~~(e.g. Gitelson, 1992; Painter et al., 2001~~;~~), and it was recently found that the spectral signatures of chlorophyll-a in the red and near-infrared (NIR) region can be utilized for mapping glacier algae (Wang et al., 2018). The red-NIR spectral signature of chlorophyll-a, i.e. absorption at 665-681 nm and reflectance around 709 nm, is present in field hyperspectral data collected over ice surfaces covered by glacier algae (Cook et al., 2020; Stibal et al., 2017). The concentration of chlorophyll-a is ~~commonly~~generally used as a proxy for algal biomass~~, upon which~~ or abundance, and based on this a number of algorithms have been developed to quantify the ~~algal~~ biomass contained in algal blooms occurring in aquatic systems (Beck et al., 2016; Blondeau-Patissier et al., 2014; Matthews, 2011; Xu et al., 2019a, 2019b). ~~Quantification of ice algae biomass from satellite data based on the chlorophyll-a feature has received less attention since the chlorophyll related satellite bands designed for land generally have coarse spectral resolutions~~Using the two-band ratio (R_{709nm}/R_{673nm}) method, Wang et al. (2018) quantified the spatial distribution of glacier algal blooms in southwest Greenland over the summer seasons in 2016 and 2017 from the Sentinel-3 Ocean and Land Colour Instrument (OLCI) data. Despite the

moderate (300 m) spatial resolution, the derived spatial pattern based on the red-NIR chlorophyll-a signature matches well with previous field observations (Stibal et al., 2015; Stibal et al., 2017; Williamson et al., 2018). As for higher spatial resolution remote sensing data, Cook et al. (2020) applied a random forest method to classify unmanned aerial vehicle (UAV) and the Sentinel-2 Multispectral Instrument (MSI) data for identification of high-algae biomass and low-algae biomass areas. However, these data have limitations in terms of spatial coverage, temporal resolution, and spectral resolution. To establish a long-term time series quantification of glacier algae distribution and study the seasonal process of glacier algal blooms and the impact on albedo change, the use of chlorophyll-a-sensitive ocean color satellite sensors is promising.

~~Recently, Wang et al. (2018) demonstrated the capability of the~~ The Sentinel-3 ~~Ocean and Land Colour Instrument (OLCI) in mapping ice algae based on the spectral signatures of chlorophyll a at the red and near infrared (NIR) spectrum range.~~ OLCI is equipped with 21 spectral bands ~~which include~~including seven narrow chlorophyll-~~sensitive~~a bands. ~~OLCI's~~The advanced band configuration of OLCI makes it a valuable sensor for mapping algal blooms not only in water but also on ice~~. The spatial pattern of ice algal abundance derived from the 709 nm to 673 nm OLCI reflectance ratio is consistent with field measurements collected on the southwest Greenland ice sheet~~ (Wang et al., 2018). OLCI was designed based on the opto-mechanical and imaging design of MEdium Resolution Imaging Spectrometer (MERIS) onboard the European Space Agency (ESA)'s Envisat satellite, operational from March 2002 to April 2012, which collected data in 15 spectral bands between 390 nm and 1040 nm. MERIS features in particular a 709 nm band where high levels of chlorophyll-a produce a characteristic reflectance peak. MERIS data have been broadly used for atmospheric and oceanic studies, with the primary goal of measuring the concentration of chlorophyll ~~pigments~~ a and suspended sediments in oceans, coastal waters, and inland lakes (Gower et al., 2008; Palmer et al., ~~2015). MERIS features in particular a 709 nm band where high levels of chlorophyll a have a characteristic reflectance peak. The similar~~2015). Similar configurations of the chlorophyll-targeted bands in terms of wavelength and bandwidth between MERIS and OLCI (Fig. 1a) point to the ~~great~~ potential of using MERIS data to reconstruct the spatial distribution of ~~ice~~glacier algae prior to 2012. In this study, we make use of the capability of MERIS for ~~mapping ice algal blooms,~~ detecting chlorophyll-a to extend the quantification of ~~ice~~glacier algae ~~extent and abundance~~ in southwest Greenland back to the 2004–2011 period, and further quantify the impact of ~~ice~~glacier algal blooms on bare ice albedo by combining the ~~multiyear~~ time series data of MERIS and MODIS.

2 Study area and data

2.1 Study area and previous field observations

Our study area is located between 66-71°N and 47-51°W in southwest Greenland. This area ~~is featured by~~features high ablation rates and low surface albedos during summertime (Alexander et al., 2014; Fettweis et al., 2011; Moustafa et al., 2015; Stroeve et al., 2013). With the progression of surface melt over time, a dark ice zone forms rapidly and reaches a maximum area from mid-July to mid-August (Tedstone et al., 2017; Wang et al., 2018). The bare ice and dark ice ~~areas~~

~~are~~areal extent is highly correlated ~~to the~~with meltwater production and surface runoff simulated by the regional climate model Modèle Atmosphérique Régionale (MAR) (Wang et al. 2018). The ~~peaking~~peak time of surface darkening coincides with the occurrence of ~~ice~~glacier algal blooms observed in the field. The ice alga Ancylonema nordenskiöldii and Mesotaenium berggrenii are the dominant species found in southwest Greenland during July and August (Lutz et al. 2018; Yallop et al. 2012; Williamson et al. 2018). Considering the growth season and surface habitat of ~~ice~~glacier algae, we focus our analysis on bare ice in July and August.

There are a limited number of field studies measuring ~~ice algal abundance and reflectance spectra over our study area. Stibal et al.~~glacier algal abundance and reflectance spectra over the study area (Cook et al., 2020; Stibal et al., 2015; Stibal et al., 2017; Williamson et al., 2018), and no field measurements were coincident with the acquisition time of the Envisat MERIS data. Here we utilized the previous field observations in a qualitative way for comparison purposes, and extended the derived empirical function from the Sentinel-3 OLCI data (Wang et al., 2018) to MERIS data for characterizing the temporal variations of algal population with surface albedo change. We utilized field data first presented by Stibal et al. (2015) and Stibal et al. (2017) to validate patterns of spatial variability in glacier algae distribution and to compare with satellite data to validate the chlorophyll-a spectral signal. Stibal et al. (2015) collected shallow surface ice cores and measured algal abundance over 14 sites in Greenland during May-September 2013, ~~in~~of which the sites DS (69°28.56'N, 49°34.838'W), KAN_M (67°3.964'N, 48°49.356'W), and KAN_L (67°5.798'N, 49°56.303'W) are within our study area. KAN_M and KAN_L ~~(Fig. 4a)~~ are located along the Kangerlussuaq transect (K-transect), and DS ~~(Fig. 4a)~~ is located near to the Jakobshavn Isbrae Glacier. ~~They~~Stibal et al. (2015) documented the algal abundance ~~(mean ± standard deviation values)~~ averaged over the sampling ~~period~~season (2013 summer) for each site, finding cell counts of 66±31 cells/ml (KAN_L), 5688±3147 cells/ml (KAN_M) and 10621±2073 cells/ml (DS), respectively. During the 2014 summer season, Stibal et al. (2017) collected both algal abundance and hyperspectral reflectance measurements via an Analytical Spectral Devices (ASD) Field Spectrometer over a site near the automatic ~~climate~~weather station S6 (67°04.779'N, 49°24.077'W) on the K-transect. They collected multiple samples each observation day and published the datasets of ~~ice~~glacier algal abundance and reflectance spectra at a 10 nm spectral resolution (Stibal et al., 2017). ~~In this study,~~Here we used ~~these~~the field ~~measurements both qualitatively and quantitatively as ground truth~~hyperspectral data to compare with the satellite spectra to validate the ~~patterns of ice algal blooms derived from satellite data~~chlorophyll-a signal.

2.2 Satellite data

2.2.1 MERIS Level-2 data

We used the full spatial resolution (300 m) MERIS Level-2 data acquired during July and August from 2004 to 2011 (https://earth.esa.int/web/guest/-/meris-full-resolution-full-swath-6015). The MERIS Level-2 data were processed from the Level-1b data (top-of-~~atmospheric~~atmosphere radiances in 15 spectral bands shown in Fig. 1a). ESA adopted different processing techniques to generate the Level-2 data over land, water, and clouds. The Level-2 data over land include the

normalized surface reflectance in 13 spectral bands, corrected for the atmospheric effects of gaseous absorption and stratospheric aerosols (ESA, 2011). The full resolution Level-2 data from May 2002 to April 2012 were released at the MERCI file archive (https://merisfrs-merci-ds.eo.esa.int/) in February 2015. We identified 146 cloudless MERIS images acquired on 135 days from July to August between 2004 and 2011. Since there were no cloudless images available for the 2002 summer season and only three images for the 2003 summer over the study area, we excluded these two years from our analysis. For those images affected by clouds over the study area, we checked the MERIS Level-2 Flag data including the pixel types classified as water, land, and cloud. However, the Flag data fail to correctly capture all the cloud pixels due to ~~algorithm~~ limitations of the algorithm in differentiating clouds from other bright surfaces like snow and ice (ESA, 2011). In this regard, we manually removed the cloud pixels (patches) from each MERIS image.

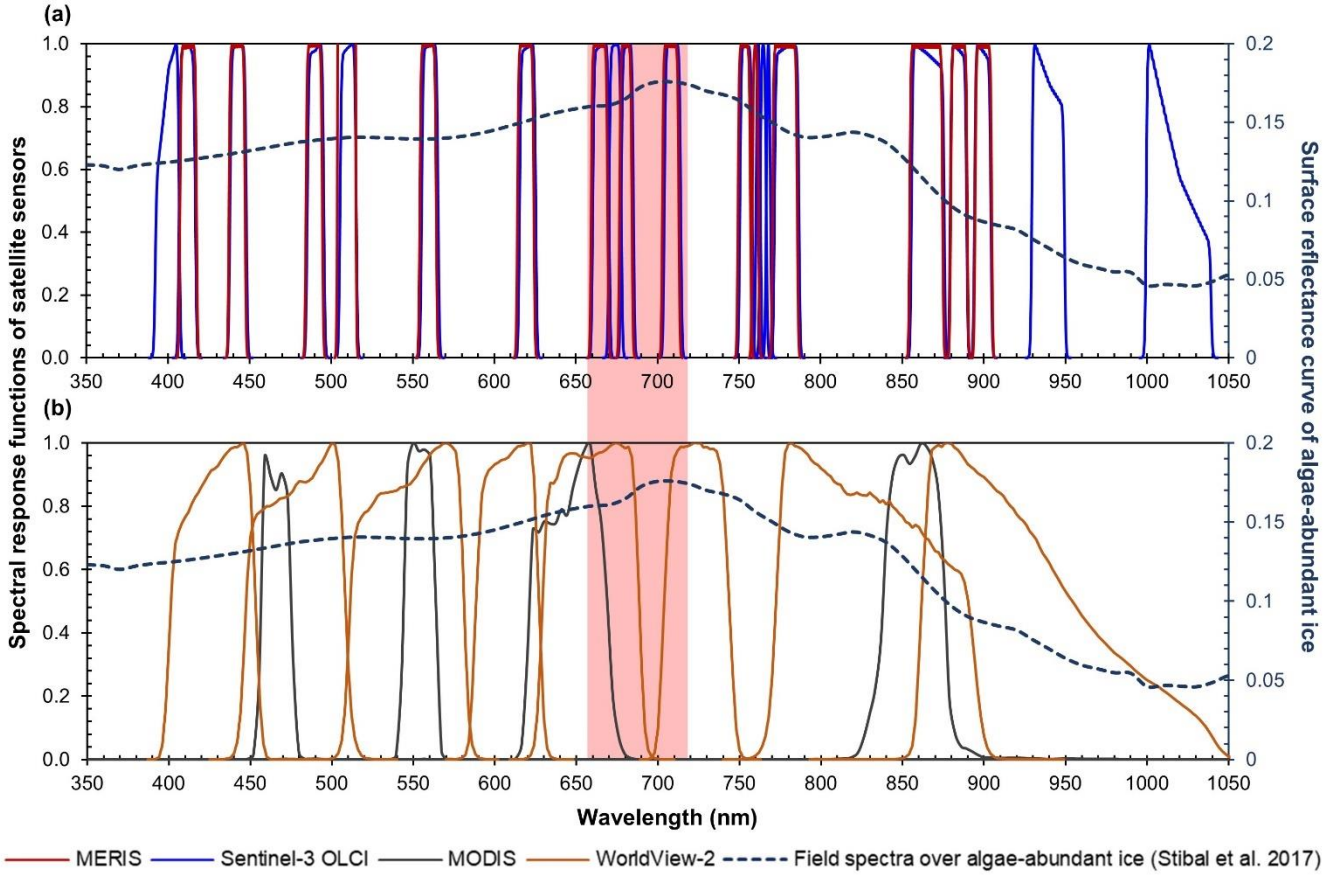

Figure 1~~:~~. Spectral response functions of (a) MERIS (red), OLCI (blue), and (b) MODIS (black), and WorldView-2 (orange) over the ~~spectrum~~wavelength range of 350-1050 nm. All the MERIS and OLCI bands are within ~~this~~the 350-1050 nm range, where photosynthetic and photoprotective pigments have spectral responses. Four MODIS bands (over land) and eight WorldView-2 bands are within this ~~spectrum~~spectral range, but with much coarser spectral resolutions. In both sub-plots, the dashed line shows hyperspectral ASD field ~~spectroradiometer~~spectrometer data (right vertical axis) collected over algae-abundant ice ~~(~~by Stibal et al~~.,~~. (2017), containing ~~the~~ chlorophyll-a signal at the red-NIR wavelengths (red highlighted region). The plotted field spectrum

(sample code: Ab.25.06.14.D1) was measured on 25 June 2014 at 67°04.779'N, 49°24.077'W (near the automatic weather station S6 along the K-transect), with an algal abundance measurement of 121664 cells/ml (Stibal et al., 2017).

2.2.2 MODIS data

We used the MODIS/Terra daily surface reflectance product (MOD09GA Version 6) and daily snow cover product (MOD10A1 Version 6). The MOD09GA data include the atmospherically corrected surface reflectance ~~at~~for the ~~MODIS bands of~~ 620-670 nm, 841-876 nm, 459-479 nm, 545-565 nm, 1230-1250 nm, 1628-1652 nm, and 2105-2155 nm MODIS bands (Fig. 1b). The MOD10A1 data include broadband albedo estimated based on the MOD09GA product. We used the version 6 data which are greatly improved in sensor calibration, cloud detection, and aerosol retrieval and correction relative to version 5 (Casey et al., 2017; Lyapustin et al., 2014; Toller et al., 2013). Version 6 data are ~~encouraged to be used~~recommended for assessing temporal variability of surface albedo ~~as~~since they are corrected for sensor degradation issues ~~impacting~~that impacted earlier versions (Casey et al., 2017). The spatial resolution of the MODIS datasets is 500 m. We resampled the MODIS data to 300 m using a nearest neighbour resampling method. The cloud masks in the MOD10A1 data were applied to exclude ~~the~~ clouds.

2.2.3 WorldView-2 imagery

~~In addition to those previous field measurements, we~~We also used WorldView-2 imagery to validate the spectral signal of ~~ice~~glacier algae ~~on~~captured by MERIS data. The WorldView-2 satellite was launched in October 2009, collecting data in nine spectral bands (~~titled~~ panchromatic, coast, blue, green, yellow, red, red edge, NIR, and NIR2, Fig. 1b) at a very high spatial resolution (~2 m for the multispectral bands). WorldView satellites have high geolocation accuracy owing to their three-axis stabilized platform equipped with high-precision GPS and attitude sensors (Wang et al., 2016). Although the WorldView-2 spectral bands have wide bandwidths, the red (630-690 nm) and red edge (705-745 nm) bands can capture the chlorophyll-a signal (Fig. 1b), ~~which~~and have been used for mapping algal species in nearshore marine habitats (Reshitnyk et al., 2014). We obtained WorldView-2 imagery acquired in July and August (2009-2011) from the Polar Geospatial Center (PGC, ~~https://www.pgc.umn.edu/).~~https://www.pgc.umn.edu/). The images were provided as orthorectified top-of-atmospheric radiances in eight multispectral bands. We performed atmospheric corrections to the radiance images and obtained surface reflectance images using the MODerate resolution atmospheric TRANsmission (MODTRAN) based Fast Line-of-sight Atmospheric Analysis of Hypercubes (FLAASH) (Anderson et al., 2002). The sub-Arctic model and rural aerosol model were used for correction of atmospheric effects caused by water vapour and aerosols (Legleiter et al., 2013).

2.3 Modèle Atmosphérique Régionale (MAR) outputs

The regional climate model Modèle Atmosphérique Régionale (MAR, Fettweis et al., 2017) combines atmospheric modelling (Gallée and Schayes, 1994) with the Soil Ice Snow Vegetation Atmosphere Transfer Scheme (De Ridder and Gallée, 1998) to simulate surface energy balance and mass balance processes over the Greenland and Antarctic ice sheets. In

this study, we examined the relationship between the MAR albedo bias (e.g. Alexander et al., 2014; Moustafa et al., 2015) and ~~ice~~glacier algal blooms. The snow albedo in MAR is determined by snowpack temperature, temperature gradient, and liquid water content, and the bare ice albedo is scaled based on the accumulated surface water (Alexander et al., 2014). Since the MAR albedo scheme does not account for impurities, there are significant biases ~~between the~~in MAR ~~albedo and MODIS~~ albedo over the southwest Greenland ablation zone (Alexander et al., 2014). We used the 7.5 km resolution MAR v3.9 daily outputs, forced by the European Centre for Medium-Range Weather Forecasts Interim Reanalysis (ERA-Interim; Dee et al., 2011). ~~MAR v3.9 features minor bug fixes and differences in tuning relative to MAR v3.5.2 (Fettweis et al., 2017).~~

3 Methods

3.1 Bare ice mapping

We mapped bare ice cover from each MERIS image using a thresholding method applied to surface reflectance data (e.g. Shimada et al., 2016; Tedstone et al., 2017; Wang et al., 2018). To be consistent with previous studies, we used MODIS-derived bare ice maps as a reference to determine the optimal threshold for the MERIS data. We removed tundra and ocean pixels using the MEaSUREs Greenland Ice Mapping Project classification mask (Howat et al., 2014). We selected 31 MOD09GA images that were coincident with MERIS overpasses and were cloud free over the study area. Following Tedstone et al. (2017), we applied a threshold to the MODIS 841-876 nm reflectance ($R_{841\text{-}876\ nm}$), using the criterion $R_{841\text{-}876\ nm}<0.6$ to extract bare ice reference maps from selected MODIS images. For coincident MERIS images, we iteratively applied a threshold value ranging from 0 to 1, increasing by 0.01 at each iteration to the MERIS band 13 (865 nm) and compared the MERIS and MODIS bare ice cover. The optimal threshold was determined based on the F1 score accuracy metric, which is the harmonic average of precision and recall, defined as ~~following~~follows:

$$F1 = 2 * (precision * recall) / (precision + recall) \quad (1)$$

where *precision* is calculated ~~using~~as $N_{TP} / (N_{TP} + N_{FP})$ and *recall* is calculated ~~using~~as $N_{TP} / (N_{TP} + N_{FN})$. N_{TP} is the number of true positives (the number of pixels classified as bare ice by both the MODIS and MERIS data), ~~-~~N_{FP} is the number of false positives (the number of pixels that are only classified as bare ice by the MERIS data), and N_{FN} is the number of false negatives (the number of pixels that are only classified as bare ice by the MODIS data). ~~Average~~The average F1 score was calculated for each threshold based on those 31 image pairs. The threshold of 0.53 yielded the highest F1 score (0.957). We ~~also~~ excluded supraglacial lakes using the modified normalized difference water index (MNDWI, Yang and Smith, 2013), defined as:

$$MNDWI = (R_{blue} - R_{red}) / (R_{blue} -+ R_{red}) \quad (2)$$

where R_{blue} is the reflectance at 442 nm (MERIS band 2) and R_{red} is the reflectance at 665 nm (MERIS band 7). Pixels with MNDWI greater than 0.14 (Yang and Smith, 2013) were identified as lake pixels and excluded from analysis. Using the same iterative method described above, we also determined an optimal threshold of 0.47 to extract dark ice pixels (pixels with bare ice containing substantial surface impurities) using the 620 nm MERIS band, following Shimada et al. (2016) and Tedstone et al. (2017). This band ~~was commonly~~has been used to delineate dark ice by applying a threshold based on the assumption that visible wavelengths including the red band are mostly affected by light-absorbing impurities rather than surface water and grain size variations (Shimada et al., 2016; Tedstone et al., 2017; Wang et al., 2018).

3.2 ~~Ice algae mapping from MERIS spectra ratio~~ Chlorophyll-a indices and impurity index

Chlorophyll-a is the primary photosynthetic pigment generated by ~~ice~~glacier algal cells (Williamson et al., 2018; Yallop et al., 2012). Hyperspectral field measurements (Fig. 2d, Cook et al., ~~2019~~2020; Stibal et al., 2017) and the Sentinel-3 OLCI spectra (Wang et al., 2018) both ~~show~~exhibit the typical spectral signatures of chlorophyll-a at the red and NIR wavelengths over ~~the~~ algae-abundant ice ~~surface, featured by~~surfaces, featuring a reflectance peak around 709 nm and absorption features around 665-681 nm. Pure ice~~, in contrast,~~ has ~~increased absorption~~lower reflectance at 709 nm ~~as~~ compared to shorter wavelengths (Hall and Martinec, 1985). The magnitude of the reflectance peak at 709 nm relative to 665-681 nm is highly dependent on the chlorophyll-a content (Binding et al., 2013; Gitelson, 1992). Figure 2d shows the MERIS spectra over a dark ice pixel, compared with ~~the~~ WorldView-2 spectra and ~~the~~ field hyperspectral measurements by Stibal et al. (2017). The selected MERIS pixel, located near to the Jakobshavn Isbrae Glacier, is close to the site DS where Stibal et al. (2015) measured a high abundance of ~~ice~~glacier algae during the 2013 summer season. The MERIS image (Fig. 2a) was acquired on 5 July 2010, and the WorldView-2 image (Fig. 2b and Fig. 2c) was acquired on 9 July 2010. The field hyperspectral curves shown in Fig. 2d were measured over dark ice (R620nm<0.4) with high algal abundance (greater than 10000 cells/ml), featuring chlorophyll-a signatures in the red-NIR region. Despite the differences in absolute values of surface reflectance, the spectral shapes of the MERIS, WorldView-2 and field spectra match quite well, particularly with regard to the presence of ~~the~~ chlorophyll-a, validating the ability of MERIS data to capture the glacier algae spectral signal~~, which validates the ice algal signal in the MERIS data~~.

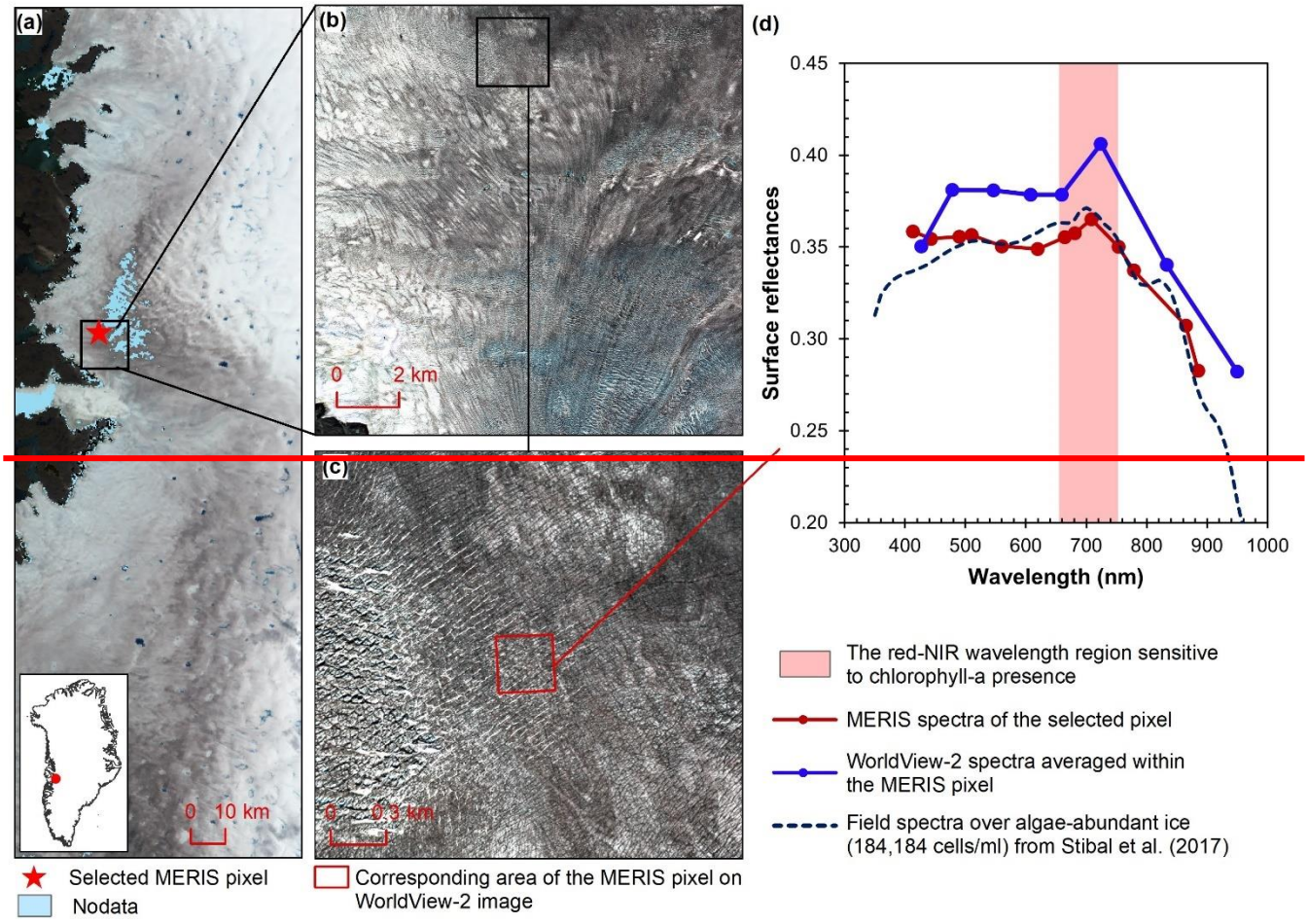
(a)
(b)
(c)
(d)
0 2 km
0 10 km
0 0.3 km
Surface reflectances
Wavelength (nm)
0.45
0.40
0.35
0.30
0.25
0.20
300
400
500
600
700
800
900
1000
The red-NIR wavelength region sensitive to chlorophyll-a presence
MERIS spectra of the selected pixel
WorldView-2 spectra averaged within the MERIS pixel
Field spectra over algae-abundant ice (184,184 cells/ml) from Stibal et al. (2017)
Selected MERIS pixel
Nodata
Corresponding area of the MERIS pixel on WorldView-2 image

270

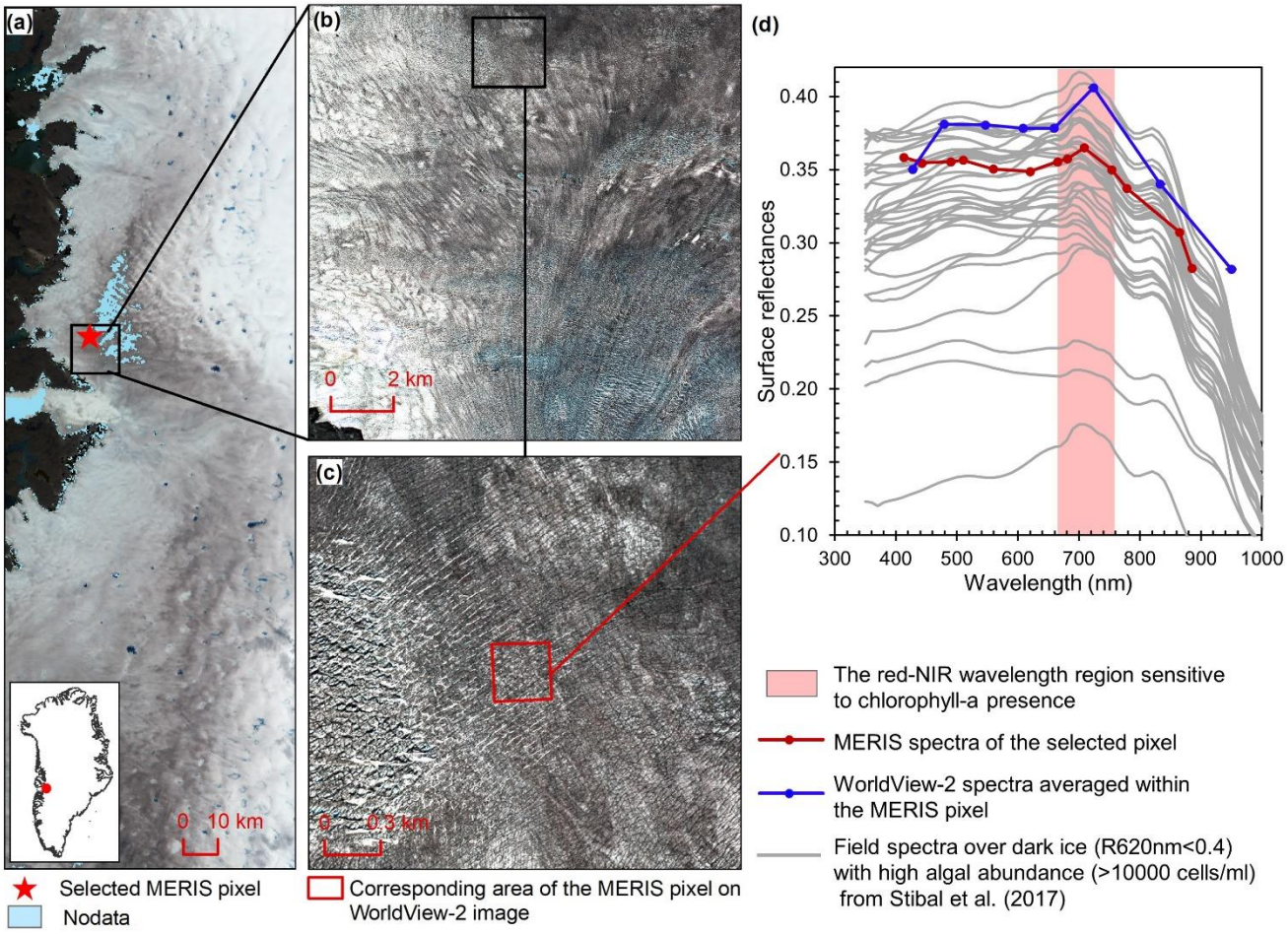

Figure 2~~.~~. Comparison between ~~the~~ MERIS, WorldView-2, and field spectra over algae-abundant dark ice. (a) MERIS Level-2 image (true colour composite) acquired on 5 July 2010. Pixels with missing data are shown in light blue. (b) WorldView-2 surface reflectance image acquired on 9 July 2010 over the square area in (a). (c) Zoomed-in WorldView-2 image, with the area (red square) corresponding to the selected MERIS pixel in (a). (d) Reflectance spectra ~~comparison between~~for MERIS~~,~~ and WorldView-2~~,~~ (2010), and ~~the~~ field hyperspectral measurements collected over the algae-abundant dark ice at S6 by Stibal et al. (2017~~).~~) in 2014.

~~In order to identify the best means of quantifying ice~~To map glacier algae using the chlorophyll-a spectral signature, we calculated ~~a number of different band ratio~~ several MERIS chlorophyll-a indices (Table 1), including the ~~well-established MERIS chlorophyll indices~~ two-band NIR–Red index (2BDA), three-band NIR–Red index (3BDA), normalized difference chlorophyll index (NDCI), and maximum chlorophyll index (MCI) (Moses et al., 2012; Mishra and Mishra, 2012; Binding et al., 2013~~) and the Impurity index (Dumont et al., 2014).~~). The ~~two-band (~~2BDA~~)~~ and ~~three-band (3BDA) red-NIR algorithms~~3BDA methods have been widely applied to ~~estimation of~~estimate chlorophyll-a concentration in aquatic systems ~~(~~using MERIS data (Beck et al., 2016; Moses et al., 2009; Xu et al., 2019a, 2019b), and have proved to be highly accurate ~~to retrieve~~for chlorophyll-a ~~content~~retrieval in turbid coastal waters ~~with~~ characterized by complex optical properties ~~from~~

MERIS data ((Moses et al., 2012). The normalized difference chlorophyll index (NDCI, (Mishra and Mishra, 2012) was defined followingbased on the concept of the normalized difference vegetation index (NDVI). The maximum chlorophyll index (MCI) measures the height of the 709 nm reflectance peak relative to the baseline interpolated by the reflectances atobtained by interpolating reflectance between 681 nm and 753 nm (Binding et al., 2013). In addition, we also calculated the impurity index (Dumont et al., 2014) to compare with the chlorophyll-a indices. The Impurityimpurity index is different from the chlorophyll indices mentioned above, as it does not utilizeratio between the chlorophyll-anatural logarithms of the spectral characteristics. This indexalbedos at the green and NIR bands, and was constructed to quantify the snow impurity content over the Greenland Ice Sheet upon the assumption that the visible wavelengths are much more sensitive to impurity content than the NIR wavelengths. Radiative transfer modelling experiments have shown that the impurity index is less affected by the snow grain size variations than the presence of impurities (Dumont et al., 2014) based on the assumption that impurities decrease the reflectance at visible bands more than the NIR bands.).

Table 1. Details on theEquations and MERIS bands used for calculation of different ratio indices.

Indices	Equation	MERIS bands
Two-band NIR–Red index (2BDA)	R_{709nm} / R_{665nm}	B7, B9
Three-band NIR–Red index (3BDA)	(R_{665nm}^{-1} - R_{709nm}^{-1}) /* R_{753nm}	B7, B9, B10
Normalized Difference Chlorophyll Index (NDCI)	(R_{709nm} - R_{665nm}) / (R_{709nm} + R_{665nm})	B7, B9
Maximum Chlorophyll Index (MCI)	(R_{709nm} - R_{681nm}) - (R_{753nm} - R_{681nm}) * (709 - 681) / (753 - 681)	B8, B9, B10
Impurity index	ln (R_{560nm}) / ln (R_{865nm})	B5, B13

3.3 Sensitivity analysis based on radiative transfer modelling

To evaluate the sensitivity of chlorophyll indices to dust presence, we performed radiative transfer modelling tests using the Snow, Ice, and Aerosol Radiation model (SNICAR; Flanner et al., 2007, 2009). SNICAR is a multi-layer, two-stream radiative transfer model for simulating the spectral albedos of snow over the 300-5000 nm wavelength range (at a 10 nm spectral resolution), accounting for various factors including illumination conditions, snow grain size, snow layer properties, and dust concentrations, etc. The SNICAR online tool (available at snow.engin.umich.edu) allows for simulating the radiative effects of dust in four size bins, in ranges of 0.1-1.0, 1.0-2.5, 2.5-5.0, and 5.0-10.0 μm. Dust optical properties in SNICAR are based on an estimate of global-mean characteristics approximated as a mixture of quartz, limestone, montmorillonite, illite, and hematite. We simulated the spectral albedos for varying sizes and concentrations of dust under the following conditions: direct incident radiation, a solar zenith angle of 60 degrees, clear sky conditions for Summit, Greenland, a snow grain effective radius of 1500 μm (approximating the ice surface), a snowpack thickness of 100 m, a snowpack density of 400 kg/m^3, a range of dust concentrations (0.1, 0.3, 0.5, 0.8, 1, 1.5, 2, 2.5, 3, 5, 8, 10, 30, 50, 80, 100,

300, 500, 800, 1000, 1500, 2000, 2500, and 3000 ppm), and four dust sizes (dust 1: 0.1–1.0μm; dust 2: 1.0–2.5μm; dust 3: 2.5–5.0μm; dust 4: 5.0–10.0 μm). We tested different values of snow grain effective radius (500 μm vs. 1500 μm) and snow density (400 kg/m^3 vs. 900 kg/m^3). The snow density value has a negligible effect on the simulation results. The simulated spectra using a snow grain effective radius of 1500 μm is the best approximation to the MERIS spectra for clean bare ice.

4 Results

4.1 Comparison between different ratio indices

Figure 3 shows the MERIS spectra over four distinct sites~~.~~ within our study area to illustrate the spectra associated with different surface types. Each site represents a typical surface type ~~such as~~, including clean bare ice, dark ice with a significant chlorophyll-a signal, dark ice with a less significant chlorophyll-a signal, ~~or~~and a supraglacial lake. Figure 3b shows that each surface type is characterized by a distinct spectral curve~~, particularly~~ . The difference between the spectral curves for the two dark ice sites~~.~~ is particularly notable. Figure 3c shows the normalized spectral curves relative to the clean ice spectrum. Both of ~~these~~the dark ice sites have a ~~surface~~ reflectance at 620 nm of less than 0.47 and are classified as 'dark ice' based on the thresholding method discussed above (Shimada et al., 2016; Tedstone et al., 2017). ~~The difference is that~~However, the northern dark ice site has a chlorophyll-a spectral signature between 665 nm and 753 nm that matches the field spectra of algae-abundant ice (Fig. 2d), while at the southern dark ice site, the reflectance peak at 709 nm is much less pronounced. The differences illustrate that pixels classified as "dark ice" can have different spectral properties, and in particular differences associated with reflectance characteristics of chlorophyll-a.

We calculated the ~~ratio indices including~~ 2BDA, 3BDA, NDCI, MCI, and ~~Impurity index~~ impurity indices over bare ice ($R_{865\ nm}$<0.53) for each MERIS image. ~~The chlorophyll indices of 2BDA, 3BDA, and NDCI use similar spectral bands and are in general very highly correlated to each other.~~ Table 2 lists the ratio indices and the ~~surface~~ reflectance at 620 nm over ~~those~~the four sites shown in Fig. 3a based on ~~the~~a MERIS image acquired on 14 August 2011~~. It is shown that~~ , to illustrate the differences between indices. The 2BDA, 3BDA, and NDCI chlorophyll-a indices ~~of 2BDA, 3BDA, and NDCI~~use similar spectral bands and are in general well-correlated; they are highest over the northern dark ice site ~~where we identified the chlorophyll signal~~, and lowest over the supraglacial lake. ~~In~~The MCI chlorophyll-a index, in contrast, ~~the chlorophyll index of MCI cannot well represent the chlorophyll signal we observed, which~~ reaches a maximum over ~~the~~ clean bare ice. ~~This may be due to the fact that~~The MCI ~~is more suitable for monitoring intense algal blooms with very high chlorophyll concentrations in water (Binding et al. 2013) while not applicable to the ice algal blooms with comparatively lower chlorophyll content. In addition, MCI~~index measures the height of the 709 nm reflectance peak relative to the baseline between 681 nm and 753 nm, ~~which could be also~~and is therefore sensitive to the bare ice spectrum. ~~Therefore, we selected the 2BDA~~This index may be less sensitive to ~~characterize the~~the relatively low chlorophyll-a content over ice, and is more suitable for monitoring intense algal ~~abundance owing to its simplicity and effectivity.~~blooms with very high chlorophyll-a concentrations in water (Binding et al. 2013). For the ~~Impurity~~impurity index, the clean bare ice has the lowest value,

345 followed by the supraglacial lake, dark ice with the weaker chlorophyll-a signal, and dark ice with the stronger chlorophyll-a signal. (Table 2 shows that the). The supraglacial lake also has a high Impurityhigher impurity index relative to clean ice, suggesting that the Impurityimpurity index may include the darkening effect caused by meltwater presence. We find that the 2BDA, 3BDA and NDCI indices are most suitable for detection of chlorophyll-a, given their specificity to chlorophyll-a signal bands, the sensitivity of the impurity index to liquid water, and the sensitivity of the MCI index to the bare ice
350 spectrum. Of these three indices, we selected the 2BDA index to characterize the glacier algae distribution owing to its simplicity and effectivity.

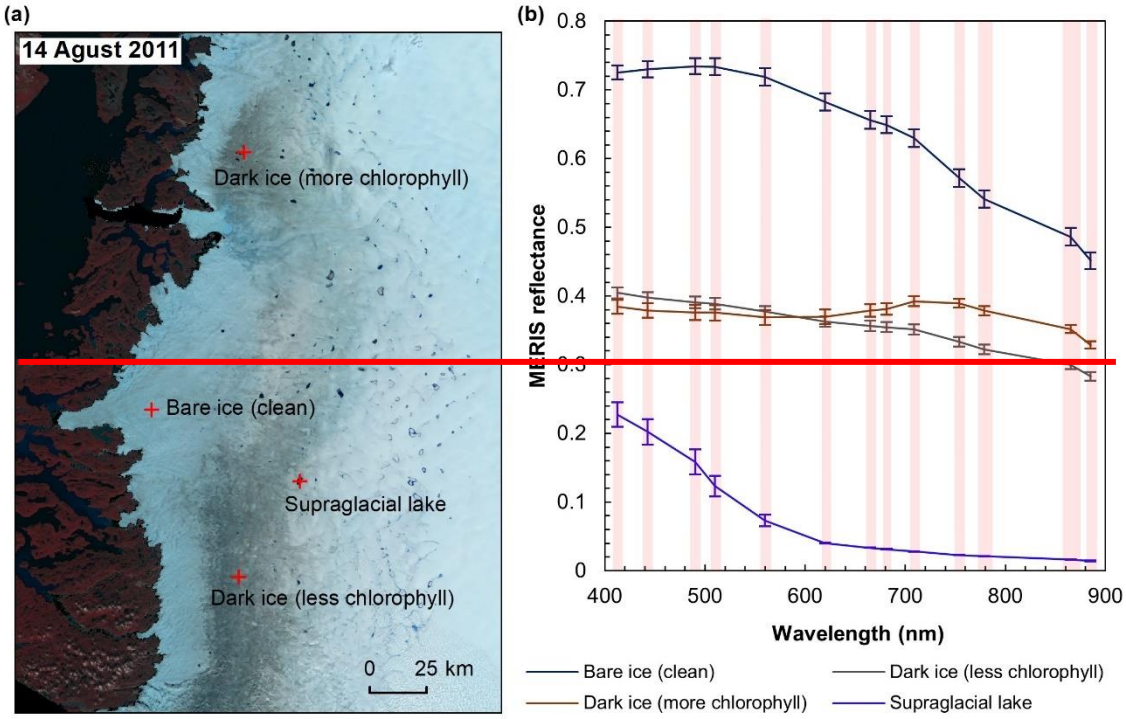

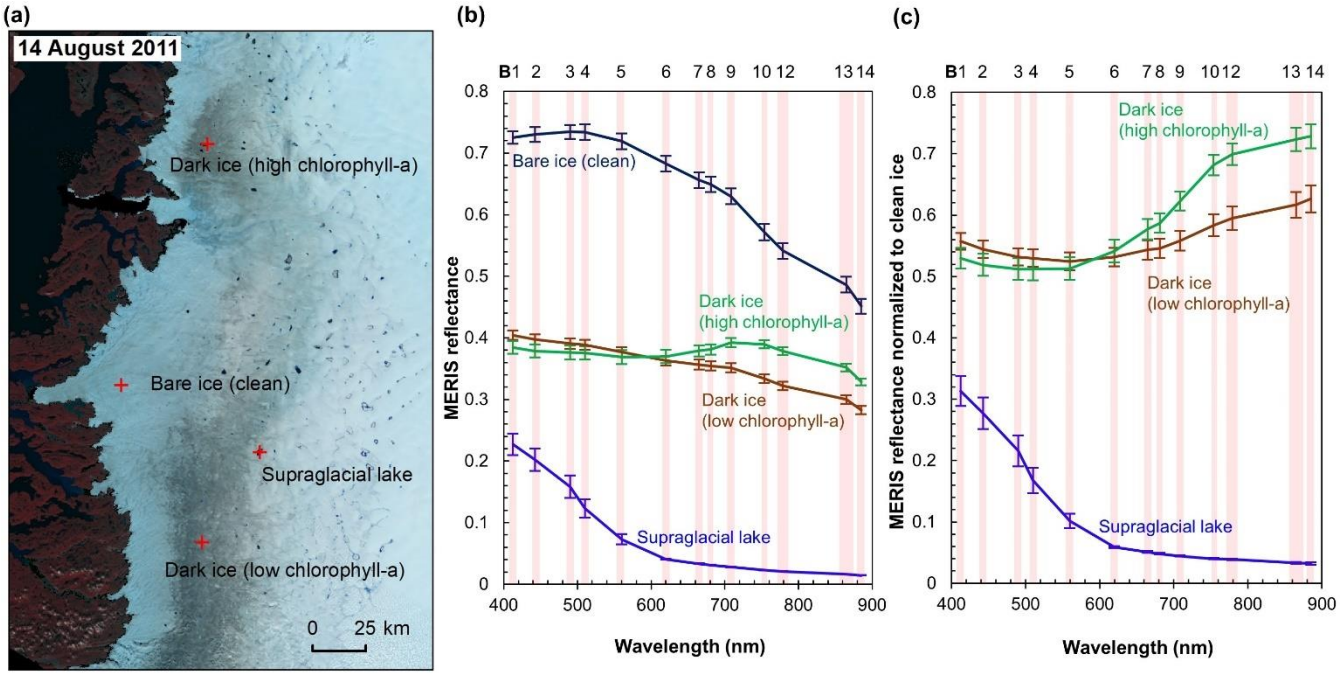

Figure 3~~:~~. MERIS spectra of different surface types. (a) MERIS Level-2 image (false colour composite) acquired on 14 August 2011 and locations of the four ~~different~~ sample sites. Each site has an area of 1.2 km by 1.2 km, composed of 16 MERIS pixels. (b) MERIS ~~surface~~ reflectance in 13 spectral bands over the four sites, illustrated by ~~the~~ mean and standard deviation values for each band over each site. (c) Normalized reflectance relative to the clean ice spectra.

Table 2. ~~The calculated~~Calculated ratio indices and ~~the~~ surface reflectance at 620 nm over the four sites.

Surface type	2BDA	3BDA	NDCI	MCI	Impurity	R_{620nm}
Bare ice (clean)	0.960	-0.~~112~~037	-0.021	0.011	0.457	0.683
Dark ice (~~more~~high chlorophyll-a)	1.035	0.~~231~~035	0.017	0.008	0.955	0.369
Dark ice (~~less~~low chlorophyll-a)	0.986	-0.~~122~~014	-0.007	0.005	0.809	0.362
Supraglacial lake	0.839	~~-250.106~~0.131	-0.087	0.000	0.635	0.040

~~**Figure 4 shows the spatial patterns of the mean 2BDA index, Impurity index, surface reflectance at 620 nm, and MODIS broadband albedo for the bare ice zone, averaged over those MERIS images acquired on 135 days from 2004 to 2011. Figure 4a suggests ice**~~**4.2 Sensitivity of the 2BDA index to non-algal factors**

Given that dust may change the spectral reflectance of bare ice and affect the 2BDA index, we analyzed the sensitivity of 2BDA index to dust presence based on the SNICAR simulations for varying dust sizes and concentrations. We should note here that there has been some discussion in past literature regarding hematite-rich dust (e.g. Tedesco et al., 2013; Cook et al., 2020), which could produce a different spectral response. However, the field study of Cook et al. (2020) found very low

concentrations of such dust, and therefore we consider its impact to be negligible. Using the simulated spectra, we calculated the 2BDA and impurity indices for each dust size and concentration. Figure 4 shows the 2BDA index vs. impurity index calculated for the SNICAR simulations (with circle diameters representing the magnitude of dust concentrations for four different dust sizes), along with the density scatterplots of impurity vs. 2BDA index calculated from the MERIS data. The SNICAR simulations show that the impurity index is more sensitive to dust than the 2BDA index. Figure 4 illustrates that the upper bound of the impurity index calculated from the MERIS data is around 1.0. This maximum value corresponds to a dust concentration of ~500 ppm (for the 5.0-10.0 μm dust range), which is consistent with the measurements of Cook et al. (2020), who reported mean and maximum dust concentrations of 342 ppm and 519 ppm respectively over a field site within the study area. However, SNICAR simulations indicate that an impurity index of 1.0 corresponds to a maximum 2BDA value of 0.99. Therefore, the presence of dust alone cannot explain the high 2BDA index values present in Fig. 4. This comparison suggests that for our study area, areas with a 2BDA index greater than 0.99 are not likely to be false positives caused by dust.

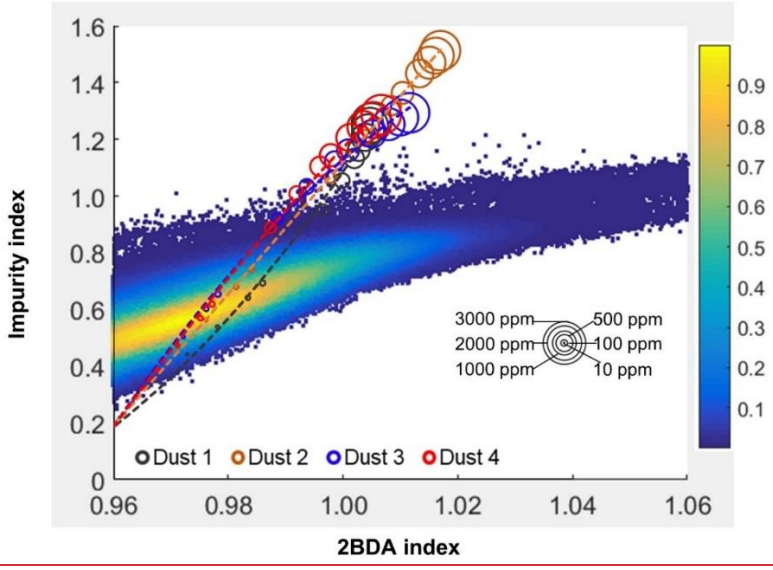

Figure 4. Impurity index vs. 2BDA index for MERIS bare ice pixels (density scatter plot with colours indicating relative frequency), excluding missing data in our study area, between 2004 and 2011. Circles show impurity vs. 2BDA index from SNICAR simulations with varying concentrations of dust (with four different dust sizes). The circle size corresponds to the dust concentration, and dashed lines show the polynomial regression for each of the different dust sizes.

Although the bare ice spectrum can also be affected by other factors such as air bubbles and meltwater presence, there is no evidence suggesting that these factors can generate the chlorophyll-a-like spectral signature with a higher reflectance at 709 nm as compared with 665 nm. In fact, ice with different concentrations of air bubbles has a consistent spectral shape between 665 nm and 709 nm (Condom et al., 2018), and meltwater exhibits a similar pattern to ice at this wavelength range (Fig. 3b), with both the ice and water spectra characterized by a decreased reflectance from 665 nm to 709 nm. The sensitivity of the 2BDA index to glacier algae can be further demonstrated using the field dataset of Cook et al. (2020). Table C1 and Figure

C2 (Appendix C) indicate strong positive correlations between measured cell abundance and the 2BDA index calculated from coincident in-situ hyperspectral data, particularly for those samples with a measured cell abundance of greater than 10000 cells/ml, which have an average 2BDA index of 1.09±0.073. In comparison, the samples with a measured cell abundance of lower than 10000 cells/ml have an average 2BDA index of 0.98±0.015.

4.3 Spatial variability

To examine spatial variability on a broader scale, Fig. 5 shows the spatial patterns of the mean 2BDA index, impurity index, reflectance at 620 nm, and MODIS broadband albedo for the bare ice zone in our study area, averaged over 135 days when MERIS images are available between 2004 and 2011. Figure 5a, which shows patterns of the 2BDA index, suggests glacier algae are abundant at the DS region close to the Jakobshavn Isbrae Glacier between the altitudes of 600 m and 1200 m, and in the middle ablation area (68.5°N-66.5°N) between 1200 m and 1400 m~~, these~~. These patterns are consistent with ~~those of ice~~glacier algal maps derived from the Sentinel-3 OLCI data for the 2016 and 2017 summer season (Wang et al., 2018). The relative magnitude of the 2BDA values between the DS, KAN_L, and KAN_M sites also matches the ~~field measurements of ice algal abundance (Stibal et al., 2015). Figure 4b indicates that the spatial extent of the high Impurity index region in the middle ablation area extends lower in elevation than the area of high algal index (1000 m to 1400 m for the Impurity index vs. 1200 m to 1400 m for the algae index). The Impurity index was designed to capture all types of impurities, indicating the presence of both abiotic (e.g.~~ relative magnitude of field measurements of glacier algal abundance (Stibal et al., 2015; circles on Fig. 5), with the highest 2BDA index and algal abundance at the DS site, a lower value at the KAN_M site, and the lowest value at the KAN_L site.~~outcropping particulates; Wientjes et al., 2012) and biological impurities, which is incapable of distinguishing ice algae from other impurities. A map of surface reflectance at 620 nm (Fig. 4c) was generated for comparison with the algal and impurity index maps, since this band was commonly used to delineate dark ice by applying a threshold (determined to be 0.47 for the MERIS data). Similar to the Impurity index, the dark ice area ($R_{620\ nm}$<0.47) is not only limited to the algae-abundant areas. Compared with the elevation level of 1200 m – 1400 m, the zone between 1000 m and 1200 m has lower surface reflectance at 620 nm (Fig. 4c) as well as lower MODIS broadband albedo (Fig. 4d). Comparison between these four maps suggests that highly abundant ice algae were present at the DS area and the middle 1200 m – 1400 m area, while the darkening at the middle 1000 m – 1200 m area could be attributed to longer exposure of bare ice and increased consolidation of particulates with melt (Tedesco et al., 2016), where the 'wavy' patterns caused by ancient dust outcropping were also observed (e.g. Wientjes and Oerlemans, 2010).~~

A comparison between Figs. 5a and 5b and an examination of variation of the indices with elevation (Fig. A1) indicate a similarity in the spatial distribution of the two indices but also notable differences. In particular, the 2BDA index reaches a peak at an elevation of 1300 m, while the impurity index peaks at 1180 m. As suggested by our sensitivity analysis discussed in Section 4.2, the 2BDA index is primarily sensitive to chlorophyll-a, while the impurity index is sensitive to materials that darken the electromagnetic spectrum in visible wavelengths, including abiotic impurities (e.g. outcropping particulates; Wientjes et al.,

2012), biological impurities, and liquid water. The map of reflectance at 620 nm, the band commonly used to delineate dark ice using a threshold (determined to be 0.47 for MERIS), is shown in Fig. 5c. Similar to the impurity index, the 620 nm reflectance and MODIS broadband albedo (Fig. 5d) reach a minimum value at 1180 m in elevation (Fig. A1; Fig. 5d). Comparison between the three indices and MODIS albedo suggests that algal abundance is highest between 1200 and 1400 m in elevation, contributing to reduced albedo, while other factors may play a more important role in albedo reduction below 1200 m in elevation. In particular, the darkening between 1000 m and 1200 m in elevation could be attributed to longer exposure of bare ice resulting in increased consolidation of particulates with melt (Tedesco et al., 2016), where "wavy" patterns of outcropping dust can be observed (Wientjes and Oerlemans, 2010; Fig. A2). In contrast, imagery (WorldView-2) suggests that these "wavy" patterns may not be present at higher elevations where the appearance of dark material is more consistent with distributed algal material (Fig. A2). Other factors that may contribute to a reduction in MODIS albedo include liquid water and surface crevasses (e.g. Ryan et al., 2018), though their fraction is small relative to other surface types (Ryan et al., 2018).

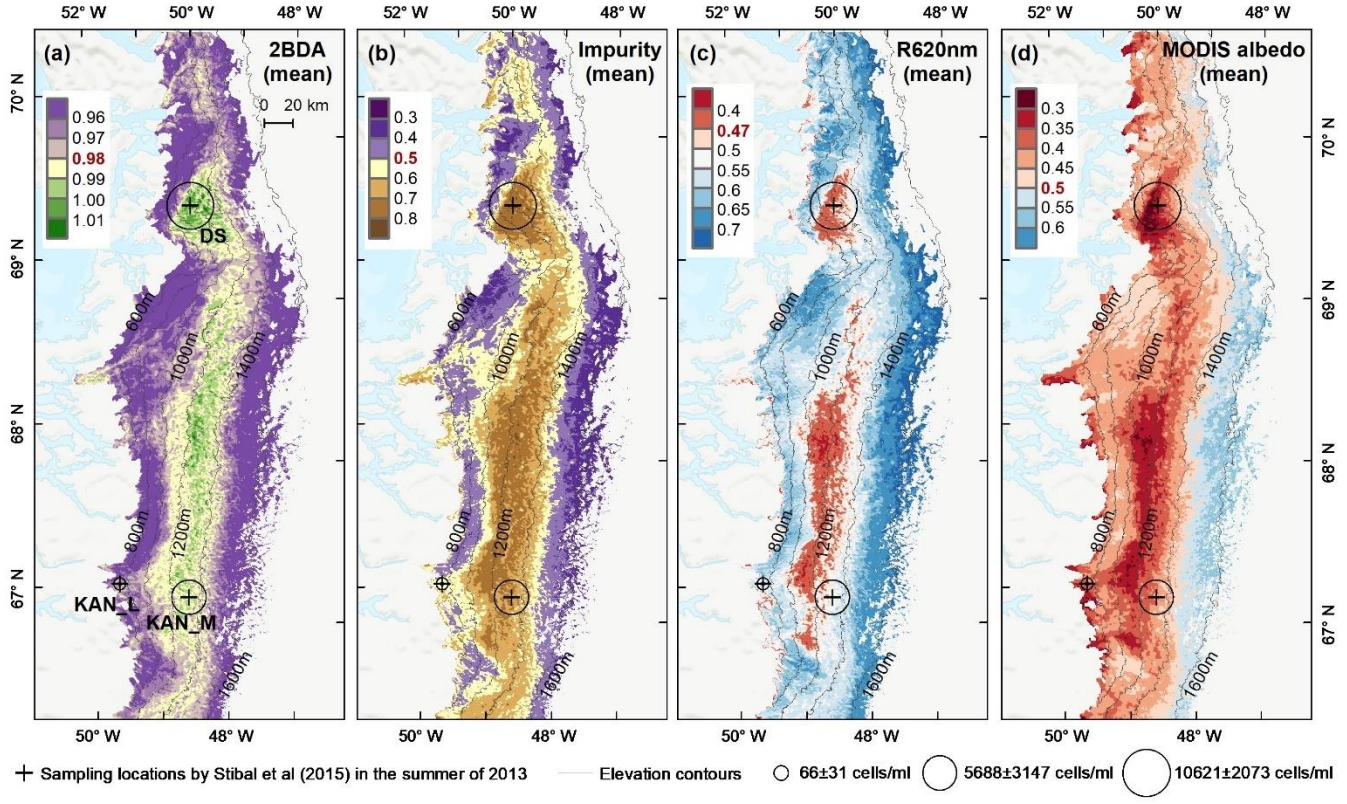

Figure ~~4:~~5. Spatial patterns of the mean 2BDA index (a), ~~Impurity~~impurity index (b), ~~surface~~ reflectance at 620 nm (c), and MODIS broadband albedo (d) over the bare ice zone during July and August from 2004 to 2011. The elevation contours illustrate the spatial variations of each variable with altitude. The cross labels show the spatial locations of the field sites DS, KAN_L, and KAN_M ~~measured by Stibal et al. (2015), along with the~~and magnitude ~~(circle labels)~~ of ~~ice~~glacier algal abundance ~~for each site.~~ (circle labels) measured by Stibal et al. (2015) in 2013.

4.24 Interannual ~~trends of ice algal blooms, impurity content, and surface albedo~~ variability

The annual time series (July-August mean) of the 2BDA index (Fig. ~~5a~~6a) and the ~~Impurity~~impurity index (Fig. ~~5b~~6b) show the interannual variability of algal abundance and impurity content, indicating a general increasing trend ~~of~~in bare ice area, algal abundance, and total impurity content ~~from~~between 2004 ~~to~~and 2011, particularly after 2006. The spatial extent of ~~ice~~glacier algae also expanded towards higher elevations (1200 m – 1400 m~~).~~) over this period. Between 2004 and 2011, the 2BDA index reached a maximum in 2010 when high air temperatures and intensive surface melt occurred over Greenland (Tedesco et al., 2011). The ~~Impurity~~impurity index ~~has~~exhibits similar interannual variability ~~to~~compared with the 2BDA index, but also exhibits different spatiotemporal variations between 1000~~ m~~ –1200 m and 1200~~ m~~ –1400 m ~~at~~in the middle ablation area. Figure A3 illustrates the interannual variability of the average 2BDA and impurity indices at different elevation levels (600-800m, 800-1000m, 1000-1200m, and 1200-1400m). In particular there are notable differences in variability of the 2BDA index between the 1000-1200m and 1200-1400m levels. The interannual variability of the 2BDA and ~~Impurity~~impurity indices is also coherent with variability in Greenland ice sheet-wide summer albedo, which was lowest in 2010 and highest in 2006 for the period 2004~~–~~–2011 (Tedesco et al., 2018).

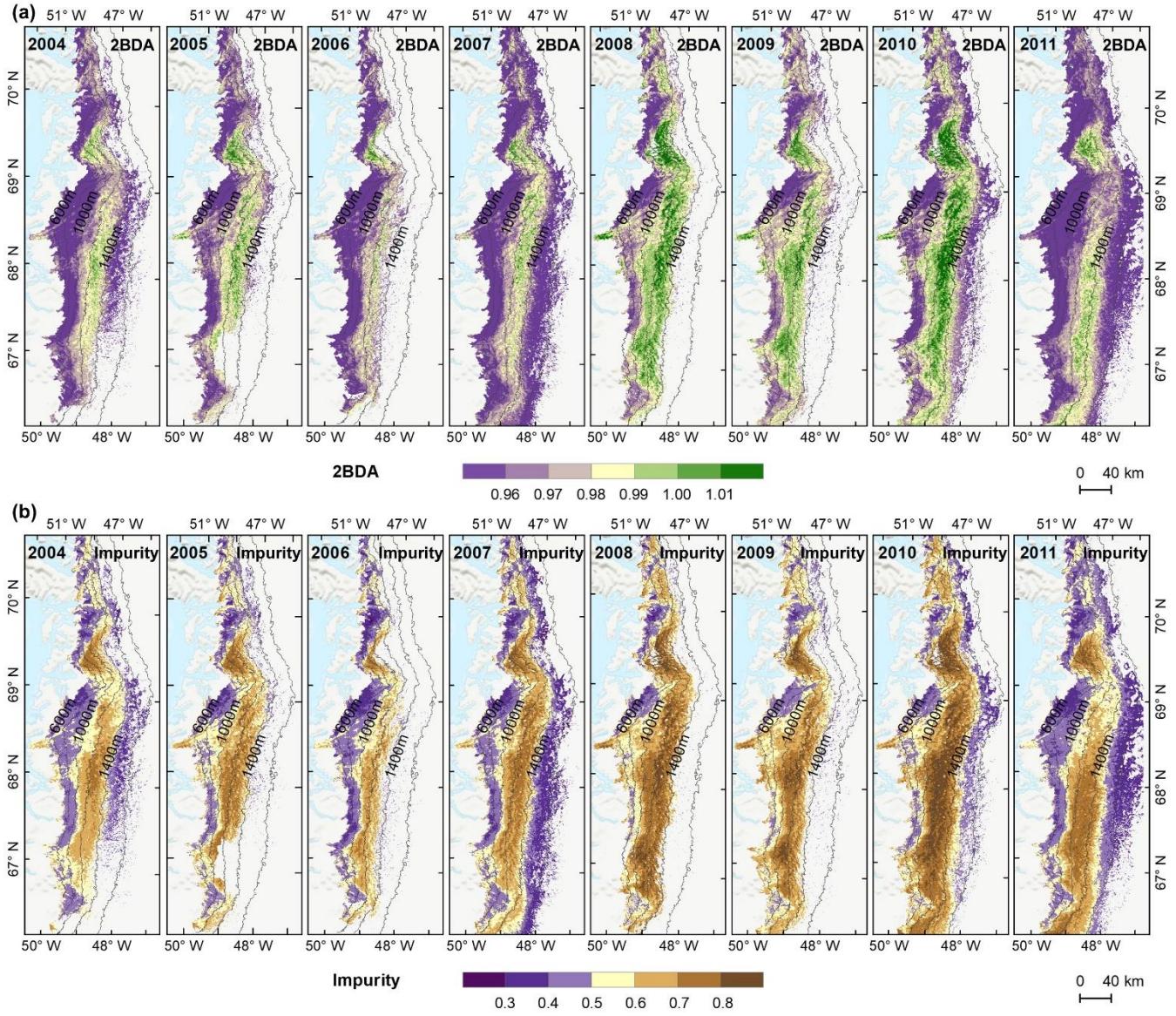

Figure ~~5:~~6. Maps of mean 2BDA index (a) and ~~Impurity~~impurity index (b) over July and August from 2004 to 2011.

We also calculated ~~the~~ interannual trends ~~of~~in the 2BDA index, ~~Impurity~~impurity index, and MODIS broadband albedo using linear regression analysis, with the mean 2BDA index, ~~Impurity~~impurity index, or MODIS albedo for each year as the dependent variable and the year as the independent variable. Pixels with observations during fewer than five years were discarded from the analysis. Figure ~~6~~7 shows the regression coefficients for 2BDA~~, Impurity~~ and impurity indices, and MODIS albedo vs. time~~, and the~~. The corresponding R^2 and P-value estimates are shown in Fig. ~~A1~~A4. There were two primary regions ~~(Fig. 6a)~~within our study area that ~~had~~exhibited significant increases in algal abundance from 2004 to 2011~~, including~~ (Fig. 7a), the DS region in the north and the southern region ~~between~~ (68.5°N ~~and~~ 66.5°N) between 1200 m and

1400 m in elevation. Other areas do not show statistically significant trends. The interannual trend of the ~~Impurity~~impurity index (Fig. ~~6b~~7b) shows a larger spatial extent with a significant increasing trend as compared with the 2BDA index. Figure ~~6c~~7c shows that the areas with increasing algal abundance and increasing impurity index also had significant albedo (July-August mean) reduction from 2004 to 2011. The albedo reduction was roughly -0.025~~~~ to -0.04 per year over the K-transect area (between 1200 m and 1400m in elevation) and within the DS area. The spatial patterns of declining albedo more closely ~~match~~resemble the patterns of impurity index as opposed to the 2BDA index, suggesting that the impurity index quantifies multiple processes related to surface darkening in addition to ~~ice~~glacier algae ~~cover~~.

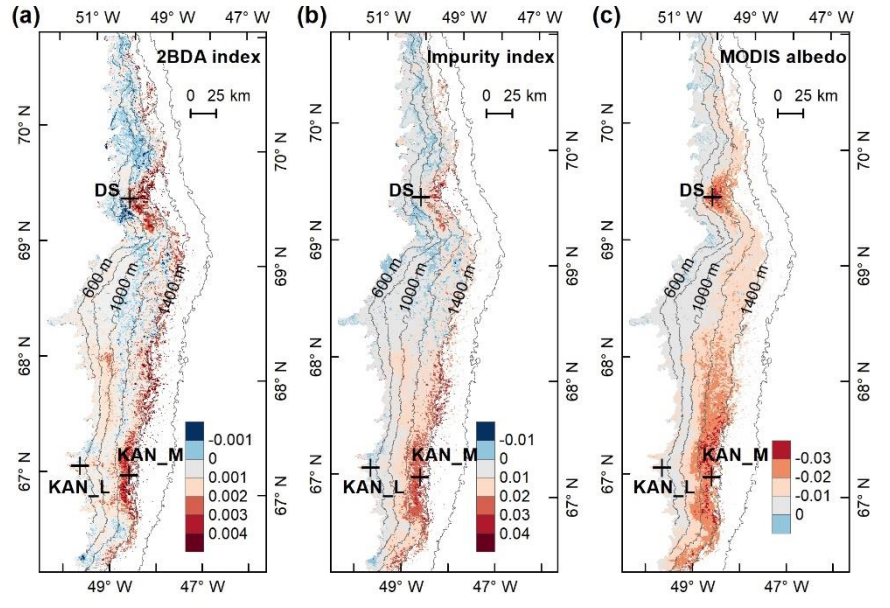

Figure ~~6:~~7. Interannual trends (regression coefficients with year) of the 2BDA index (a), Impurity index (b), and MODIS albedo (c) from 2004 to 2011.

4.~~3 Ice~~ 5 Seasonal trends of algal ~~development~~growth over ~~summer months of~~ July and August

To better understand seasonal dynamics of ~~ice~~glacier algae, we examined intra-annual trends in the 2BDA index during the months of July and August. We estimated the temporal trend of the 2BDA index from July to August for each MERIS pixel. For each pixel and each day, we calculated the average 2BDA index using the same ~~-~~day 2BDA indices of multiple years. To account for the differences between different years, we applied a temporal smoothing function with a window size of three days to the daily average 2BDA data. Pixels with more than 15 days of observations were kept for linear regression analysis, with the daily 2BDA index as the dependent variable and the time (~~day~~in days) as the independent variable. ~~Our results indicate that the 2BDA index can also capture the temporal dynamics of ice algal development during summer.~~

Figure ~~7 shows a comparison between~~ 8 illustrates the pattern of seasonal trends across the southwest Greenland ablation area. Figures 8b and 8c show the spatial distribution of seasonal trends across the area, while Fig. 8a shows examples of the

daily 2BDA time series ~~of the 2BDA index and the field measurements of ice algal abundance over the K-transect observation site (S6)~~ at ~~67° 04.779' N, 49° 24.077' W (Stibal et al., 2017). The field measurements were collected during the 2014 summer season. We calculated~~ the ~~mean algal abundance for each observation day~~three field sites KAN_L, KAN_M, and ~~converted it to cell doubling scale using~~DS. At the ~~logarithmic function. The daily 2BDA index (left axis in Fig. 7) was~~ ~~calculated by aggregating~~coastal KAN_L site, which had the ~~same day 2BDA indices of multiple years between 2004~~ lowest algal cell concentration (66 ± 31 cells/ml), the average 2BDA index is less than 0.98 during July and ~~2011. It~~August, and there is ~~shown that 2BDA index has coherent~~no significant temporal ~~trends~~trend. At the KAN_M and DS sites, with ~~the field measurements, particularly the~~ higher cell concentrations (5688±3147 and 10621±2073 cells/ml respectively), 2BDA values were mostly greater than 0.98, and there were significant increases in the 2BDA index during July and August (of 0.0004 and 0.0007 day^{-1} respectively), suggesting dramatic algal growth. The results indicate that the higher concentrations of algae are associated with a significant increasing trend ~~from~~ over the course of a season. Indeed, the highest seasonal trends in the middle ablation area (68.5°N-66.5°N) are found in the 1200 to 1400 m elevation band, also the region of highest 2BDA index.

The time series in Fig. 8a suggest that the period of algal growth at KAN_M occurred primarily between mid-July ~~to~~and mid-August~~.~~, beginning later than at the DS site. Between 20 July and 20 August, the regression slope was 0.0009 day^{-1} for both DS and KAN_M. This time window is consistent with the rapid algal colonization observed in field (Stibal et al., 2017; Williamson et al., 2018; Yallop et al., 2012; Lutz et al. ~~2018). A similar mid-July to mid-August increase was also found by Wang et al. (2018) using Sentinel-3 OLCI data.~~2018) and the patterns of temporal variability derived from Sentinel-3 data (Wang et al., 2018). To test whether higher growth rates later in the season were present across the region, we also examined region-wide trends between 20 July and 20 August (Fig. 8c). The magnitude of trends for the shorter period are higher over a broad region, and R^2 values are higher, indicating a shorter growth period across much of the region, with the exception of the area around the DS site in the north. We also explored the interannual variability of seasonal patterns over the DS and KAN_M sites (Fig. A5). Despite the interannual variations of 2BDA index, the regression slopes of 2BDA versus time (day) through mid-July to mid-August for different years were comparable to the slope of the aggregated time series between 2004 and 2011, particularly for the KAN_M site. Over the DS site, the algal growth rates were above-average during the growth seasons in 2005, 2009, and 2011 (Fig. A5). The DS site is located in lower elevations, where warmer temperatures may promote a faster growth rate.

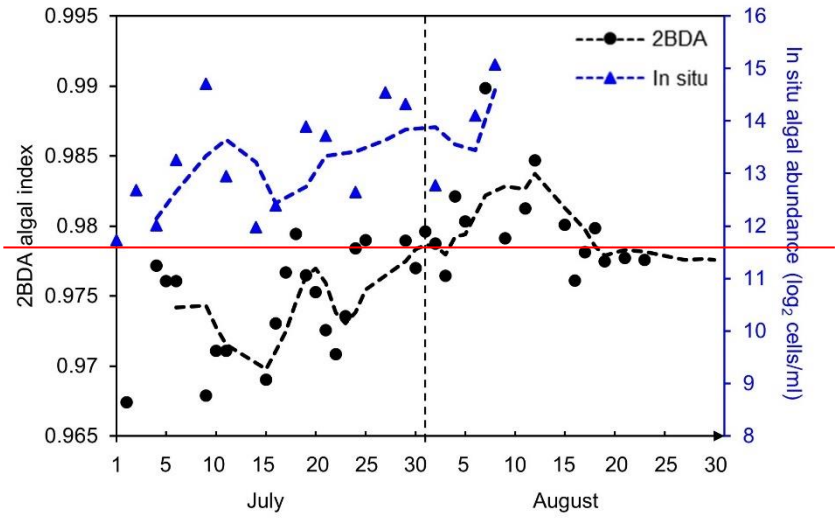

~~**Figure 7: The July-August time series of the 2BDA index (2004-2011) and the field measurements of ice algal abundance (2014) at the Stibal et al. (2017) field site S6.**~~

~~Figure 8a shows the daily 2BDA time series at the three field sites KAN_L, KAN_M, and DS, as examples of areas with different seasonal trend patterns, while Figs. 8b and c show the spatial distribution of seasonal trends across the west coast ablation area. The three field sites illustrate the temporal evolution of algal abundance. There was no significant temporal trend in 2BDA index at KAN_L, and the 2BDA index was less than 0.98 through July and August. In comparison, the 2BDA index at KAN_M and DS had statistically significant increasing trends with time, and the 2BDA values were mostly greater than 0.98, indicating that dramatic algal growth occurred at KAN_M and DS through the summer season. This pattern is highly consistent with the measured ice algal abundance during the 2013 summer (Stibal et al., 2015). The site KAN_L had fewer ice algal cells (66±31 cells/ml) than the sites KAN_M (5688±3147 cells/ml) and DS (10621±2073 cells/ml), and ice algal blooms appeared to be more intense at DS than KAN_M. The time series in Fig. 8a suggest that the period of algal growth at the KAN_M occurred primarily between mid July and mid August, with the start of growth occurring later than at the DS site. Between 20 July and 20 August, the regression coefficient was 0.0009 day^{-1} for both DS and KAN_M, suggesting a nearly constant growth rate during the fast proliferation stage of ice algae. Throughout July and August, the regression coefficient was 0.0007 and 0.0004 for DS and KAN_M, respectively. To test whether this period of algal growth was consistent, across the region, we calculated temporal trends for 20 July–20 August (Fig. 8c). The magnitude of trends is larger for this period and R^2 values are higher over a broader region, suggesting that this shorter period of growth occurs over a wide region. In the DS region, however, the R^2 values and magnitude of trends are similar for the two periods, indicating that the growth period is longer in the DS region relative to other areas (consistent with the KAN_M vs. DS time series).~~

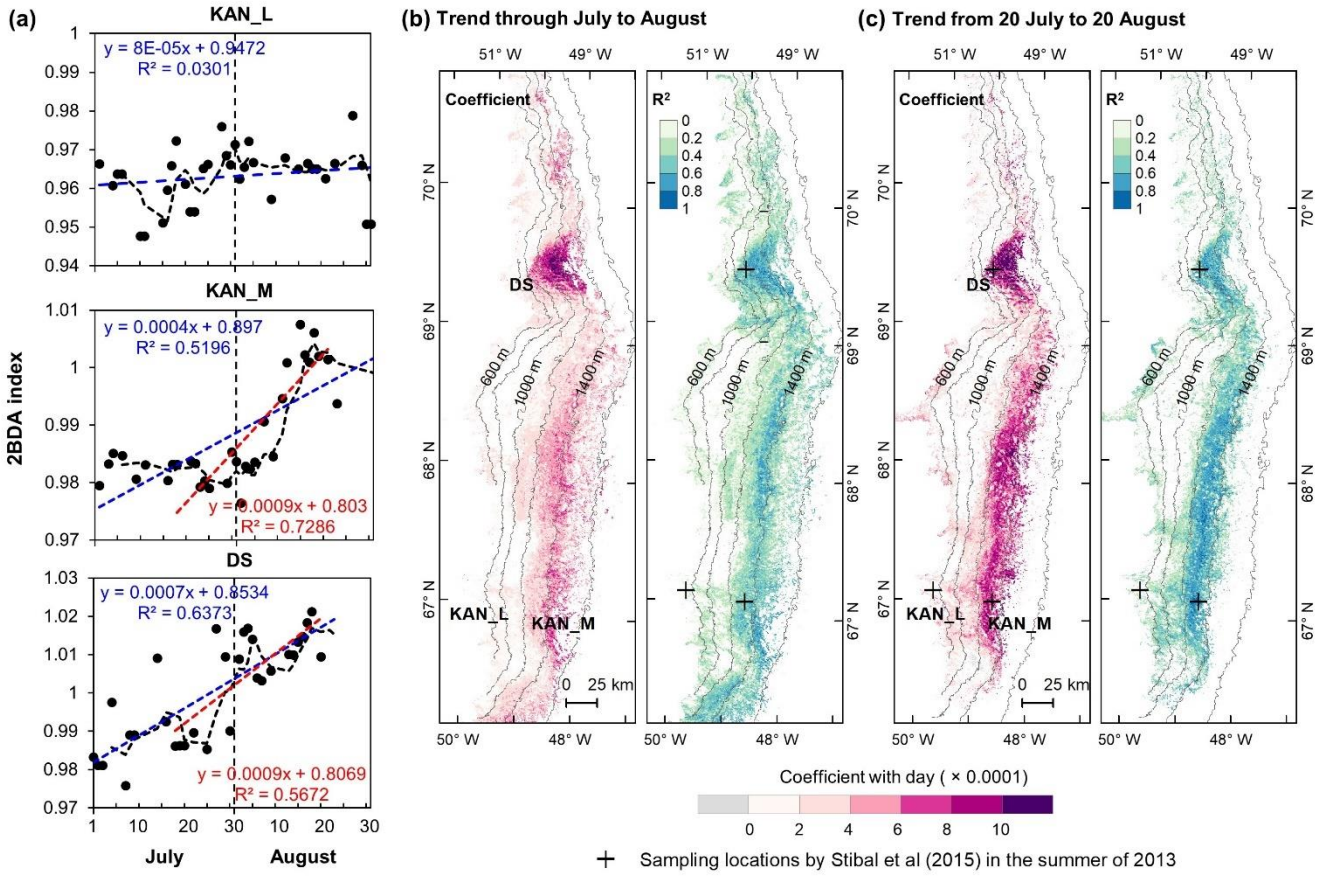

Figure 8~~.~~. Temporal trends of the 2BDA index over July and August. (a) 2BDA time series and temporal trend analysis over the KAN_L, KAN_M, and DS sites. (b) Regression ~~coefficients~~slope and R^2 estimates of the temporal trend analysis for the period of July–August~~.~~ (for areas where the p value <=0.05). (c) Regression ~~coefficients~~slope and R^2 estimates of the temporal trend analysis for the period of 20 July–20 August~~.~~ (for areas where the p value <=0.05).

To make our estimates ~~more~~ comparable to previous studies, we calculated the algal population doubling time ~~for~~from the ~~different regression coefficients of~~seasonal trends in the 2BDA index ~~with time~~. Wang et al. (2018) derived an empirical relationship between the Sentinel-3 OLCI reflectance ratio R_{709nm}/R_{673nm} and the ~~ice algal abundance,~~glacier algal abundance (Stibal et al., 2015; Williamson et al., 2018) using an exponential fit. The empirical relationship is represented as

$$y=10^{-35}\, e^{87.015x} \quad (3)$$

where x denotes the reflectance ratio and y denotes the algal abundance (cells/ml). Given the similarity between the OLCI and MERIS band configurations and the negligible differences between the 673 nm and 665 nm reflectance, we used Eq. (3) to derive the relationship between the MERIS 2BDA index (x) and algal population doubling ~~($\log_2 y$ cells/ml) as~~level ($\log_2 y$ cells/ml, i.e. the number of times the observed number of cells has doubled). Taking the base-2 logarithm of Eq. (3) gives the equation:

$$\log_2 y = \log_2 e * 87.015 * x - 35 * \log_2 10 \quad (4)$$

~~Therefore, based on the regression coefficient (denoted as *a*) of 2BDA versus time, the algal population doubling time can be approximated as 1 / ($\log_2 e$ * 87.015 * *a*), as~~The algal population doubling time can then be derived by examining the regression coefficient (denoted as *a*) of 2BDA versus time, which gives the rate of change of 2BDA with time (*dx/dt*). From Eq. (4), the rate of change of population doubling with respect to the 2BDA index ($dlog_2y/dx$) is $\log_2 e$ * 87.015. Combining $dlog_2y/dx$ with the regression coefficient *a* (*dx/dt*) the change in population doubling level with time ($dlog_2y/dt$) is $\log_2 e$ * 87.015 * a, and the time for one algal population doubling is therefore estimated as 1 / ($\log_2 e$ * 87.015 * *a*). Values of population doubling time corresponding to various values of *a* are listed in Table 3. The areas with significant algal growth trend (R^2>0.5) between 20 July and 20 August (Fig. 8c) had a mean regression coefficient of 0.00076±0.0002, ~~and~~corresponding to a mean algal population doubling time of 11.2±2.6 days. The DS area had faster algal growth rate than other areas, ~~which was estimated to be~~with a doubling time of 9.6±2.7 days. This estimate is comparable to the field study by Williamson et al. (2018) who reported a doubling time of 7.18±1.04 days for algae-abundant ice (at the K-transect).

Table 3. Algal population doubling time for different regression coefficients of 2BDA index with day

Regression coefficient	Population doubling time (days)
0.0004	19.91
0.0005	15.93
0.0006	13.28
0.0007	11.38
0.0008	9.96
0.0009	8.85
0.~~001~~0010	7.97
0.0015	5.31
0.0020	3.98

4.~~4~~6 Impact of ~~ice~~glacier algal blooms on surface albedo in July and August

~~We~~To investigate potential impact of algal changes on albedo variability, we quantified the ~~impact of ice~~relationship between glacier algal blooms ~~on~~and surface albedo in July and August based on the daily time series data of the 2BDA index and MODIS broadband albedo. ~~Similar to deriving the July-August trend of 2BDA index, we generated a~~A daily albedo time series ~~after~~obtained by averaging and smoothing the MODIS daily albedo data from 2004 to 2011~~.~~ was derived using the same method for deriving the 2BDA seasonal trends. Figure 9 shows the derived temporal trends ~~of~~in MODIS albedo from 1 July to 20 August. The days after 20 August were excluded from the analysis since snowfalls often ~~happened~~happen in late August. The DS area had the most significant albedo reduction over July and August, up to 0.4~0.6% per day. In the middle

ablation zone between the altitudes of 1000 m and 1200 m the albedo reduction rate was 0.2~0.4% per day, and the reduction rate was 0.2~0.3% per day in the zone between 1200 m and 1400 m in elevation.

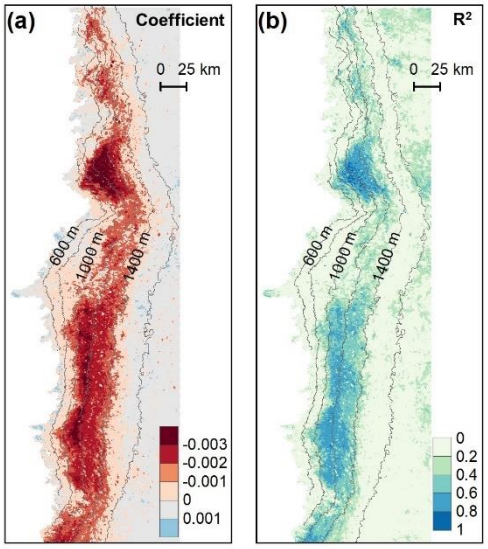

Figure 9~~:~~. Temporal trends ~~of~~in MODIS broadband albedo ~~in~~during July and August~~.~~ (over 2004-2011). (a) Regression coefficients of surface albedo with time (day) from 1 July to 20 August. (b) Corresponding R^2 estimates.

We converted the 2BDA index (x) to the algal population doubling level ($\log_2 y$) using the derived Eq. (4) in section 4.~~3~~5. Figure 10 shows results of a regression analysis for algal population doubling vs. surface albedo. The analysis shows a statistically significant correlation between algal growth and albedo reduction at the DS area between the altitudes of 800 m and 1200 m, the middle ablation zone between the altitudes of 1200 m and 1400 m, and the 1000–1200 m area nearby the K-transect. Over these areas, the regression coefficient ranged between -0.04 to -0.02, indicating a surface albedo decrease of 2~4% for each algal population doubling. This estimate is comparable to results from the field study by Stibal et al. (2017) who estimated a net albedo reduction of 0.038±0.0035 for each algal population doubling based on ~~the~~ in-situ measurements of ~~ice~~glacier algal abundance and coincident surface albedo. In general, ~~ice~~glacier algal growth explains most of the temporal variability of surface albedo in July and August between 1000 and 1400 m in elevation, except the middle area between 1000 m and 1200 m in elevation where ~~there are probably~~ other factors ~~contributing~~likely contribute to the observed albedo reduction.

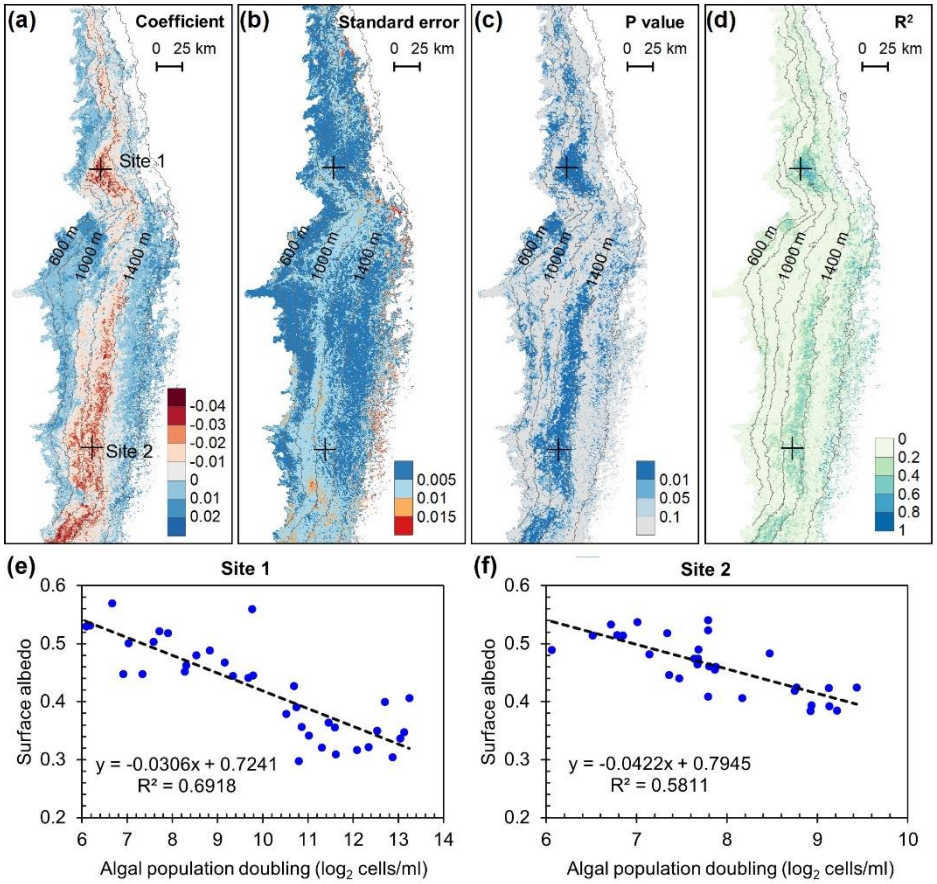

Figure 10~~:~~. Relationship between algal population doubling and surface albedo. (a) Regression coefficients. (b) Standard errors of the correlation coefficients. (c) P values. (d) R^2 values. (e) and (f) show algal population doubling versus surface albedo at Site 1 and Site 2, respectively.

5 Discussion

~~In this study, we demonstrated that MERIS data can be used for characterization of the spatial distribution and temporal dynamics of ice algal blooms in southwest Greenland. This enables the construction of a long-term time series data of ice algae in combination with the new-generation satellite sensor Sentinel-3 OLCI in the future. Despite the moderate spatial resolution of the MERIS sensor, its narrow bandwidths and specific band wavelengths designed for chlorophyll make the MERIS archive data a powerful tool to study the spatiotemporal variability of algal communities in supraglacial environment. The chlorophyll signal of ice algae presented in the MERIS spectra is very consistent with the coincident (nearly) WorldView-2 data and the field hyperspectral measurements collected over algae-abundant ice. Similar to the Sentinel-3 OLCI ratio index R_{709nm}/R_{673nm}, the MERIS 2BDA index R_{709nm}/R_{665nm} can effectively quantify the algal growth pattern through July to August. This ratio index is further supported by a very recent study (Cook et al., 2019) which shows~~

~~that the ratio of the reflectance peak at 709 nm relative to 665 nm increases with ice algal abundance based on the field measurements of algal abundance and coincident reflectance spectra.~~

5.1 Sensitivity to subpixel variability

In this study, we utilized the chlorophyll-a signal generated by glacier algae in the red-NIR region (Fig. 2d) to quantify the spatiotemporal variability of glacier algae at a regional scale for the summer seasons of 2004-2011 in southwest Greenland. The specific wavelengths and narrow bandwidths of MERIS designed for chlorophyll-a detection make MERIS archive data a powerful tool for studying supraglacial algal communities. The chlorophyll-a signal present in the MERIS spectra is consistent with (nearly) coincident WorldView-2 data and hyperspectral field measurements collected over dark ice with high algal abundance (Fig. 2d). Similar to the Sentinel-3 OLCI ratio index R_{709nm}/R_{673nm}, the MERIS 2BDA index R_{709nm}/R_{665nm} can effectively quantify the algal growth pattern during July and August (Fig. 8). Using SNICAR simulations, we examined the potential impact of dust on the 2BDA index. The comparison between SNICAR simulations and MERIS ratio indices indicates a high sensitivity of the 2BDA index to glacier algae as compared to dust (Fig. 4). Here we explore the sensitivity of the 2BDA index to subpixel variability using a linear mixing method based on the field spectral measurements of Cook et al. (2020) and the SNICAR-simulated spectra for dust (size 4 with a concentration of 500 ppm). The spectra used for linear mixing experiments are shown in Fig. C3a. By specifying the areal percentage of the impurity-covered (algae or dust) surface at subpixel scale, we calculated the mixed spectra by linearly combining the algae (four samples with different measured algal abundance) or dust spectra (SNICAR-simulated) with the bare ice spectrum (measured algal abundance as 0) weighted by areal percentage. Figure C3b shows the 2BDA index calculated from the mixed spectra varying with the areal percentage of algae or dust at the subpixel scale. It is shown that the 2BDA index dramatically increases with the areal percentage of glacier algae, being consistent with the positive correlation between the 2BDA index and algal abundance. In contrast, the 2BDA index is much less sensitive to dust areal coverage. The results indicate that even with sub-pixel variability of surface materials, the satellite-derived 2BDA index is still strongly sensitive to the presence of algae. High-resolution UAV mapping by Ryan et al. (2018) suggests that the areal percentage of distributed impurities is up to 65%~95% within individual MODIS pixels (500-meter resolution) over the dark zone in southwest Greenland, indicating that a high sub-pixel areal percentage of algae is possible. Our linear mixing experiments (Fig. 3Cb) indicate that the relatively high 2BDA values derived from satellite are unlikely to be achieved without the presence of glacier algae, and that the MERIS 2BDA index can effectively capture the glacier algae variability, especially within the dark zone.

5.2 Relationship between regional climate model albedo bias and glacier algae

Our analysis ~~indicates~~suggests that surface albedo decreases by 0.02~0.04 for each algal population doubling during July and August primarily in algae-abundant areas close to the Jakobshavn Isbrae Glacier and within the middle ablation zone (68.5°N-66.5°N) between 1200 m and 1400 m in elevation. It is also important to know whether the MERIS 2BDA index could explain the discrepancy between the satellite-measured albedo and ~~climate model~~bare ice albedo~~,~~ in climate models

which ~~is fundamental to improve~~do not currently simulate the ~~albedo scheme and surface energy budget estimates in~~ effects of biology and other impurities. The MAR regional climate ~~models like MAR. Previous studies~~model, for instance, exhibits a positive albedo bias along the southwestern Greenland ice sheet margin because of this (e.g. Alexander et al., 2014~~) have demonstrated a positive albedo bias of MAR in comparison with the MODIS albedo along the southwest Greenland Ice Sheet, which results from the fact that the algae and other impurities are not yet included in the albedo scheme.~~). Figure 11a shows ~~the~~a comparison between MODIS albedo and MAR albedo over the study area (including both bare ice and snow), indicating the overestimation of MAR albedo for the dark areas with MODIS albedo less than 0.5. There ~~was~~is a significant negative correlation between the albedo difference (MODIS albedo minus MAR albedo) and the 2BDA index (Fig. 11b), ~~which means~~indicating that the positive MAR albedo bias increases with ~~the~~ algal abundance.

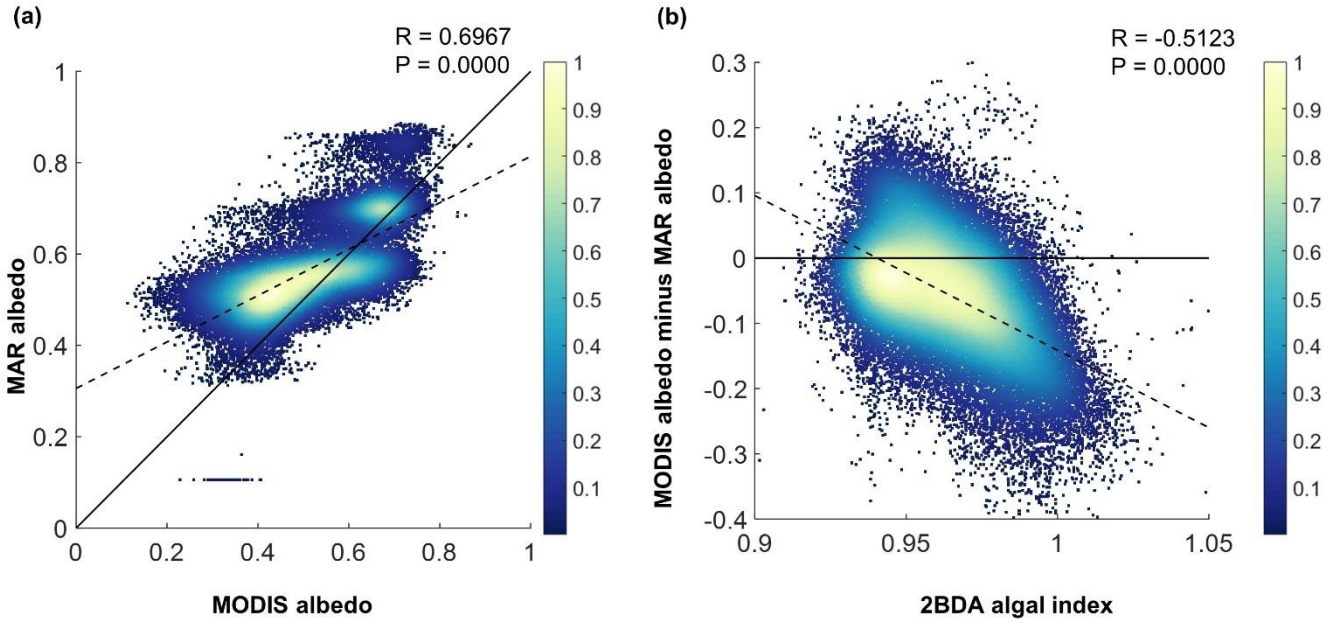

Figure 11~~:~~. (a) Comparison between MAR albedo and MODIS albedo over the study area for July and August from 2004 to 2011. The dashed line ~~and equation show~~shows the linear ~~fitting~~fit between MODIS albedo and MAR albedo. The black line is the 1:1 reference line. (b) Relationship between the MERIS 2BDA index and the albedo difference between MODIS and MAR~~,~~ with the dashed-line showing the linear fit. The colour scheme in both (a) and (b) illustrates the relative data distribution density (yellow means higher density, and blue means lower density).

The spatial pattern of the MAR albedo bias (Fig. 12a) is consistent with the satellite-derived impurity distribution~~.~~ (e.g. Fig. 5b). Over the dark areas, the MAR albedo was overestimated by 0.16±0.03 as compared to the MODIS albedo. We further examined the relationship between the albedo bias (MODIS albedo minus MAR albedo) and the algal population for the seasonal trend between 1 July and 20 August, finding a significant correlation ~~between them~~ in the DS ~~area (Fig~~site region (Figs. 12b ~~and Fig.~~, 12c, 12d). Figure 12d indicates that each population doubling can explain a -0.0274 bias between the

MODIS and MAR albedos~~. Although there are also negative correlations between the algal population and the MODIS-MAR albedo difference like Fig. 12d~~ at the DS site. In comparison, the albedo bias in the middle zone between 1000 m and 1400 m~~, the correlations are~~ is less ~~significant as compared to the DS area.~~well-explained by glacier algae. This is partially consistent with our previous analysis that the albedo reduction at 1000 m~~–~~–1200 m is poorly related to algal growth. Between 1200 m and 1400 m the correlation between the derived algal population and the MAR bias is not strong (Fig. 12c) even though there is a fairly strong correlation between algal population and MODIS albedo. This suggests that in this area, although MAR does not include the effects of algae, the decrease in albedo associated with liquid water ponding in MAR may approximate the trends associated with increasing algae concentrations. In addition to parameterizing ~~the ice~~glacier algal growth, other processes related to albedo reduction ~~caused by impurities~~ such as consolidation of impurities melted from snow should be also accounted for in the future.

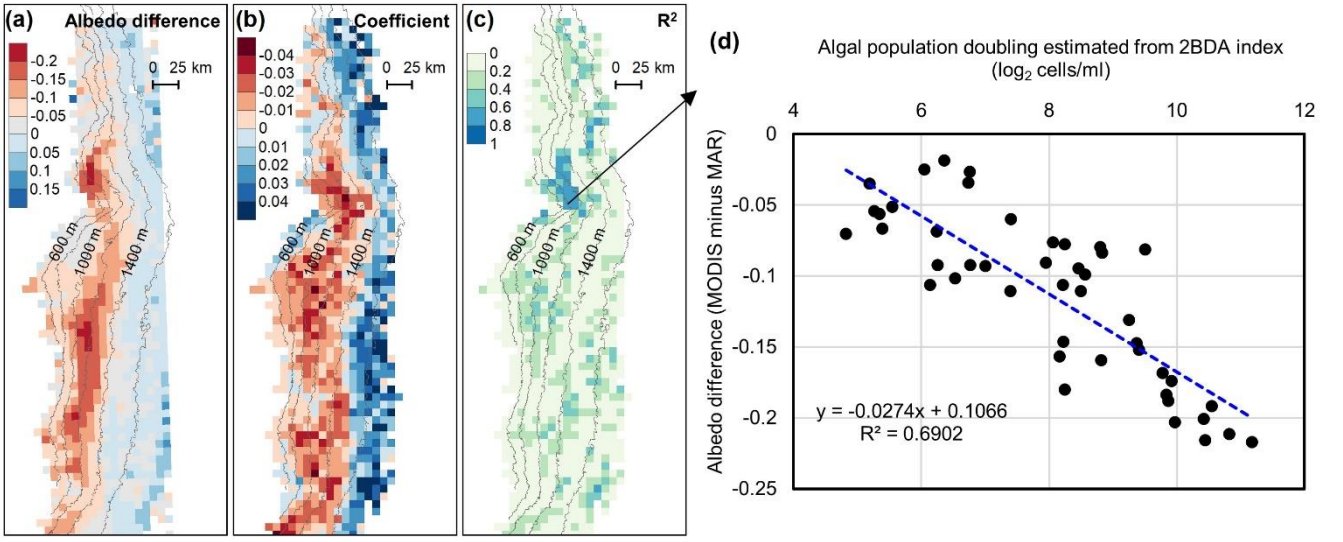

Figure 12~~:~~. (a) Albedo difference between MODIS albedo and MAR albedo (MODIS albedo minus MAR albedo) averaged over the study period. (b) Regression coefficients of albedo difference with 2BDA-derived algal population doubling (log_2 cells/ml). (c) R^2 estimates for the regression analysis. (d) Scatterplot of albedo difference versus algal population doubling over the DS algae-abundant area and the ~~linear fitting~~ equation for the linear fit.

5.3 Potential drivers for glacier algae variability

Due to the ~~increasing trend~~ impact of ~~ice~~glacier algal blooms ~~and their significant impact~~ on bare ice albedo, it is fundamental to understand the factors affecting ~~the~~ algal growth. Lutz et al. (2018) analysed the composition of ~~ice~~glacier algal communities near the K-transect between 27 July and 14 August 2016 using high-throughput sequencing and subsequent oligotyping techniques. The ~~ice~~glacier algae species of Ancylonema nordenskiöldii and Mesotaenium berggrenii were found as the dominant taxa. ~~Ice~~Glacier algae lack a flagellated stage and are less capable of migrating upwards to snow

layers at the beginning of melting season (Anesio et al., 2017). Therefore, ~~the ice~~glacier algal growth is restricted to the bare ice surface, which is consistent with our finding that ~~ice~~glacier algal blooms tend to occur extensively from late-July to mid-August when the bare ice is ~~mostly~~ exposed ~~and less affected by snowfalls. The~~. However, somewhat paradoxically, the areas at lower altitude have longer duration of bare ice exposure, whereas intense ~~ice~~glacier algal blooms occur at higher altitude up to 1200 ~~m~~ -1400 m along the middle ablation zone. ~~The~~ One possible reason for this discrepancy could be that the growth of ~~ice~~glacier algae ~~also depends on the availability of~~ is influenced by liquid water ~~and nutrients in addition to the surface habitat of bare ice. Particulates melted from ancient ice layers have been suggested to be an important nutrient source for ice algae growth (Stibal~~(e.g. Tedstone et al., 2017~~; Wientjes et al., 2012).~~) and nutrient availability. Although liquid water is a prerequisite for algal growth, Wang et al. (2018) found a negative correlation between algal abundance and meltwater production, which was attributed to hydrological flushing of algae during periods of excessive meltwater and surface runoff (Takeuchi, 2001; Uetake et al., 2010). ~~Figure 13a-b show~~These results do not contradict the importance of liquid water to algal growth as indicated by Tedstone et al. (2017), but rather suggest that there is an optimal amount of melt that may be required to support algal growth, with too little or too much melt resulting in lower algal concentrations.

To examine potential drivers of algal growth, we explored the relationships between the 2BDA index and ~~the~~ topographic variables as well as ~~the~~ near surface temperature and meltwater production simulated by MAR~~. For each two variables, we separated~~ (Fig. B1), by separating the data into two-dimensional bins and ~~calculated~~calculating the average 2BDA index for each bin. ~~It is suggested~~The comparison suggests that ~~ice~~glacier algae are mostly distributed over flat areas with ~~less~~fewer topographic undulations (Fig. ~~13a~~B1a). The areas suitable for ~~ice~~glacier algal growth have moderate but not excessive melting ~~conditions~~ (Fig. ~~13b~~B1b). This further supports the hypothesis that ~~active hydrological processes have~~high melt has a negative effect on algal development. In regard to the suitable temperature, ~~ice~~glacier algae are so far known to be well adapted to ~~the temperature~~temperatures close to ~~the freezing point of water~~ 0°C (Anesio et al., 2017). Although no significant correlations have been found between algal abundance and air temperature, ~~the algal growth appears to be affected by cold freezing temperatures as suggested by Fig. B1 which~~Figure B2 shows ~~the daily simulated near surface temperature along with the~~ dips in ~~situ~~ measured daily algal abundance (Stibal et al~~.~~., 2017) coinciding with below-freezing near-surface MAR-simulated daily air temperatures at the K-transect S6 station ~~in~~during the 2014 summer~~. Figure 13c-e show~~, suggesting that freezing temperatures negatively impact algal growth.

We also examined interannual variations in climate variables in relation to the 2BDA index. Figure 13 shows the MAR-simulated shortwave and longwave downward radiation fluxes, cloud cover, snowfall, rainfall, meltwater production, and near surface air temperature averaged over July and August across the study area from 2004 to 2011. The high 2BDA algal index ~~in~~during 2008-2010 (Fig. 5a and Fig. 13a) coincides with ~~less~~reduced cloud cover and ~~more~~higher incoming shortwave radiation (Fig. ~~13c~~13b). This period is also characterized by less ~~rainfalls~~rainfall (Fig. ~~13d~~13c), reducing the possibility of hydro-flushing ~~possibility. .~~ Figure ~~13e~~13d shows that the high algal index years of 2008 and 2009 ~~with high algal index had~~exhibited less melting and lower temperature than the other years, suggesting that ~~meltwater production and air temperature~~ these variables may play a less ~~dominant~~important role in algal growth than shortwave radiation ~~in ice algal~~

~~development.~~. Given the importance of shortwave radiation for photosynthesis of ~~ice~~glacier algae, ~~we argue~~the results suggest that air temperature, surface melt, and bare ice exposure ~~are~~may be important factors at the beginning stage of ~~ice~~glacier algal habitat development, while downward shortwave radiation ~~has a primary control on~~could be most important during the proliferation stage ~~of ice algae.~~. These dynamics ~~may relate to the~~could be influenced by recent atmospheric circulation ~~change~~changes in Greenland, with patterns of anomalous anticyclonic circulation and higher 500 hPa geopotential height becoming more frequent (e.g. Hanna et al., 2016; Mioduszewski et al., 2016), associated with reduced cloud cover (Hofer et al., ~~2016~~2017) and increased downward shortwave radiation. ~~Therefore~~However, more research is required to fully understand these relationships and quantify the effects of various factors on glacier algal growth. In the context of future ice sheet change, it is therefore vital to understand the interactions between the supraglacial microbiome and climate change (Cavicchioli et al., 2019) for better projection of future ice sheet mass balance.

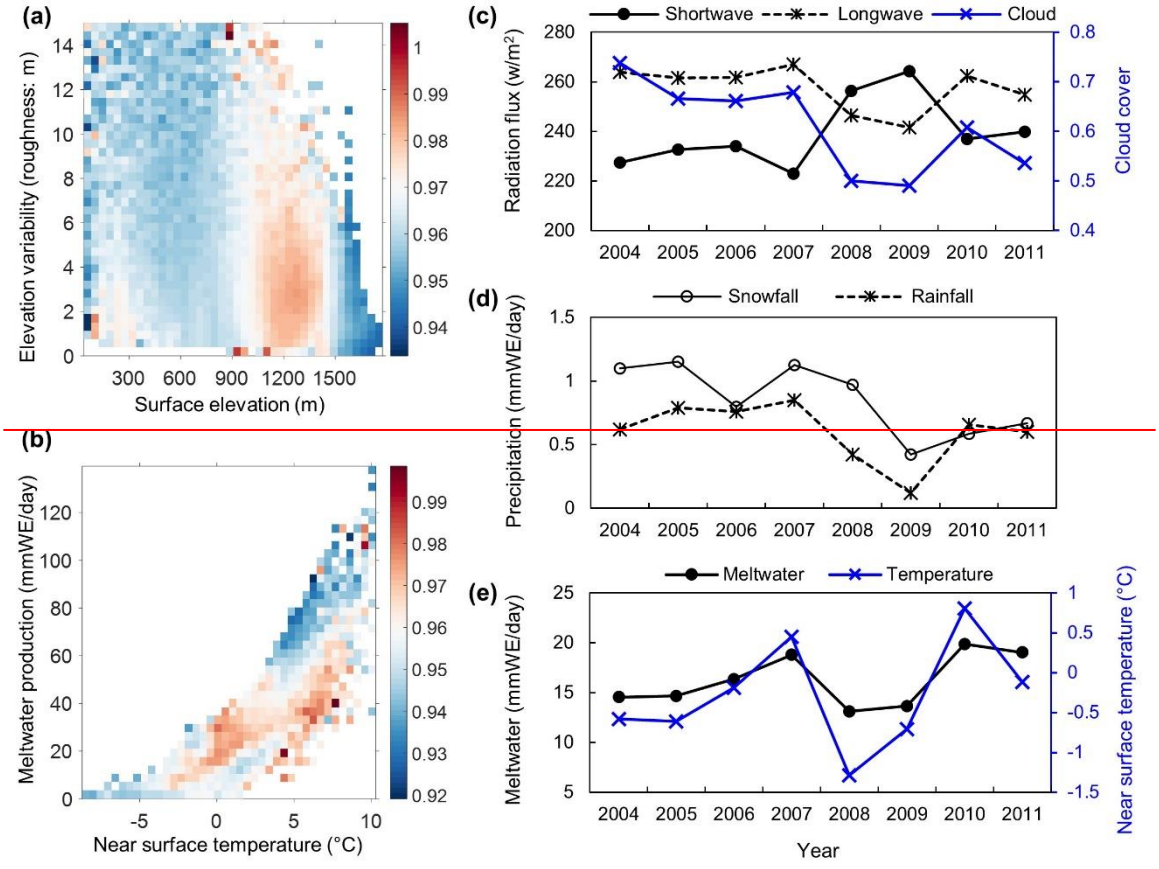

~~Figure 13:~~

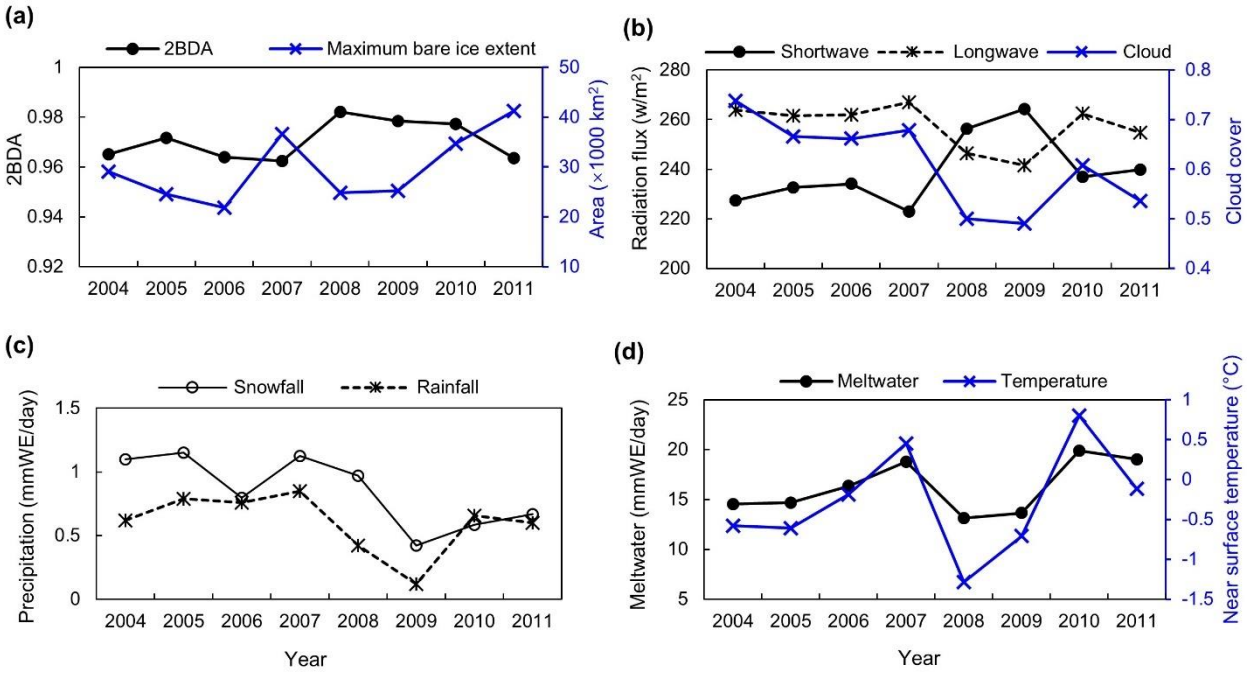

Figure 13. (a) Average 2BDA index over bare ice and maximum bare ice area from 2004 to 2011 (MERIS). (b ~~(a) 2BDA index versus surface elevation and roughness (elevation variability within each MERIS pixel). (b) 2BDA index versus near surface temperature and meltwater production simulated by MAR. The colour bars in (a) and (b) indicate the average 2BDA index for each two-dimensional bin defined by the two variables on horizontal and vertical axis. (c~~) July-August mean of downward shortwave and longwave radiation fluxes and cloud cover over the study area from 2004 to 2011~~.~~ (MAR). (c) July-August mean of rainfall and snowfall (MAR). (d) July-August mean of ~~rainfall and snowfall. (e) July-August mean of~~ meltwater production and near surface temperature~~.~~ (MAR).

6 Conclusions

We examined the spatiotemporal variability of ~~ice~~glacier algal blooms in southwest Greenland during July and August from 2004 to 2011 using the chlorophyll-a detection capability of MERIS. We calculated a number of remote sensing ratio indices including chlorophyll-a indices and the impurity index. The results indicate that similar to the Sentinel-3 OLCI ratio index of R_{709nm}/R_{673nm}, the MERIS 2BDA index of R_{709nm}/R_{665nm} can effectively quantify the spatial distribution and seasonal growth pattern of ~~ice~~glacier algae, with results highly consistent with field measurements. There was an increasing trend of ~~ice~~glacier algal abundance and impurity content at the dark area close to Jakobshavn Isbrae Glacier and the area close to K-transect at altitude of 1200 m~~—~~–1400 m, ~~being coherent~~in conjunction with ~~the reducing~~a declining trend of surface albedo ~~in this~~over the 2004 to 2011 period. We quantified the impact of ~~ice~~glacier algal growth on surface albedo over July and August, and found that each algal population doubling ~~would decrease~~decreases the surface albedo by 2~4 percent. Our analysis points to the great potential of using ~~the~~ satellite ratio ~~index~~indices to parameterize the impact of ~~ice~~glacier algae on

surface albedo ~~and~~, thereby reducing the albedo bias in regional climate models. Nevertheless, the surface darkening along the middle ablation zone between 1000 m and 1200 m in elevation cannot be well explained by algal growth, indicating that other processes related to surface darkening need further investigation and quantification. Future research should also be directed toward understanding the climate drivers of ~~ice~~glacier algae variability and parameterizing their ~~growing~~growth dynamics using regional climate model outputs.

Data availability

~~The~~ MERIS level-2 data are available at the MERCI file archive (https://merisfrs-merci-ds.eo.esa.int/), courtesy of the European Space Agency. ~~The~~ MODIS MOD09GA and MOD10A1 data can be accessed from the NASA Land Processes Distributed Active Archive Center (https://search.earthdata.nasa.gov/). ~~The~~ WorldView-2 imagery were provided by the Polar Geospatial Center (PGC, https://www.pgc.umn.edu/) at the University of Minnesota. MAR v3.9.3 outputs are available at ftp://ftp.climato.be/fettweis/.MARv3.9.3. -

Appendix A

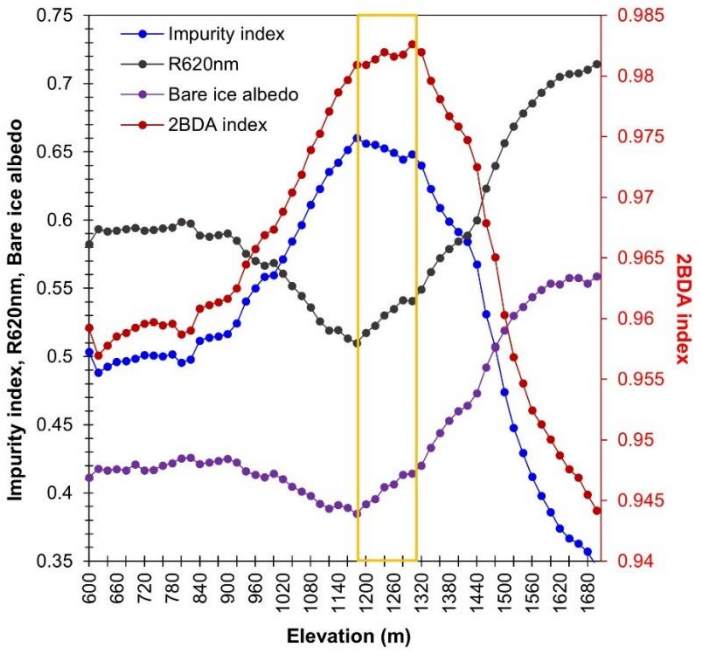

Figure A1. Spatial variations of the average 2BDA index, impurity index, 620 nm reflectance, and MODIS albedo over bare ice at different elevations within the study area (20-meter elevation interval). For surface elevation, we used the 30-meter resolution MEaSUREs Greenland Ice Mapping Project (GIMP) Digital Elevation Model (Howat et al., 2014; 2015).

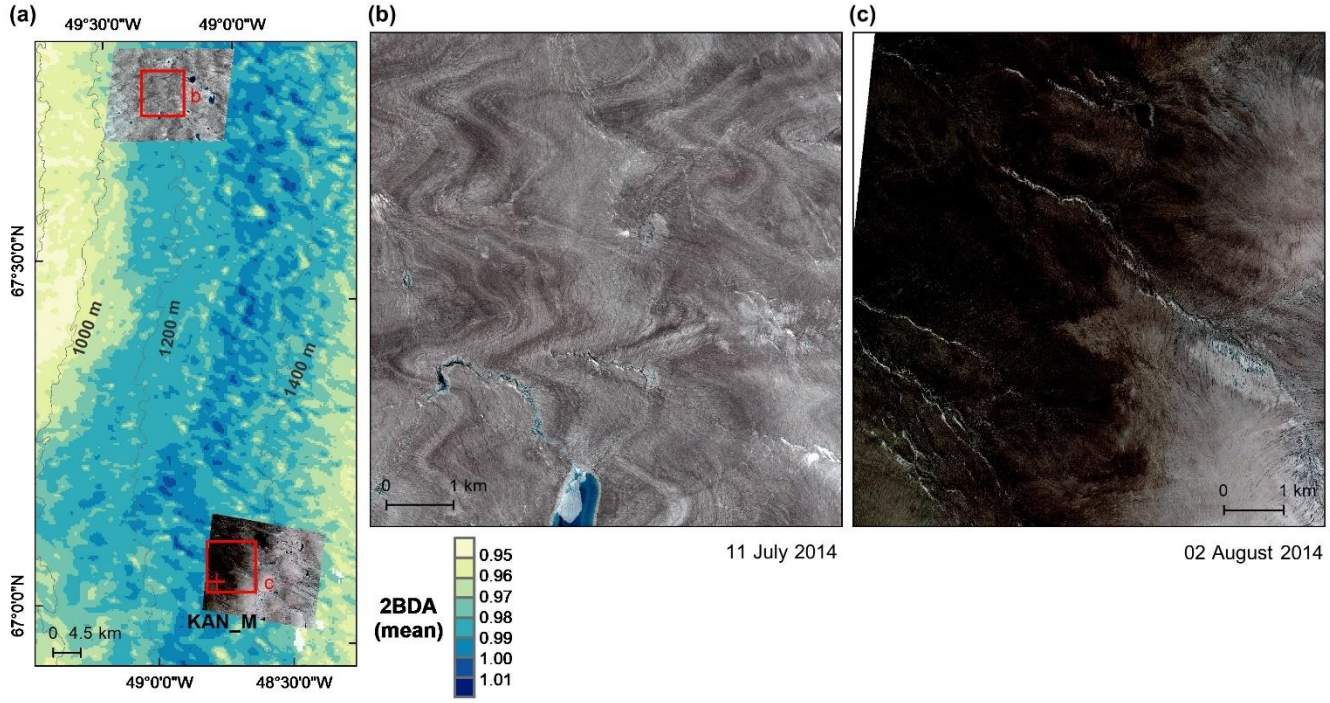

Figure A2. Average 2BDA index (2004-2011) for a subset of our study area (a) and comparison between WorldView-2 imagery over a dark ice site with low 2BDA index at 1000-1200m elevation (b) and a dark ice site with high 2BDA index at 1200-1400m elevation (c). The WorldView-2 image in (b) illustrates the 'wavy' pattern that Wientjes and Oerlemans (2010) suggested was caused by ancient ice outcropping.

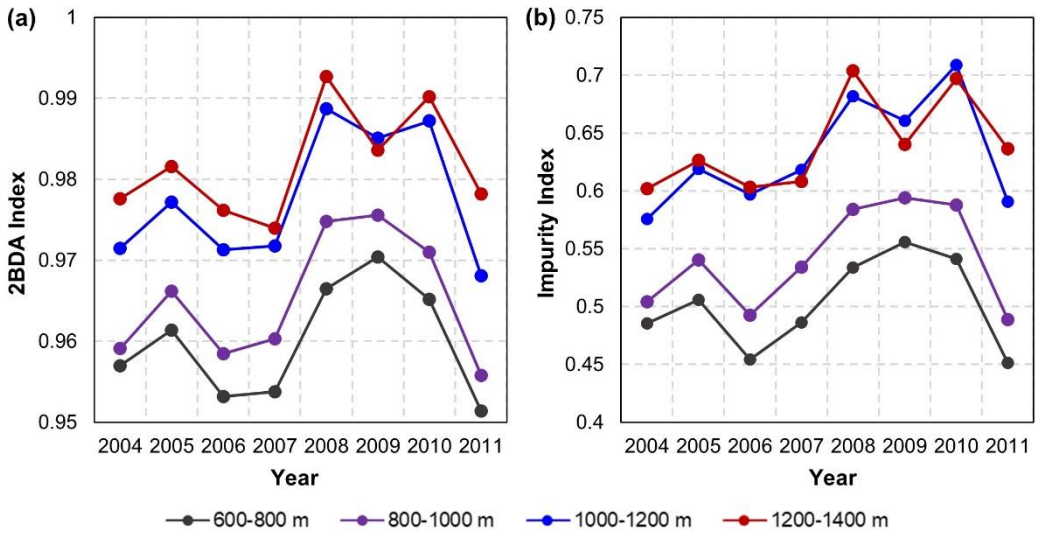

Figure A3. Interannual variability of the 2BDA index (a) and impurity index (b) at the elevation levels of 600-800m, 800-1000m, 1000-1200m, and 1200-1400m within the study area.

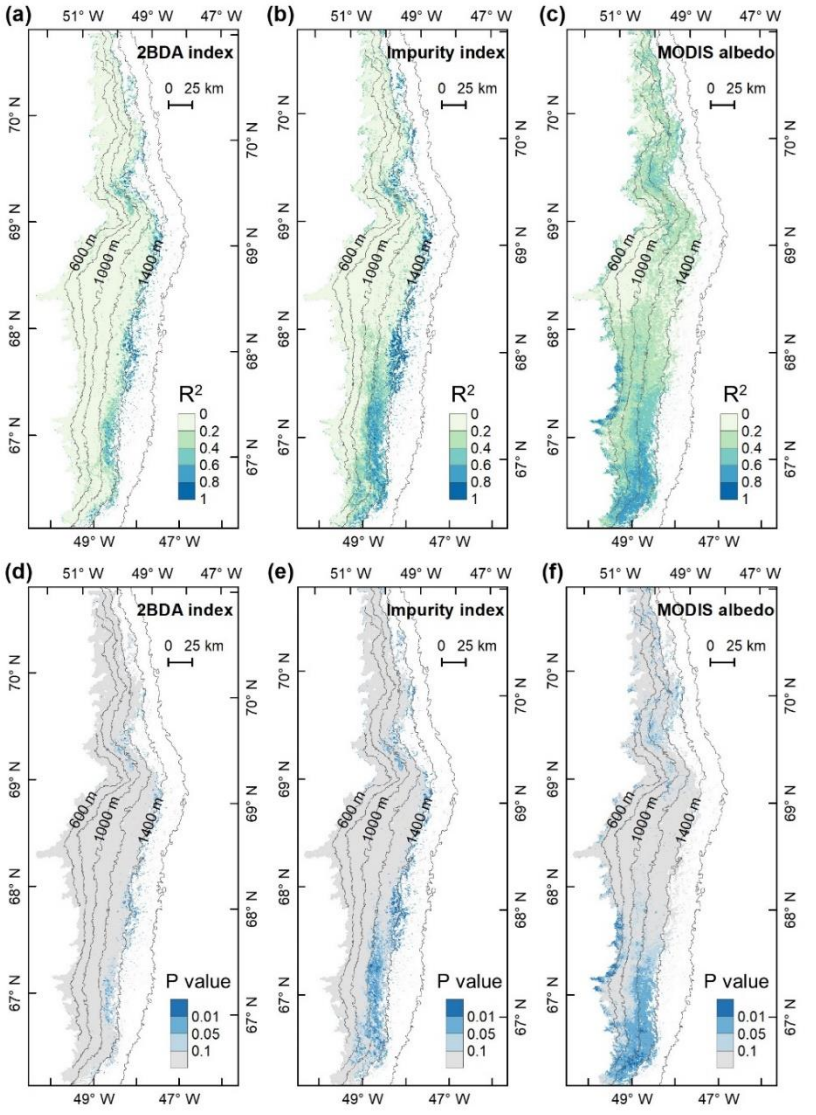

Figure A4. R^2 ~~of~~and P values for the interannual trends of the 2BDA index ~~(a), Impurity~~, impurity index ~~(b),~~ and MODIS albedo ~~(c)~~ from 2004 to 2011.

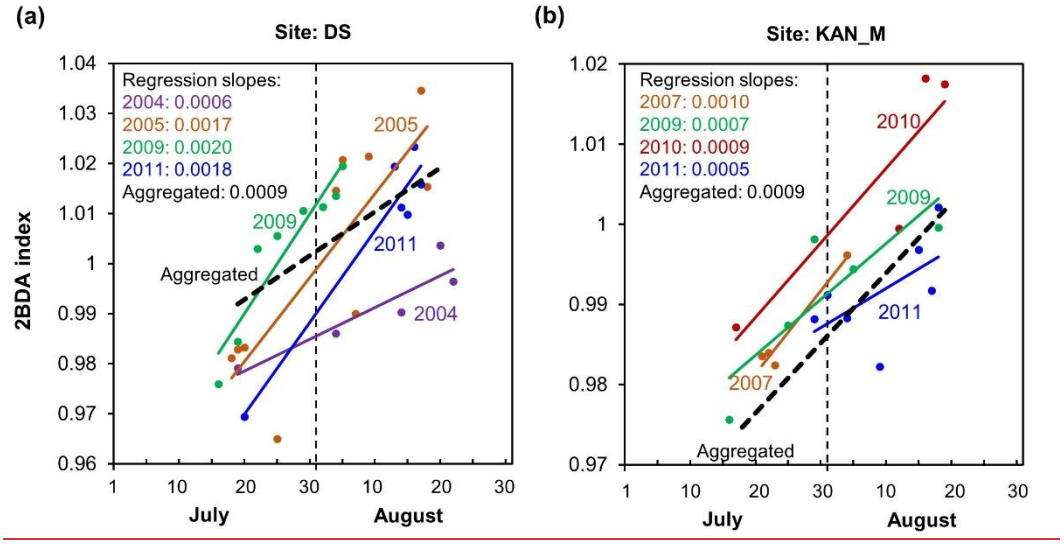

Figure A5. Temporal trends of 2BDA index from mid-July to Mid-August in different years at sites DS (a) and KAN_M (b).

Appendix B

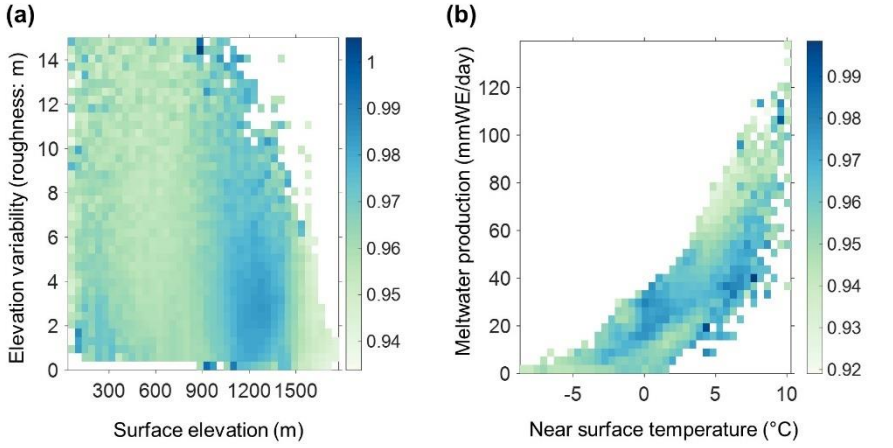

Figure B1. (a) 2BDA index versus surface elevation and roughness (elevation variability within each MERIS pixel). (b) 2BDA index versus near surface temperature and meltwater production simulated by MAR. The colour bars in (a) and (b) indicate the average 2BDA index for each two-dimensional bin defined by the two variables on the horizontal and vertical axes.

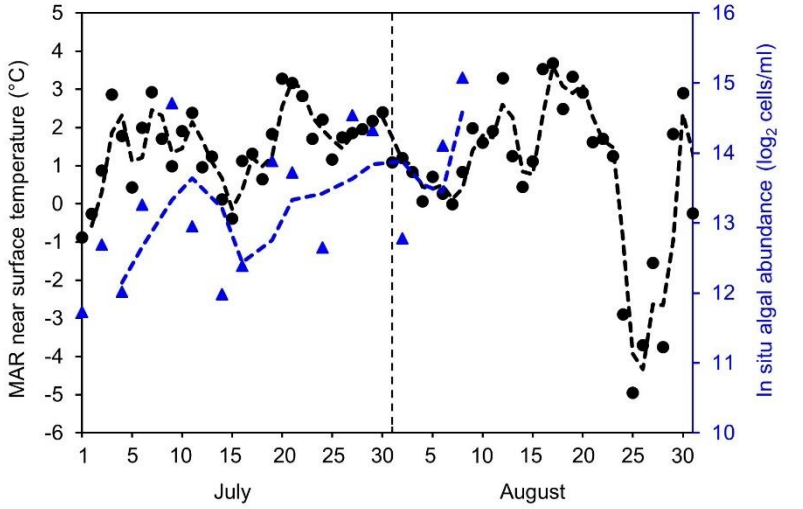

Figure ~~B1~~B2. MAR-simulated near surface temperature (°C, black circle, left axis) and in situ measured algal abundance (log_2 cells/ml, blue ~~triangle~~triangles, right vertical axis) ~~over~~at the S6 weather station at the K-transect during ~~2014~~ July-August 2014 by Stibal et al. (2017).

790

Appendix C

Table C1. Measured algal cell abundance from the field dataset of Cook et al. (2020) with the 2BDA index calculated from coincident hyperspectral measurements. The highlighted rows are samples with cell abundance of greater than 10000 cells/ml.

Sample ID	Cell abundance (cells/ml)	2BDA index
13_7_SB1	2688	0.9614
13_7_SB2	13375	1.0075
13_7_SB3	938	0.9813
13_7_SB4	4500	1.0371
13_7_SB5	0	0.9653
14_7_SB1	30313	1.0953
14_7_SB2	3063	0.9868
14_7_SB3	7938	0.9554
14_7_SB4	17938	0.9939
14_7_SB5	41000	1.2218
14_7_SB6	0	0.9555
14_7_SB7	12438	1.0850
14_7_SB8	0	0.9863
14_7_SB9	21875	1.0808
14_7_SB10	24875	1.1257
15_7_SB1	1438	0.9908
15_7_SB2	7250	0.9497
15_7_SB3	30313	1.0810
15_7_SB4	4250	0.9665
15_7_SB5	938	0.9839
20_7_SB1	11375	1.0536
20_7_SB2	7563	0.9939
20_7_SB3	7625	1.0122
21_7_SB1	92250	1.2635
21_7_SB2	44861	1.1411
21_7_SB3	750	0.9922
21_7_SB4	14313	1.0296
21_7_SB5	1063	0.9731
21_7_SB7	33229	1.0794
21_7_SB8	1188	0.9440
21_7_SB9	313	1.0097
21_7_SB10	17563	1.0763
23_7_SB1	250	0.9765
23_7_SB2	938	0.9754
23_7_SB3	8563	1.0141
23_7_SB4	21125	0.9975
23_7_SB5	28563	1.1131
24_7_SB1	1875	0.9985

795

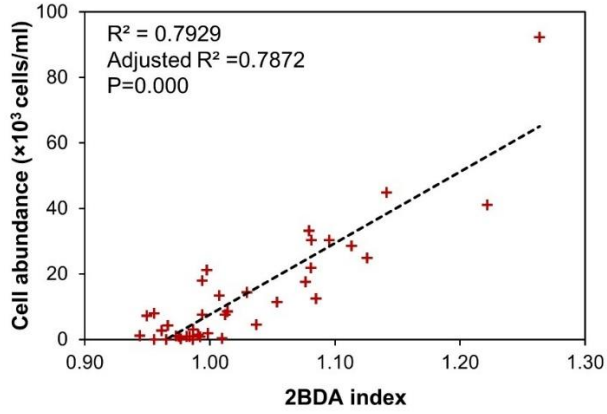

Figure C2. Scatterplot of measured cell abundance versus 2BDA index listed in Table C1.

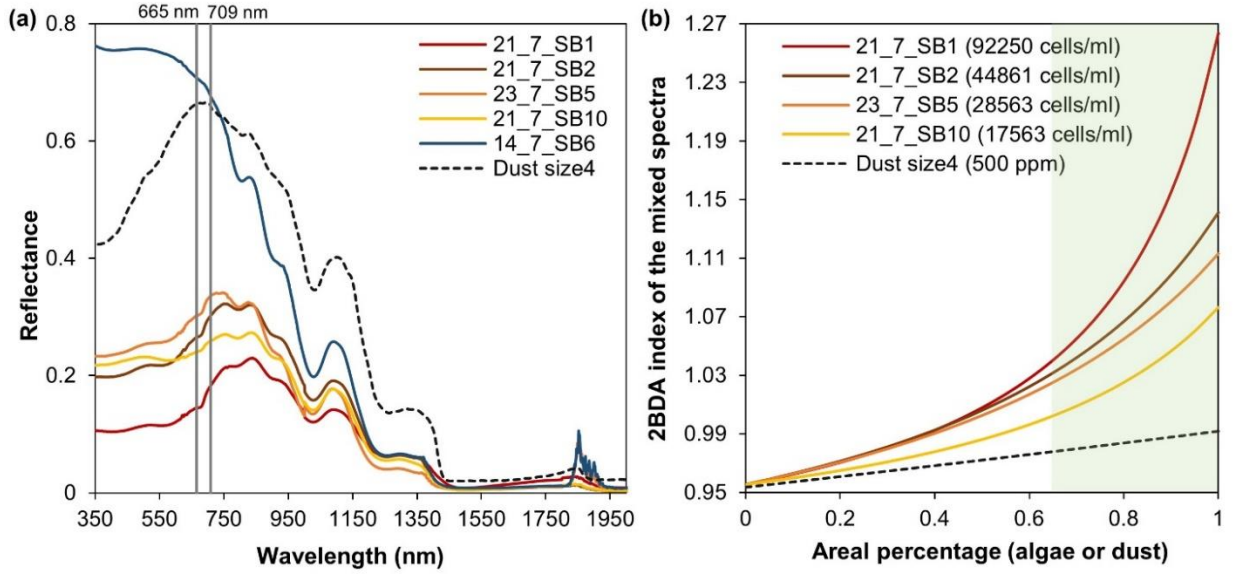

Figure C3. Spectral linear mixing experiments. (a) Field hyperspectral measurements of four algae-abundant samples (21_7_SB1, 21_7_SB2, 23_7_SB5, and 21_7_SB10) and one bare ice sample (zero algal abundance, 14_7_SB6) from Cook et al. (2020), and the SNICAR-simulated spectra for the dust scenario (size 4 at concentration of 500 ppm). (b) 2BDA index calculated from the linearly mixed spectra with varying areal percentage at subpixel scale for algae (different algal abundances) and dust scenarios.

Author contribution

S. W., M. T., and P. A. designed the study. S. W. processed the MERIS, MODIS, and WorldView-2 data. S. W. and M. X. tested the MERIS ratio indices. X. F. provided the MAR v3.9 outputs. S. W., M. T., and P. A. analysed the results and generated figures. S. W. wrote the manuscript. All authors discussed the results and contributed to the final manuscript.

Competing interests

The authors declare that they have no conflict of interest.

Acknowledgements

This work was supported by National Science Foundation ANS #1713072, National Science Foundation PLR-1603331, NASA Exobiology award #80NSSC18K0814, NASA MAP #80NSSC17K0351, NASA #NNX17AH04G, and the Heising-Simons foundation. We would like to thank the Polar Geospatial Center (https://www.pgc.umn.edu/) for providing the WorldView-2 imagery, the European Space Agency for distributing the MERIS data, and the NASA Land Processes Distributed Active Archive Center for distributing the MODIS data. Thanks to David Porter (Lamont-Doherty Earth Observatory, Columbia University) and Rafael Antwerpen (Utrecht University) for ~~commenting~~providing comments on the final manuscript.

References

Alexander, P. M., Tedesco, M., Fettweis, X., van de Wal, R. S. W., Smeets, C. J. P. P. and van den Broeke, M. R.: Assessing spatio-temporal variability and trends in modelled and measured Greenland Ice Sheet albedo (2000–2013), The Cryosphere, 8(6), 2293–2312, 2014.

Anderson, G. P., Felde, G. W., Hoke, M. L., Ratkowski, A. J., Cooley, T. W., Chetwynd, J. H., Gardner, J. A., Adler-Golden, S. M., Matthew, M. W., Berk, A., Bernstein, L. S., Acharya, P. K., Miller, D. P. and Lewis, P. E.: MODTRAN4-based atmospheric correction algorithm: FLAASH (fast line-of-sight atmospheric analysis of spectral hypercubes), in Algorithms and Technologies for Multispectral, Hyperspectral, and Ultraspectral Imagery VIII, vol. 4725, pp. 65–72, International Society for Optics and Photonics., 2002.

Anesio, A. M., Lutz, S., Chrismas, N. A. M. and Benning, L. G.: The microbiome of glaciers and ice sheets, NPJ Biofilms Microbiomes, 3, 10, 2017.

Beck, R., Zhan, S., Liu, H., Tong, S., Yang, B., Xu, M., Ye, Z., Huang, Y., Shu, S., Wu, Q., Wang, S., Berling, K., Murray, A., Emery, E., Reif, M., Harwood, J., Young, J., Nietch, C., Macke, D., Martin, M., Stillings, G., Stump, R. and Su, H.: Comparison of satellite reflectance algorithms for estimating chlorophyll-a in a temperate reservoir using coincident

hyperspectral aircraft imagery and dense coincident surface observations, Remote Sens. Environ., 178(Supplement C), 15–30, 2016.

Binding, C. E., Greenberg, T. A. and Bukata, R. P.: The MERIS Maximum Chlorophyll Index; its merits and limitations for inland water algal bloom monitoring, J. Great Lakes Res., 39, 100–107, 2013.

Blondeau-Patissier, D., Gower, J. F. R., Dekker, A. G., Phinn, S. R. and Brando, V. E.: A review of ocean color remote sensing methods and statistical techniques for the detection, mapping and analysis of phytoplankton blooms in coastal and open oceans, Prog. Oceanogr., 123, 123–144, 2014.

Box, J. E., ~~Cappelen, J., Decker, D., Fettweis, X., Mote, T., Tedesco, M. and van de Wal, R. S. W. Greenland [in Arctic Report Card 2010]. Retrieved from https://arctic.noaa.gov/Report-Card/Report-Card-Archive, 2010.~~

~~Box, J. E.,~~ Fettweis, X., Stroeve, J. C., Tedesco, M., Hall, D. K. and Steffen, K.: Greenland ice sheet albedo feedback: thermodynamics and atmospheric drivers, The Cryosphere, 6(4), 821–839, 2012.

Casey, K. A., Polashenski, C. M., Chen, J. and Tedesco, M.: Impact of MODIS sensor calibration updates on Greenland Ice Sheet surface reflectance and albedo trends, The Cryosphere, 11(4), 1781–1795, 2017.

Cavicchioli, R., Ripple, W. J., Timmis, K. N., Azam, F., Bakken, L. R., Baylis, M., Behrenfeld, M. J., Boetius, A., Boyd, P. W., Classen, A. T., Crowther, T. W., Danovaro, R., Foreman, C. M., Huisman, J., Hutchins, D. A., Jansson, J. K., Karl, D. M., Koskella, B., Mark Welch, D. B., Martiny, J. B. H., Moran, M. A., Orphan, V. J., Reay, D. S., Remais, J. V., Rich, V. I., Singh, B. K., Stein, L. Y., Stewart, F. J., Sullivan, M. B., van Oppen, M. J. H., Weaver, S. C., Webb, E. A. and Webster, N. S.: Scientists' warning to humanity: microorganisms and climate change, Nat. Rev. Microbiol., doi:10.1038/s41579-019-0222-5, 2019.

Chandler, D. M., Alcock, J. D., Wadham, J. L., Mackie, S. L. and Telling, J.: Seasonal changes of ice surface characteristics and productivity in the ablation zone of the Greenland Ice Sheet, The Cryosphere, 9(2), 487–504, 2015.

Condom, T., Dumont, M., Mourre, L., Sicart, J. E., Rabatel, A., Viani, A. and Soruco, A.: Technical note: A low-cost albedometer for snow and ice measurements – theoretical results and application on a tropical mountain in Bolivia, Geoscientific Instrumentation, Methods and Data Systems, 7(2), 169–178, doi:10.5194/gi-7-169-2018, 2018.

Cook, J. M., Tedstone, A. J., Williamson, C., McCutcheon, J., Hodson, A. J., Dayal, A., Skiles, M., Hofer, S., Bryant, R., McAree, O., McGonigle, A., Ryan, J., Anesio, A. M., Irvine-Fynn, T. D. L., Hubbard, A., Hanna, E., Flanner, M., Mayanna, S., Benning, L. G., van As, D., Yallop, M., McQuaid, J. B., Gribbin, T. and Tranter, M.: Glacier algae accelerate melt rates on the south-western Greenland Ice Sheet, The Cryosphere, 14(1), 309–330, doi:10.5194/tc-~~2019-58, 2019~~14-309-2020, 2020.

Dee, D. P., Uppala, S. M., Simmons, A. J., Berrisford, P., Poli, P., Kobayashi, S., Andrae, U., Balmaseda, M. A., Balsamo, G., Bauer, P., Bechtold, P., Beljaars, A. C. M., van de Berg, L., Bidlot, J., Bormann, N., Delsol, C., Dragani, R., Fuentes, M., Geer, A. J., Haimberger, L., Healy, S. B., Hersbach, H., Hólm, E. V., Isaksen, L., Kållberg, P., Köhler, M., Matricardi, M., McNally, A. P., Monge-Sanz, B. M., Morcrette, J.-J., Park, B.-K., Peubey, C., de Rosnay, P., Tavolato, C., Thépaut, J.-N.,

and Vitart, F.: The ERA-Interim reanalysis: configuration and performance of the data assimilation system, Q. J. Roy. Meteorol. Soc., 137, 553–597, doi:10.1002/qj.828, 2011.

De Ridder, K. and Gallée, H.: Land Surface–Induced Regional Climate Change in Southern Israel, J. Appl. Meteorol., 37(11), 1470–1485, 1998.

~~Di Mauro, B., Fava, F., Ferrero, L., Garzonio, R., Baccolo, G., Delmonte, B. and Colombo, R.: Mineral dust impact on snow radiative properties in the European Alps combining ground, UAV, and satellite observations, J. Geophys. Res. D: Atmos., 120(12), 6080–6097, 2015.~~

Dumont, M., Brun, E., Picard, G., Michou, M., Libois, Q., Petit, J.-R., Geyer, M., Morin, S. and Josse, B.: Contribution of light-absorbing impurities in snow to Greenland's darkening since 2009, Nat. Geosci., 7, 509, 2014.

European Space Agency (ESA): MERIS Product Handbook, Issue 3.0, 1 August 2011.

European Space Agency (ESA): MERIS Algorithm Theoretical Basis Document 2-17-Pixel Classification, Issue 5.0, 30 May 2011.

Fettweis, X., Tedesco, M., van den Broeke, M. and Ettema, J.: Melting trends over the Greenland ice sheet (1958–2009) from spaceborne microwave data and regional climate models, The Cryosphere, 5(2), 359–375, doi:10.5194/tc-5-359-2011, 2011.

Fettweis, X., Box, J., Agosta, C., Amory, C., Kittel, C., Lang, C., van As, D., Machguth, H. and Gallée, H.: Reconstructions of the 1900--2015 Greenland ice sheet surface mass balance using the regional climate MAR model, Cryosphere (The), 11, 1015–1033, 2017.

Flanner, M. G., Zender, C. S., Randerson, J. T. and Rasch, P. J.: Present-day climate forcing and response from black carbon in snow, J. Geophys. Res., 112(D11), 3131, 2007.

Flanner, M. G., Zender, C. S., Hess, P. G., Mahowald, N. M., Painter, T. H., Ramanathan, V. and Rasch, P. J.: Springtime warming and reduced snow cover from carbonaceous particles, Atmospheric Chemistry and Physics, 9(7), 2481–2497, doi:10.5194/acp-9-2481-2009, 2009.

Gallée, H. and Schayes, G.: Development of a Three-Dimensional Meso-γ Primitive Equation Model: Katabatic Winds Simulation in the Area of Terra Nova Bay, Antarctica, Mon. Weather Rev., 122(4), 671–685, 1994.

Ganey, G. Q., Loso, M. G., Burgess, A. B. and Dial, R. J.: The role of microbes in snowmelt and radiative forcing on an Alaskan icefield, Nat. Geosci., 10, 754, 2017.

Gitelson, A.: The peak near 700 nm on radiance spectra of algae and water: relationships of its magnitude and position with chlorophyll concentration, Int. J. Remote Sens., 13(17), 3367–3373, 1992.

Goelles, T. and Bøggild, C. E.: Albedo reduction of ice caused by dust and black carbon accumulation: a model applied to the K-transect, West Greenland, J. Glaciol., 63(242), 1063–1076, 2017.

Gower, J., King, S. and Goncalves, P.: Global monitoring of plankton blooms using MERIS MCI, Int. J. Remote Sens., 29(21), 6209–6216, 2008.

Hall, D. K. and Martinec, J.: Remote sensing of snow and ice, Principles and Applications of Imaging Radar, edited by FM Henderson and AJ Lewis, 677–703, 1985.

Hanna, E., Cropper, T. E., Hall, R. J. and Cappelen, J.: Greenland Blocking Index 1851-2015: a regional climate change signal, Int. J. Climatol., 36(15), 4847–4861, 2016.

Hofer, S., Tedstone, A. J., Fettweis, X. and Bamber, J. L.: Decreasing cloud cover drives the recent mass loss on the Greenland Ice Sheet, Sci Adv, 3(6), e1700584, 2017.

Howat, I. M., Negrete, A. and Smith, B. E.: The Greenland Ice Mapping Project (GIMP) land classification and surface elevation data sets, The Cryosphere, 8(4), 1509–1518, 2014.

Howat, I. M., Negrete, A. and Smith, B.: MEaSURES Greenland Ice Mapping Project (GIMP) Digital Elevation Model, Version 1., Boulder Colo. USA NASA Natl. Snow Ice Data Cent, Distrib. Act. Arch. Cent., doi, 10, 2015.

Huovinen, P., Ramírez, J. and Gómez, I.: Remote sensing of albedo-reducing snow algae and impurities in the Maritime Antarctica, ISPRS J. Photogramm. Remote Sens., 146, 507–517, 2018.

Legleiter, C. J., Tedesco, M., Smith, L. C. and Overstreet, B. T.: Mapping the bathymetry of supraglacial lakes and streams on the Greenland Ice Sheet using field measurements and high resolution satellite images, The Cryosphere Discussions, 7(5), 4741–4773, doi:10.5194/tcd-7-4741-2013, 2013.

Lutz, S., Anesio, A. M., Jorge Villar, S. E. and Benning, L. G.: Variations of algal communities cause darkening of a Greenland glacier, FEMS Microbiol. Ecol., 89(2), 402–414, 2014.

Lutz, S., Anesio, A. M., Raiswell, R., Edwards, A., Newton, R. J., Gill, F. and Benning, L. G.: The biogeography of red snow microbiomes and their role in melting arctic glaciers, Nat. Commun., 7, 11968, 2016.

Lutz, S., Anesio, A. M., Edwards, A. and Benning, L. G.: Linking microbial diversity and functionality of arctic glacial surface habitats, Environ. Microbiol., 19(2), 551–565, 2017.

Lutz, S., McCutcheon, J., McQuaid, J. B. and Benning, L. G.: The diversity of ice algal communities on the Greenland Ice Sheet as revealed by oligotyping, Microb Genom, doi:10.1099/mgen.0.000159, 2018.

Lyapustin, A., Tucker, J., Hall, F., Sellers, P., Wu, A., Angal, A., Wang, Y., Xiong, X., Meister, G., Platnick, S. and Others: Scientific impact of MODIS C5 calibration degradation and C6+ improvements, Atmospheric Measurement Techniques, 7(12) [online] Available from: https://ir.library.oregonstate.edu/concern/articles/b2773x521, 2014.

Matthews, M. W.: A current review of empirical procedures of remote sensing in inland and near-coastal transitional waters, Int. J. Remote Sens., 32(21), 6855–6899, 2011.

Mioduszewski, J. R., Rennermalm, A. K., Hammann, A., Tedesco, M., Noble, E. U., Stroeve, J. C. and Mote, T. L.: Atmospheric drivers of Greenland surface melt revealed by self-organizing maps, J. Geophys. Res. D: Atmos., 121(10), 2015JD024550, 2016.

Mishra, S. and Mishra, D. R.: Normalized difference chlorophyll index: A novel model for remote estimation of chlorophyll-a concentration in turbid productive waters, Remote Sens. Environ., 117, 394–406, 2012.

Moses, W. J., Gitelson, A. A., Berdnikov, S. and Povazhnyy, V.: Satellite Estimation of Chlorophyll-a Concentration Using the Red and NIR Bands of MERIS—The Azov Sea Case Study, IEEE Geoscience and Remote Sensing Letters, 6(4), 845–849, doi:10.1109/lgrs.2009.2026657, 2009.

Moses, W. J., Gitelson, A. A., Berdnikov, S., Saprygin, V. and Povazhnyi, V.: Operational MERIS-based NIR-red algorithms for estimating chlorophyll-a concentrations in coastal waters—The Azov Sea case study, Remote Sens. Environ., 121, 118–124, 2012.

Moustafa, S. E., Rennermalm, A. K., Smith, L. C., Miller, M. A., Mioduszewski, J. R., Koenig, L. S., Hom, M. G. and Shuman, C. A.: Multi-modal albedo distributions in the ablation area of the southwestern Greenland Ice Sheet, The Cryosphere, 9(3), 905–923, 2015.

Nordenskiöld, A. E.: I.—Account of an Expedition to Greenland in the year 1870, Geol. Mag., 9(97), 289–306, 1872.

Painter, T. H., Duval, B., Thomas, W. H., Mendez, M., Heintzelman, S. and Dozier, J.: Detection and quantification of snow algae with an airborne imaging spectrometer, Appl. Environ. Microbiol., 67(11), 5267–5272, 2001.

Palmer, S. C. J., Hunter, P. D., Lankester, T., Hubbard, S., Spyrakos, E., N. Tyler, A., Présing, M., Horváth, H., Lamb, A., Balzter, H. and Tóth, V. R.: Validation of Envisat MERIS algorithms for chlorophyll retrieval in a large, turbid and optically-complex shallow lake, Remote Sens. Environ., 157, 158–169, 2015.

Remias, D., Schwaiger, S., Aigner, S., Leya, T., Stuppner, H. and Lütz, C.: Characterization of an UV-and VIS-absorbing, purpurogallin-derived secondary pigment new to algae and highly abundant in M esotaenium berggrenii (Zygnematophyceae, Chlorophyta), an extremophyte living on glaciers, FEMS Microbiol. Ecol., 79(3), 638–648, 2012.

Reshitnyk, L., Costa, M., Robinson, C. and Dearden, P.: Evaluation of WorldView-2 and acoustic remote sensing for mapping benthic habitats in temperate coastal Pacific waters, Remote Sens. Environ., 153, 7–23, 2014.

Ryan, J. C., Hubbard, A., Stibal, M., Irvine-Fynn, T. D., Cook, J., Smith, L. C., Cameron, K. and Box, J.: Dark zone of the Greenland Ice Sheet controlled by distributed biologically-active impurities, Nat. Commun., 9(1), 1065, 2018.

Shimada, R., Takeuchi, N. and Aoki, T.: Inter-Annual and Geographical Variations in the Extent of Bare Ice and Dark Ice on the Greenland Ice Sheet Derived from MODIS Satellite Images, Front. Earth Sci., 4, 2293, 2016.

Skiles, S. M., Flanner, M., Cook, J. M., Dumont, M. and Painter, T. H.: Radiative forcing by light-absorbing particles in snow, Nat. Clim. Chang., 8(11), 964–971, 2018.

Stibal, M., Gözdereliler, E., Cameron, K. A., Box, J. E., Stevens, I. T., Gokul, J. K., Schostag, M., Zarsky, J. D., Edwards, A., Irvine-Fynn, T. D. L. and Jacobsen, C. S.: Microbial abundance in surface ice on the Greenland Ice Sheet, Front. Microbiol., 6, 225, 2015.

Stibal, M., Box, J. E., Cameron, K. A., Langen, P. L., Yallop, M. L., Mottram, R. H., Khan, A. L., Molotch, N. P., Chrismas, N. A. M., Calì Quaglia, F., Remias, D., Smeets, C. J. P. P., van den Broeke, M. R., Ryan, J. C., Hubbard, A., Tranter, M., van As, D. and Ahlstrøm, A. P.: Algae Drive Enhanced Darkening of Bare Ice on the Greenland Ice Sheet, Geophys. Res. Lett., 44(22), 2017GL075958, 2017.

Stroeve, J., Box, J. E., Wang, Z., Schaaf, C. and Barrett, A.: Re-evaluation of MODIS MCD43 Greenland albedo accuracy and trends, Remote Sens. Environ., 138, 199–214, 2013.

Takeuchi, N.: The altitudinal distribution of snow algae on an Alaska glacier (Gulkana Glacier in the Alaska Range), Hydrol. Process., 15(18), 3447–3459, 2001.

Takeuchi, N., Dial, R., Kohshima, S., Segawa, T. and Uetake, J.: Spatial distribution and abundance of red snow algae on the Harding Icefield, Alaska derived from a satellite image, Geophys. Res. Lett., 33(21), 570, 2006.

~~Takeuchi, N., Nagatsuka, N., Uetake, J. and Shimada, R.: Spatial variations in impurities (cryoconite) on glaciers in northwest Greenland, Bull. Glaciol. Res., 32, 85–94, 2014.~~

Tedesco, M., Fettweis, X., van den Broeke, M. R., van de Wal, R. S. W., C J P, van de Berg, W. J., Serreze, M. C. and Box, J. E.: The role of albedo and accumulation in the 2010 melting record in Greenland, Environ. Res. Lett., 6(1), 014005, 2011.

Tedesco, M., Foreman, C. M., Anton, J., Steiner, N. and Schwartzman, T.: Comparative analysis of morphological, mineralogical and spectral properties of cryoconite in Jakobshavn Isbrae, Greenland, and Canada Glacier, Antarctica, Ann. Glaciol., 54(63), 147–157, 2013.

Tedesco, M., Doherty, S., Fettweis, X., Alexander, P., Jeyaratnam, J. and Stroeve, J.: The darkening of the Greenland ice sheet: trends, drivers, and projections (1981–2100), The Cryosphere, 10(2), 477–496, 2016.

Tedesco, M., Box, J. E., Cappelen, J., Fausto, R. S., Fettweis, X., Andersen, J. K., Mote, T., Smeets, C. J. P. P., van As, D. and

van de Wal, R. S. W.: Greenland Ice Sheet [in Arctic Report Card 2018]. Retrieved from https://arctic.noaa.gov/Report-Card/Report-Card-2018/ArtMID/7878/ArticleID/781/Greenland-Ice-Sheet, 2018.

Tedstone, A. J., Bamber, J. L., Cook, J. M., Williamson, C. J., Fettweis, X., Hodson, A. J. and Tranter, M.: Dark ice dynamics of the south-west Greenland Ice Sheet, The Cryosphere, 11(6), 2491–2506, 2017.

Tedstone, A. J., Cook, J. M., Williamson, C. J., Hofer, S., McCutcheon, J., Irvine-Fynn, T., Gribbin, T. and Tranter, M.: Algal growth and weathering crust state drive variability in western Greenland Ice Sheet ice albedo, The Cryosphere, 14(2), 521–538, 2020.

Toller, G., Xiong, X. J., Sun, J., Wenny, B. N., Geng, X., Kuyper, J., Angal, A., Chen, H., Madhavan, S. and Wu, A.: Terra and Aqua moderate-resolution imaging spectroradiometer collection 6 level 1B algorithm, JARS, 7(1), 073557, 2013.

Uetake, J., Naganuma, T., Hebsgaard, M. B., Kanda, H. and Kohshima, S.: Communities of algae and cyanobacteria on glaciers in west Greenland, Polar Sci., 4(1), 71–80, 2010.

Wang, S., Liu, H., Yu, B., Zhou, G. and Cheng, X.: Revealing the early ice flow patterns with historical Declassified Intelligence Satellite Photographs back to 1960s, Geophys. Res. Lett., 43(11), 2016GL068990, 2016.

Wang, S., Tedesco, M., Xu, M. and Alexander, P. M.: Mapping Ice Algal Blooms in Southwest Greenland From Space, Geophys. Res. Lett., 45(21), 11,779–11,788, 2018.

Warren, S. G.: Optical properties of snow, Rev. Geophys., 20(1), 67, 1982.

Wientjes, I. G. M. and Oerlemans, J.: An explanation for the dark region in the western melt zone of the Greenland ice sheet, The Cryosphere, 4(3), 261–268, 2010.

Wientjes, I. G. M., Wal, R. S. W. V. de, Reichart, G. J., Sluijs, A. and Oerlemans, J.: Dust from the dark region in the western ablation zone of the Greenland ice sheet, The Cryosphere, 5(3), 589–601, 2011.

Wientjes, I. G. M., Van De Wal, R. S. W., Schwikowski, M., Zapf, A., Fahrni, S. and Wacker, L.: Carbonaceous particles reveal that Late Holocene dust causes the dark region in the western ablation zone of the Greenland ice sheet, J. Glaciol., 58(210), 787–794, 2012.

Williamson, C. J., Anesio, A. M., Cook, J., Tedstone, A., Poniecka, E., Holland, A., Fagan, D., Tranter, M. and Yallop, M. L.: Ice algal bloom development on the surface of the Greenland Ice Sheet, FEMS Microbiol. Ecol., 94(3), doi:10.1093/femsec/fiy025, 2018.

Williamson, C. J., Cameron, K. A., Cook, J. M., Zarsky, J. D., Stibal, M. and Edwards, A.: Glacier Algae: A Dark Past and a Darker Future, Front. Microbiol., 10, 524, 2019.

Williamson, C. J., Cook, J., Tedstone, A., Yallop, M., McCutcheon, J., Poniecka, E., Campbell, D., Irvine-Fynn, T., McQuaid, J., Tranter, M., Perkins, R. and Anesio, A.: Algal photophysiology drives darkening and melt of the Greenland Ice Sheet, Proc. Natl. Acad. Sci. U. S. A., doi:10.1073/pnas.1918412117, 2020.

Xu, M., Liu, H., Beck, R., Lekki, J., Yang, B., Shu, S., Kang, E. L., Anderson, R., Johansen, R., Emery, E., Reif, M. and Benko, T.: A spectral space partition guided ensemble method for retrieving chlorophyll-a concentration in inland waters from Sentinel-2A satellite imagery, Journal of Great Lakes Research, 45(3), 454–465, doi:10.1016/j.jglr.2018.09.002, 2019a.

Xu, M., Liu, H., Beck, R., Lekki, J., Yang, B., Shu, S., Liu, Y., Benko, T., Anderson, R., Tokars, R., Johansen, R., Emery, E. and Reif, M.: Regionally and Locally Adaptive Models for Retrieving Chlorophyll-a Concentration in Inland Waters From Remotely Sensed Multispectral and Hyperspectral Imagery, IEEE Transactions on Geoscience and Remote Sensing, 57(7), 4758–4774, doi:10.1109/tgrs.2019.2892899, 2019b.

Yallop, M. L., Anesio, A. M., Perkins, R. G., Cook, J., Telling, J., Fagan, D., MacFarlane, J., Stibal, M., Barker, G., Bellas, C., Hodson, A., Tranter, M., Wadham, J. and Roberts, N. W.: Photophysiology and albedo-changing potential of the ice algal community on the surface of the Greenland ice sheet, ISME J., 6(12), 2302–2313, 2012.

Yang, K. and Smith, L. C.: Supraglacial streams on the Greenland Ice Sheet delineated from combined spectral--shape information in high-resolution satellite imagery, IEEE Geoscience and Remote Sensing Letters, 10(4), 801–805, 2013.